DOE/AL/85802--T1

Contract Report

Sustainable Hydrogen Production

FSEC-CR-857-95
DOE Contract #DE-FG04-94AL85802
January 1996

Submitted to:
U.S. Department of Energy
Advanced Utility Concepts Division (EE-142)
Mr. Neil Rossmeissl
1000 Independence Ave., S.W.
Washington, DC 20585

Submitted by:
David L. Block
Clovis Linkous
Nazim Muradov

Florida Solar Energy Center
1679 Clearlake Road
Cocoa, Florida 32922-5703

PREFACE

This report describes the Sustainable Hydrogen Production research conducted at the Florida Solar Energy Center (FSEC) for the past year. The report presents the work done on the following four tasks:

Task 1. Production of Hydrogen by Photovoltaic-Powered Electrolysis - This task represents the final effort of a cooperative project between the U.S. Department of Energy, NASA/Kennedy Space Center, FSEC and the Florida Energy Office. The activities covered five years of effort at a total funding of $216,809. These results represent a successful coordination of two state agencies and two federal agencies.

Task 2. Solar Photocatalytic Hydrogen Production from Water Using a Dual-Bed Photosystem - This task established the basis of the dual-bed concept by selectively evolving hydrogen or oxygen. A number of redox mediators were found to facilitate hydrogen production.

Task 3. Development of Solid Electrolytes for Water Electrolysis at Intermediate Temperatures - Several ionomers were synthesized and fabricated into proton exchange membranes. Laboratory testing in an electrolysis cell gave comparable performance to the commercial product.

Task 4. Production of Hydrogen by Thermocatalytic Cracking of Natural Gas - The experimental unit was constructed and a number of catalysts for methane cracking reactions were tested. Laboratory experiments established catalyst activity and identified stability problems.

This report was prepared by the Florida Solar Energy Center/University of Central Florida as an account of work sponsored by the U.S. Department of Energy (Contract #DE-FG04-94AL85802)). The work reported in this document does not imply endorsement by U.S. Department of Energy.

David L. Block
Clovis Linkous
Nazim Muradov

DISCLAIMER

TABLE OF CONTENTS

Task 1 Report

Production of Hydrogen by Photovoltaic-Powered Electrolysis

FSEC-CR-857-95

Submitted to:
Mr. Michael Ashworth
Ms. Jan Rickey
Florida Energy Office
Department of Community Affairs
2740 Centerview Drive
Tallahassee, FL 32399-2100

FEO Contract #914
FSEC Account #26-56-729

Mr. Neil P. Rossmeissl
Advanced Utilities Concepts Division (EE-142)
U.S. Department of Energy
1000 Independence Ave., S.W.
Washington, DC 20585

DOE Contract #DE-FG04-94AL85802
FSEC Account #26-56-118

Mr. H. T. Everett
Ms. Joyce E. Beeson
NASA/Kennedy Space Center
Kennedy Space Center, FL 32899

NASA Grant #NAG10-0123
FSEC Account #26-25-206

December 1995

Submitted by:
David L. Block
Florida Solar Energy Center
1679 Clearlake Road
Cocoa, Florida 32922-5703

PRODUCTION OF HYDROGEN BY PHOTOVOLTAIC-POWERED ELECTROLYSIS

Prepared by:

David L. Block
Florida Solar Energy Center
1679 Clearlake Road
Cocoa, FL 32922-5703

December 1995

1.0 SUMMARY

The report presents results of a cooperative effort among the Florida Energy Office, NASA/Kennedy Space Center, the U.S. Department of Energy and the Florida Solar Energy Center (FSEC). It reports on a task to evaluate hydrogen production from photovoltaic (PV)-powered electrolysis. The resulting activities covered five years of effort funded at a total of $216,809. The results represent a successful, coordinated effort among two state agencies and two federal agencies.

Results are reported on two separate investigations:

1) The first investigation looked at the use of line focus concentrating photovoltaics coupled with single-cell electrolyzers to produce gaseous hydrogen. The concept, and its design, construction and operation, are presented. The objectives of the line focusing PV system are to reduce overall system cost under the assumptions that lenses and mirrors are cheaper to deploy than are PV cells, and that low-voltage, high-current dc electricity can efficiently power a single-cell electrolyzer to produce hydrogen.

2) The second investigation evaluated a base case cost of PV electrolysis hydrogen production based on present-day PV and electrolyzer costs and efficiencies. A second step analyzed the hydrogen costs based on a "best" prediction of where PV costs and efficiencies will be in 10 years. These results set the minimum cost standards that other renewable production technologies must meet or better.

Line Focus Concentrating PV Electrolysis Hydrogen Production

The basic idea of the concentrating PV electrolysis concept is to combine the least-cost concentrator technology with high-efficiency photovoltaic cells and to use low-voltage, high-current power produced by the PV for water electrolysis using a single-cell electrolyzer. An assessment of water electrolysis as a matched load to concentrating PV systems looks very good. Electrolysis requires high-amperage, low-voltage dc electricity, and its load profile is very similar to charging lead-acid batteries. Ideally, the water electrolysis unit can be direct-coupled to the PV system without significant mismatch losses in efficiency and reliability-robbing electronics. Acknowledgment for development of this concept is given to Dr. Kirk Collier, a former FSEC employee.

The major components of the hydrogen production system that was installed at FSEC are a parabolic trough concentrator, a photovoltaic receiver assembly, a cooling system and electrolyzer cells. The parabolic trough concentrator was purchased from Industrial Solar Technology, Denver, Colorado, at a cost of approximately $\$100/m^2$ and consists of four 20-foot-long collectors, each 7.5 feet wide. The nominal focal width is 2 inches, which yields a geometric concentration of 56:1. The reflector material chosen for the FSEC installation was 3M aluminized film. The electrolyzer cells were supplied by The Electrolyzer Corporation Ltd., Toronto, Canada. The cells are alkaline cells of unipolar design, each rated at 250 amps and between 1.8 and 2 volts. Water from an above-ground swimming pool is used to cool the PV cells. Bonding and electrically connecting the PV cells proved to be a difficult and time-consuming task during construction, and failure of cooling of the system was a problem.

The system was continuously operated over the five-month period of July to December 1993; data were segregated between the summer (July-September) and fall (October-December) seasons. The most important measured parameter is the amount of hydrogen produced from a given amount of solar energy. Due to the complexity of accurately measuring gaseous quantities of hydrogen, the amount of current passing through the electrolyzer was used as the measure of the quantity of hydrogen produced. The trend of the electrical current supplied to the electrolyzer as a function of the direct normal solar flux at solar noon was reasonably linear for both summer and fall seasons. Of particular interest, however, is the performance at high values of solar radiation, approximately 800 W/m^2, where the current

deviates significantly from the linear behavior. This deviation is thought to be caused by mismatch between the PV output and the electrolyzer load.

The PV cells had a poor conversion efficiency -- less than 6% under concentration. Plots show the system conversion efficiency as a function of solar time for a typical summer and fall day. The system conversion efficiency is defined as the higher heating value of the hydrogen produced (assuming a coulombic efficiency of 100%) divided by the available solar energy. The overall system efficiency for the time period July through December was 2.8% based on total direct-normal radiation, and 1.8% based on total global radiation. Although these efficiencies seem extremely low at first glance, they do show that the mismatch losses between the PV cells and array and the electrolyzer are very low when compared to the PV and electrolyzer losses. The best instantaneous efficiency achieved was about 3.8% (based on direct-normal radiation).

Although the PV cells used in this system were of low efficiency, the data taken verified the design goals of the project. The system demonstrated that a relatively inexpensive concentrator system can be successfully employed in a direct-coupled PV-electrolysis system with minimal losses. Both mismatch losses between PV cells and between PV and electrolyzer were minimal, and the system operated relatively well under totally unattended operation.

To achieve acceptable conversion efficiencies, much higher efficiency PV cells must be used. Also, higher electrolyzer efficiencies are possible using alkaline technology if the cell temperatures are kept significantly above ambient temperature. The use of the cooling water from the concentrating PV would be an excellent candidate to increase the temperature and, thus, efficiency of the electrolyzer.

Photovoltaic-Electrolysis-Produced Hydrogen Costs

The efficiencies, costs and resulting performance of PV and electrolyzer systems for the present and for 10 years in the future were carefully evaluated in this investigation. Values of photovoltaic modules costs and efficiencies for the present and for the future were established using the DOE Five-Year Research Plan for Photovoltaics, with modifications

based on FSEC experience and other published data. These values were also examined with respect to present materials, process costs, and achieved efficiency results.

FSEC contacted major PV manufacturers and determined a quoted price of $4 per peak watt of power as the present cost for large-scale PV. The calculations assumed a cost of $400/m^2 and a 12% efficiency. The PV systems considered were flat plate, flat-plate tracking, and concentrating, rather than cells, in terms of materials or technology.

To predict performance of a PV system, specific sites must be selected to establish input values for solar insolation. Twenty regionally representative cities were selected, and Typical Meteorological Year (TMY) data for these cities were used to establish the site-specific insolation values. For each of these 20 sites, insolation enhancement factors for latitude tilt, tracking and direct-normal PV arrays were calculated. To produce representative insolation values for fixed, tracking and concentrating arrays, data from the 20 cities were averaged to represent four U.S. regions -- southwest, south, middle and north.

PV power was calculated for each of the four regions using site insolation times PV efficiencies. The PV life-cycle cost calculations were then made for the lifetimes of the equipment by equating the present value of the PV equipment (module cost plus balance-of-system cost) and operating cost (discounted to present value) to the power produced times the cost of power (inflated at the energy escalation rate). As an example, this calculation gives a dc life-cycle cost of $0.15/kWh for a present-day flat-plate system located in the Southwest.

Results of the PV electricity cost calculations for dc electricity show that present PV-produced dc electricity costs $0.14 to $0.36/kWh, and that costs of $0.06 to $0.09/kWh are achievable in 10 years. PV system costs are $500 to $800/m^2 ($46 to $74/ft^2) for the present, and $325 to $565/m^2 ($30 to $53/ft^2) in a 10-year period. The variance between types of PV systems is slight, with flat-plate tracking producing slightly lower values.

A present-day ac electrolyzer was taken to have a conversion efficiency of 60% and an initial cost of $780 per gaseous hydrogen (H_2) production unit of 1000 Nm^3/year. The elimination of the need for ac-to-dc conversion equipment reduced the initial electrolyzer cost by 30%, giving a cost of $550 for 1000 Nm^3/year. In 10 years, the electrolyzer efficiencies were assumed to increase to 70%, with the initial costs remaining the same as at present.

Calculations of gaseous hydrogen production by PV electrolysis were performed, assuming that a constant value of 1000 Nm^3/year of H_2 would be produced. These calculations used the PV-produced dc electricity cost results.

The results for the cost of gaseous H_2 show present-day prices of $76 to $99/MMBtu for the desert Southwest, and prices of $127 to $185/MMBtu for the northern U.S. The cost of hydrogen from conventional $0.05/kWh electricity is $34/MMBTU. Thus, present PV-produced hydrogen costs for the desert Southwest are approximately 2.5 times those of hydrogen produced with conventional electricity. Gaseous hydrogen for future PV costs were $34 to $46/MMBtu for the desert Southwest, and $55 to $82/MMBtu for the northern U.S. These results show that PV-produced hydrogen costs in 10 years may be as little as 20% higher than the cost of hydrogen produced with conventional electricity at $0.05/kWh. All calculations show flat-plate tracking to be the minimum cost option. The calculations also show that the electrolysis equipment cost makes up 11% of the total H_2 cost.

2.0 INTRODUCTION

The project presented in this report is a cooperative effort among the Florida Energy Office, NASA/Kennedy Space Center, the U.S. Department of Energy and the Florida Solar Energy Center (FSEC). The report presents results of a task to evaluate hydrogen production from photovoltaic (PV)-powered electrolysis. PV-powered electrolysis is important in advancement of renewable hydrogen production, as it is the most straightforward of the renewable production technologies, and it sets the minimum cost standards that other renewable production technologies must meet or better.

The Florida Energy Office initiated this project in 1990 when it provided a $94,921 contract to FSEC to design, construct and operate a photovoltaic-powered electrolyzer system for the production of gaseous hydrogen. The design and construction of a line focus concentrating photovoltaic and single-cell electrolyzer unit was completed in 1991. This system operated for two days in December 1991, after which the PV cells were destroyed by overheating caused by failure of the cooling system. The system design, construction and operation were reported to the Florida Energy Office in Reference 1; system details are presented in the Results section of this report.

As part of the Florida Energy Office project, FSEC provided $73,355 to redesign the PV and cooling system and to install new PV cells. The resulting system was operated from June to December 1993. These results are presented in the Results section and are also reported in Reference 2.

In December 1993, NASA/Kennedy Space Center funded a $30,000 project to engineer a PV-electrolysis production unit for KSC to use in fueling its fleet vehicles. This project evaluated the line focus concentrating PV electrolysis system and KSC's method of producing gaseous hydrogen. Recommendations were made to NASA/Kennedy Space Center to install a PV-electrolysis system for their gaseous hydrogen needs, although no such system was constructed.

In 1994, $18,533 of U.S. Department of Energy funds and the remaining NASA funds were allocated to be used to improve the efficiency of the PV cells and the PV electrolysis system by thermal management and to continue monitoring of the PV electrolysis system. The PV

system was operated until FSEC relocated to new facilities in Cocoa, Florida. Relocation required that operation be discontinued, and the system was dismantled. The system is now in storage at the FSEC Field Test Site and can be reconstructed should the need arise.

The major objective of this project was to evaluate the price of hydrogen from PV-powered electrolysis. A "best-effort" detailed analysis of the cost of hydrogen from PV-powered electrolysis was conducted to accomplish this objective. This analysis updated work originally done five years ago, as reported in Reference 3.

3.0 RESULTS

The results of this $216,809 multi-agency project are presented in this section. These results can be grouped into two separate investigations, as follows:

1) The first investigation looked at the use of line focus concentrating photovoltaics coupled with single-cell electrolyzers to produce gaseous hydrogen. The concept, and its design, construction and operation, are presented. The objectives of the line focusing PV system are to reduce overall system cost under the assumptions that lenses and mirrors are cheaper to deploy than are PV cells, and that low-voltage, high-current dc electricity can efficiently power a single-cell electrolyzer to produce hydrogen.

2) The second investigation evaluated a base case cost of PV electrolysis hydrogen production based on present-day PV and electrolyzer costs and efficiencies. A second step analyzed the hydrogen costs based on a "best" prediction of where PV costs and efficiencies will be in 10 years. These results set the minimum cost standards that other renewable production technologies must meet or better.

3.1 Line Focus Concentrating PV Electrolysis Hydrogen Production

A hydrogen production facility utilizing a parabolic trough, concentrating-photovoltaic electrolysis system was designed, constructed and operated by FSEC. The project began in 1990, and the six-month operational period occurred in summer and fall of 1993. The initial project was funded by the Florida Energy Office and FSEC. Initial operation of the system took place over two days in December 1991 (reported in Reference 1). The limited operational

time was due to failure of the cooling system, which caused the PV cells to be destroyed by overheating. The PV cells were then reinstalled, and the system was made operational again in 1993.

The basic idea of the concentrating PV electrolysis concept is to combine the least-cost concentrator technology with high-efficiency photovoltaic cells and to use the resulting low-voltage, high-current power for water electrolysis using a single-cell electrolyzer. Acknowledgment for development of this concept is given to Dr. Kirk Collier, former FSEC employee [References 1 and 2]. The key to this concept is the use of low voltage and high current. Dr. Alexander Stuart of Electrolyzer Corporation supplied the single-cell electrolyzers to utilize the PV system's low voltage and high current. Dr. Stuart, in personal communication [Reference 4], indicated that there are three other similar applications of the concept, as follows:

1. A flat-plate PV-electrolyzer system of 3-4 kWp on the Electrolyzer Corporation roof in Toronto, Canada, that was installed five years ago and that has operated for four years.

2. A flat-plate PV-electrolysis system at the University of California, Riverside, that is still operational.

3. A PV electrolysis system at Xerox Corporation in Los Angeles that became operational in 1995.

On November 15, 1995, D. Block visited the University of California at Riverside and discussed the PV electrolysis system with Mr. James Heffel [5]. The description of the University of California site is as follows:

- Purpose - To demonstrate production, storage and utilization of hydrogen in one complete location. Refueling of vehicles is done as part of demonstration.

- Photovoltaics system array - Flat-plate Siemens modules of 3.5 kW size, wired to produce 24 volts.

- Electrolyzer - Twelve 7.3 kW electrolyzer cells from Electrolyzer Corporation which are wired in series to use the 24-volt PV power. Each individual electrolyzer looked exactly the same as the single cell used at FSEC.

- Other components - The produced hydrogen gas is compressed to 5000 psi and stored. The site has a refueling station for vehicles and has operated for approximately two years. The system is still in operation.

- Performance - A report from the University of California is near completion but has not yet been released.

Mr. Heffel [5] has described the PV electrolysis system at Xerox Corporation as follows:

- Purpose - To supply a refueling station for two pure hydrogen vehicles, with the hydrogen being supplied by PV electrolysis.

- Photovoltaics system - Concentrating PV using 11″ x 11″ Fresnel lenses and Siemens PV cells. The system size for 15″ x 15″ Fresnel lenses was to be 48 kW. With 11″ x 11″ lenses, the system is less than 48 kW (exact size not known). The author estimates the concentrator ratio of this system at 10 to 1. The array produces 24 volts and 300 amps.

- Electrolyzer - The electrolyzer is the same as used at the University of California at the Riverside site. Other details are not known.

Review of the PV electrolysis literature has shown that the other reported PV electrolysis systems all use the more conventional high-voltage PV and electrolyzers [6,7,8].

3.1.1 Concept Description

Concentrating PV has been demonstrated for a considerable period of time, with the majority of the applications in the area of utility power [9, 10, 11]. These applications of photovoltaics and parabolic trough technology have not been successful because of the concentrator's optical characteristics and the requirement of the electrical load for 120-240 volts. The 120-240

voltage requirement mandates that up to 300 individual PV cells must be wired in series, as a single PV cell provides approximately 1 volt, so cells must be added to reach the voltage requirement.

Because of the physics of a PV cell, the solar flux distribution at the focus of solar concentrators must be extremely uniform to maintain high system efficiency. Such solar flux uniformity is required so that the electrical current produced by the PV cell is proportional to the incident solar flux. If the solar flux doubles, then the current produced by the PV cell approximately doubles. The voltage characteristics are different. Output voltage remains almost constant with large changes in the incident solar flux.

The practical implications of this behavior are that PV cells are easy to voltage-match under varying solar flux levels, but will not current-match under these same conditions. This means that cells wired in series must be subjected to identical solar fluxes in order for their current outputs to be the same. If they are not the same, the low-current cells will behave like resistors to the high-current cells, and the efficiency of the string will decrease accordingly.

The solar flux distribution along the focal line of available parabolic trough concentrators is not uniform enough to maintain high efficiency for applications requiring the relatively high voltages needed for power production. However, for low-voltage applications, the situation is reversed. This is the concept proposed by this PV electrolysis system.

When PV cells are wired in parallel, the output currents of individual cells simply add to one another. They do not need to be matched to maintain efficiency. This means that parallel configurations of PV cells will maintain high efficiency in conditions of non-uniform solar fluxes.

This situation offers benefits when applied to water electrolysis. Water electrolysis requires only 1.5 to 2.0 volts dc to operate. For this application, only three to four parallel PV "strings" need to be operated in series rather than the 200-300 needed for utility-grid applications. Because the PV output is dc, the costs and inefficiencies of electrical inverters are also eliminated.

3.1.2 System and Design Considerations

Electrolysis provides a near-perfect electrical load for a line focus concentrating PV system, since most single electrolysis cells require hundreds of amps at between 1.5 and 2.0 volts. For a parabolic trough concentrator and available PV cells, a receiver length of about 30 to 45 cm should provide 200 amps of current. To create the 1.5 to 2.0 volts necessary, three to four strings of parallel cells must be connected in series. The optical requirements of solar uniformity are now much less stringent. The average solar flux over the total 30 to 45 cm length now must match over the 5 cm series connection length. Present parabolic trough systems can accomplish this quite well.

A first-cut assessment of water electrolysis as a matched load to concentrating PV systems looked very good. Electrolysis requires high-amperage, low-voltage dc electricity, and its load profile is very similar to charging lead-acid batteries. Ideally, the water electrolysis unit can be direct-coupled to the PV system without significant mismatch losses in efficiency and reliability-robbing electronics.

The major components of the hydrogen production system are the parabolic trough concentrator, the photovoltaic receiver assembly, the cooling system and the electrolyzer cells. These components are shown schematically in Figure 1.

The parabolic trough concentrator was purchased from Industrial Solar Technology (IST), Denver, Colorado, at a cost of approximately $\$100/m^2$. The IST concentrator system, as shown in Figure 2, consists of four 20-foot-long collectors that are each 7.5 feet wide. The nominal focal width is 2 inches, which yields a geometric concentration of 56:1. The construction of the IST concentrator is an inherently low-cost design, since it incorporates lightweight aluminum with maximum structural rigidity. The reflector material chosen for the FSEC installation was 3M aluminized film. Although the reflectivity of this film is lower relative to silver film (84% vs. 93%), the manufacturer recommended aluminum film for environmental reliability in Florida's climate.

A cross-section of the PV installation on the focal receiver assembly is shown in Figure 3. The PV cells are mounted in a single plane and are water cooled via jet-impingement on the back side of the mounting surface. Specially manufactured single-crystal silicon concentrator

PV cells was obtained from AstroPower Inc., Newark, DE. The nominal size of the cells was 10 x 5 cm. The PV cells are bonded to a square (3.8 cm x 3.8 cm) aluminum tube with a thermally conductive (relative to air) glass-filled epoxy adhesive (.2 mm thick).

Not shown in Figure 3 is the protective covering. First, the face of the cells is covered with optically clear silicone RTV potting compound; then the entire assembly is placed inside a heat-shrinkable Teflon tube.

Electrical connections from the cells to the copper bus bars are made with solder-coated copper ribbon (0.125 mm thick) soldered to the cell edges and the copper bus bars. Electrical isolation among components is achieved through the use of glass-filled epoxy adhesive.

Electrically, seven cells are connected in parallel, and four seven-cell strings are connected in series for a total of 28 cells. Because each cell is only 9.5 cm long, each parallel string is approximately 66.5 cm long. Series connections are created by reversing the polarity of the cells relative to the bus bars. Bonding and electrically connecting the PV cells proved to be a difficult, time-consuming task during construction of the receiver system.

Finally, a ½ inch (U.S. pipe size) PVC pipe is inserted inside the square aluminum tube for receiver cooling. Cooling water enters the PVC pipe and exits through a small hole opposite the back of the PV cell. The water then exits the aluminum tube at the other end of the receiver assembly. This design improves the convective heat transfer at the area of contact with the PV cells.

The system is designed such that a flow rate of 6 gallons per minute would yield a maximum cell temperature that is approximately 13°C above the water coolant temperature. The water used to cool the PV cells is itself cooled by an above-ground swimming pool. Aeration and passive evaporation/convection are the available cooling mechanisms. An emergency cooling system was also incorporated into the system design in case of power failure while the receiver is in focus. The back-up system is accomplished with a normally closed electromagnetic valve separating the city water supply and the PV cooling system. If electric power fails, this valve opens, allowing city water to circulate through the receiver tube for cooling.

The electrolyzer cells, shown in Figure 4, were supplied by The Electrolyzer Corporation Ltd., Toronto, Canada. These alkaline cells of unipolar design are rated at 250 amps and between 1.8 and 2 volts. Unipolar cell design was chosen as such cells are considered to perform better under transient electrical input than are bipolar cells. Make-up water for the electrolysis cells was obtained from a solar still and was processed by water treatment hardware shown in Figure 5.

The hydrogen and oxygen gases produced in the electrolyzer are transported to a water seal via 1.5″ black iron pipe. The water seal allows adjustment of back pressure on the electrolyzer while ensuring that no outside air enters the system during times of non-production, such as at night.

Data acquisition for the system consisted of a Campbell 21X system with the ability to record direct-normal insolation, 28.5° tilt insolation, water temperature in and out of the receivers, temperature of the PV cells, pool temperature, electrolyzer temperatures, current and voltage output of the PV array, current and voltage across the electrolyzer, and hydrogen output. The data acquisition system was designed to test six different receiver designs at a time. All weather conditions are also available from the on-site FSEC weather station (e.g., temperature, wind speed and direction, relative humidity, etc.).

3.1.3. Hydrogen Production Results

The system was continuously operated over the five-month period of July to December 1993, and data were segregated between the summer (July-September) and fall (October-December) seasons. Occasional system shutdowns occurred when the cooling water flow rate sensor became inoperable due to debris in the line. The system controller was programmed to monitor cooling water flow rate. The controller required a flow of 2 liters/minute or it would shut the system down to avoid overheating the receiver.

The most important parameter to be measured is the amount of hydrogen produced from a given amount of solar energy. Due to the complexity of accurately measuring gaseous quantities of hydrogen, the amount of current passing through the electrolyzer was used as the measure of hydrogen production.

Figure 6 shows the electrical current supplied to the electrolyzer as a function of the direct-normal solar flux at solar noon for both summer and fall conditions. The trend of the data for both seasons appears reasonably linear. Of particular interest, however, is the performance at high values of solar radiation. It appears that at around 800 W/m^2, the current deviates significantly from linear behavior. A possible reason for this deviation may be mismatch between the output of the PV system and the electrolyzer load.

Figure 6 also shows that the current output of the electrolyzer is slightly lower during fall than in summer. A possible reason for this deviation may be the lower electrolyzer efficiency caused by lower electrolyzer operating temperatures in the cooler fall season. These two situations will be further discussed in this section.

Further examination of Figure 6 shows that the maximum current supplied by the PV system during summer would be about 140 amps without load mismatch. This corresponds to about 20 amps per PV cell. Figure 7 shows the current/voltage (IV) curve for an individual AstroPower PV cell as measured by Sandia National Laboratories, Albuquerque, New Mexico. At an irradiance of 33 suns, the maximum current is 22 amps. Measurements with a reference cell showed the optical concentration ratio to be approximately 39:1 at solar noon. The geometric concentration ratio for the IST system is 56:1, which yields a system optical efficiency of approximately 70%. A direct-normal radiation of 800 W/m^2 will correspond to approximately 31 suns at the receiver. Thus, the system of 28 PV cells is responding very closely to the sum of the individual cells.

Further examination of Figure 7 also shows how poorly these cells perform. With a PV cell conversion efficiency of less than 6% under concentration, the total system performance cannot be expected to be exemplary. Figures 8 and 9 bear this out. These plots show the system conversion efficiency as a function of the solar time for a typical summer and fall day. The system conversion efficiency is defined as the higher heating value of the hydrogen produced (assuming a coulombic efficiency of 100%) divided by the available solar energy. The available solar energy is defined as the direct-normal pyreheliometer measurement corrected by projection into the plane of the local meridian. This is the component of the direct-normal radiation that a single-axis, north-south tracking system can use.

The overall system efficiency for July through December was 2.8% based on total direct-normal radiation and 1.8% based on total global radiation. Although these efficiencies seem extremely low at first glance, they do show that the mismatch losses between the PV cells, the PV array and the electrolyzer are very low when compared to the PV system and electrolyzer losses. The best instantaneous efficiency achieved was about 3.8% (based on direct-normal radiation).

Of particular interest is the system's behavior during fall, as shown in Figure 9, where efficiency decreases symmetrically about solar noon. A possible explanation for this behavior may be the mismatch between the PV system and the electrolyzer, and the fact the electrolyzer operating temperatures are much lower in fall than in summer. For higher values of solar flux, the IV curve of the PV cell is higher, requiring higher voltages to power the electrolyzer. The colder the electrolyzer, the higher this voltage requirement becomes. Figure 10 shows the electrolyzer temperature as a function of solar time for summer and fall conditions. As one would expect, the electrolyzer temperature is higher for a longer portion of the day in summer than in fall.

Figure 11 shows the electrolyzer efficiency as a function of current. For these calculations, Gibbs Free Energy, rather than the more common Helmholtz Energy, is used as the baseline. Gibbs uses the higher heating value of hydrogen based on 1.24 volts rather than 1.43 volts. If the higher Helmholtz voltage were used, overall system efficiency (solar to hydrogen) results could be misleading, since an efficiency of greater than 100% would be possible.

Although the PV cells used in this system were of low efficiency, the data taken have verified the design goals of the project. The system has shown that a relatively inexpensive concentrator system can be successfully employed in a direct-coupled PV electrolysis system with minimal losses. Both mismatch losses between PV cells and between the PV system and the electrolyzer were minimal, and the system operated relatively well under totally unattended operation.

To achieve acceptable conversion efficiencies, much higher efficiency PV cells must be used. Also, much higher electrolyzer efficiencies are possible using alkaline technology, if the cell temperatures are kept significantly above ambient temperature. The heated cooling water

from the concentrating PV system would be an excellent candidate for increasing the efficiency of the electrolyzer.

3.2 Cost of Hydrogen Produced from Photovoltaic Electrolysis

The efficiencies, costs and resulting performance of PV and electrolyzer systems for the present and for 10 years in the future were carefully evaluated in this task. The process updated work originally performed approximately five years ago and reported in Reference 3.

3.2.1 Photovoltaic Efficiencies, Power Output and Costs

The first step in evaluating photovoltaics output is to establish the cost and efficiencies of present and future photovoltaic modules. These PV costs and efficiencies were initially established using those published in the DOE Five-Year Research Plan for Photovoltaics [12]. These values were then modified by FSEC experience and other published data. They were also examined with respect to present materials and process costs, and achieved PV cell efficiency results. FSEC contacted major PV manufacturers and determined a quoted price of $4 per peak watt for the present cost of large-scale PV. For a module with an efficiency of 12%, a balance-of-system efficiency of 90% and a power efficiency of 95%, the ratio of the area to peak watts is 9.75 m^2/kW_p. Using $\$4/W_p$ as the module cost, the PV cost per m^2 is $410. The calculations assumed a cost of $\$400/m^2$.

Table I presents the efficiencies and costs that were selected for the calculations herein. The PV systems in Table I are presented as flat plate, flat-plate tracking, and concentrating, rather than in terms of cell materials or technology.

The 10-year future costs were also based on the DOE Research Plans for PV [12, 13] and on FSEC experience. These future values appear to be realistic. The following points were considered when establishing the values:

- Efficiencies greater than the module values assumed have already been achieved in laboratory cells [13]. Experience has shown that the timing between laboratory cell achievements and production cells realization lags by approximately 10 years.

- Future costs for modules (the largest cost factor) of thin-film cells are given as $\$51.45/m^2$ [14] and as $\$26.31/m^2$ [15]. These two values are both lower than the $\$250/m^2$ number assumed for the 10-year cost.

- All cell materials are common and are in plentiful supply. No problems of availability or escalating prices are anticipated [15].

- Balance-of-system and power conditioning efficiencies are already at the values expected in the late 1990s, and future expectations are excellent.

To predict performance of a PV system, specific sites must be designated to establish input values for solar insolation. This analysis required three insolation values: global at latitude tilt (fixed flat-plate), global normal (two-axis flat-plate tracking) and direct normal (concentrating two-axis tracking). Twenty regionally representative cities were selected, and Typical Meteorological Year (TMY) data for these cities were used to establish the site-specific insolation values [16]. TMY data represent the long-term climatic mean for a particular location.

For each of these 20 sites, insolation enhancement factors for latitude tilt, tracking and direct-normal PV arrays were calculated using the method developed by Liu and Jordan [17]. To produce representative insolation values, data from the 20 cities were then averaged to determine values for four U.S. regions -- southwest, south, middle and north. Table II presents the horizontal insolation data and the enhancement factors for the cities and for the four regional averages.

PV electricity costs were next computed using the efficiencies, cost values and lifetimes of Table I and the average insolation data of Table II. The economic assumptions made in the calculations were a discount rate of 6% and an energy escalation rate of 4%. Yearly PV operation and maintenance costs were taken for the present as $\$3/m^2$ per year. This value corresponds to a reported value of approximately \$0.01/kWh. Ten-year O&M values were based on the future DOE values [12].

The PV life-cycle costs were made by first calculating the PV power produced at a specific location (insolation times efficiencies). For example, the present-day flat-plate case fixed at

latitude for the desert Southwest will produce 252.8 kWh/m^2 · year, calculated by multiplying 5.83 kWh/m^2 · day x 0.12 x 0.90 x 1.10 x 365 days/year. The life-cycle cost calculations for the equipment were made by equating the present value of the PV equipment (module cost plus balance-of-system cost) and operating cost (discounted to present value) to the power produced times the cost of power (inflated at the energy escalation rate). This calculation gives a dc life-cycle cost of $0.15/kWh for the present-day flat-plate Southwest example.

Results of the PV electricity cost calculations for dc electricity are presented in Table III. These results show that present PV-produced dc electricity costs $0.14 to $0.36/kWh, and that $0.06 to $0.09/kWh is achievable in 10 years. PV system costs are $500 to $800/$m^2$ ($46 to $74/ft^2$) for the present, and $325 to $565/m ^{2}($30 to $53/ft) in a 10-year period. The variance between types of PV systems is slight, with flat-plate tracking producing slightly lower values.

Although not presented, the cost of PV-produced ac electricity (which requires use of an inverter) increased the dc electricity cost by $0.01 to 0.015/kWh for the present day, and $0.003 to 0.007/kWh for the 10-year case. Thus, power conditioning costs are minimal.

3.2.2 Electrolyzer Performance and Gaseous Hydrogen Production

Calculating representative present and future values for the efficiencies and costs of an electrolyzer was the next objective of this analysis. Personal communication [18] indicated that present-day ac electrolyzers have a conversion efficiency of 60% and that a commercial unit's initial cost is $780 per gaseous hydrogen (H_2) production unit of 1000 Nm^3/year. It was assumed that the elimination of the need for ac-to-dc conversion equipment in the electrolyzer would reduce the initial cost by 30%. The resulting cost would be $550 for 1000 Nm^3/year. In 10 years, the electrolyzer efficiencies were assumed to increase to 70%, with the initial costs remaining the same as present values.

Calculations of gaseous hydrogen production by PV electrolysis were performed by assuming that a constant value of 1000 Nm^3/year of H_2 would be produced. These calculations used the PV-produced dc electricity cost results. The other electrolyzer parameters used were lifetimes of 20 and 25 years, and yearly operation and maintenance costs of 10% and 7.5% of the initial cost. These electrolyzer values are presented in the bottom of Table I.

Table IV shows the flat-plate PV array area necessary to produce 1000 Nm^3/year. As expected, the desert Southwest requires the smallest PV array. Note that the reductions in size from the present to the 10-year values are due to increases in system efficiencies. PV array sizes for other H_2 production rates may be scaled linearly from Table IV.

The main parameter of interest is the cost of gaseous H_2. These costs were calculated in terms of $/MMBtu, and the results are presented in Table V. The values of Table V are obtained by calculating the cost per year to produce the specified amount of hydrogen from the PV electricity costs of Table III plus the yearly cost of the electrolyzer equipment using a 6% discount rate and the electrolyzer lifetimes.

For clarity, an example calculation for the present-day flat-plate desert Southwest case follows. The cost of gaseous H_2 is the electricity (kWh) needed to produce the H_2 times the dc electricity price of Table III, with the result converted to MMBtu, or

$$H_2\ (\$/MMBtu) = 1 \times 10^6/0.60 \times kWh/3413\ Btu \times \$0.155/kWh = \$76/MMBtu \qquad (1)$$

The annualized equipment cost is the initial cost annualized over the lifetime plus the yearly operation and maintenance cost. The initial cost of the electrolyzer for a 1000 Nm^3/year production is $565. For a 20-year lifetime at a 6% discount rate, the annual cost of the electrolyzer is $56. The operation and maintenance cost is 10% of initial cost, or $56. The total equipment cost is then $112 for a 1000 Nm^3/year production, which is $9.10/MMBtu.

The total H_2 cost is $76 for electricity plus $9.10 for equipment or $85/MMBtu. This calculation shows that the electrolysis equipment cost is 11% of the total H_2 cost. The last line of Table V presents the H_2 cost using conventionally produced electricity at $0.05/kWh and the present-day electrolyzer initial cost of $780/1000 Nm^3/year.

The results for the cost of gaseous H_2 show present day prices of $76 to $99/MMBtu for the desert Southwest and prices of $127 to $185/MMBtu for the northern U.S. The cost of hydrogen for conventional $0.05/kWh electricity is $34/MMBTU. Thus, present PV-produced hydrogen costs for the desert Southwest are approximately 2.5 times those of hydrogen produced with conventional electricity. Gaseous hydrogen for future PV costs were $34 to $46/MMBtu for the desert Southwest and $55 to $82/MMBtu for the northern U.S. These

results show that PV-produced hydrogen costs in 10 years can be as little as 20% more than the cost of hydrogen produced with conventional electricity at $0.05/kWh. All calculations show flat-plate tracking to be the minimum cost option.

4.0 CONCLUSIONS

This project has demonstrated the ability to coordinate the efforts of two state agencies and two federal funding agencies and to produce successful results.

A hydrogen production facility utilizing a parabolic trough, concentrating-photovoltaic electrolysis system was designed, constructed and operated by the Florida Solar Energy Center. The project began in 1990, and the six-month operational period occurred in summer and fall of 1993. The data have been segregated between the summer (July-September) and fall (October-December) seasons. The major components of the hydrogen production system are the parabolic trough concentrator, the photovoltaic receiver assembly, the cooling system and the electrolyzer cells.

The overall system efficiency for the time period of July through December was 2.8% based on total direct-normal radiation and 1.8% based on total global radiation. Although these efficiencies seem extremely low at first glance, they do show that the mismatch losses between the PV cells, the PV array and the electrolyzer are very low when compared to PV system and electrolyzer losses. The best instantaneous efficiency achieved was about 3.8% (based on direct-normal radiation).

The data taken have verified the design goals of the project, and the system has shown that a relatively inexpensive concentrator system can be successfully employed in a direct-coupled PV-electrolysis system with minimal losses. Both mismatch losses between PV cells and between PV and electrolyzer were minimal, and the system operated relatively well under totally unattended operation.

To achieve acceptable conversion efficiencies, much higher efficiency PV cells must be used. Also, much higher electrolyzer efficiencies are possible using alkaline cell technology if the cell temperatures are kept significantly above ambient temperature. Water heated by cooling

of the concentrating PV would be an excellent candidate to increase the efficiency of the electrolyzer.

The costs of gaseous hydrogen from PV electrolyzer systems for the present and for 10 years in the future were carefully evaluated in the second investigation. Results of the PV electricity cost calculations for dc electricity show that present PV-produced dc electricity costs $0.14 to $0.36/kWh, depending upon the U.S. location, and that $0.06 to $0.09/kWh is achievable in 10 years. PV system costs are $500 to $800/$m^2$ ($46 to $74/$ft^2$) for the present, and $325 to $565/$m^2$ ($30 to $53/$ft^2$) in a 10-year period. The variance between types of PV systems is slight, with flat-plate tracking producing slightly lower values.

The costs of PV-produced hydrogen for the present day vary between $76 to $185/MMBtu. For the desert Southwest, these costs are approximately 2.5 times those of hydrogen produced with conventional electricity at $0.05/kWh. Results also show that PV-produced hydrogen costs in 10 years can be as little as 20% more than the cost of hydrogen produced with conventional electricity at $0.05/kWh.

5.0 ACKNOWLEDGMENTS

Special acknowledgment for the concentrating PV electrolysis part of this report is given to Dr. Kirk Collier, who designed and analyzed the production system and who was the project manager for the activities associated with the concentrating PV electrolysis system. Special acknowledgment is also given to the Florida Energy Office, which supplied the funds to purchase and construct the PV-electrolysis system.

6.0 REFERENCES

1. Collier, K., "Production of Hydrogen by Photovoltaic-Powered Electrolysis," FSEC-CR-485-92, Florida Solar Energy Center, 1992.

2. Collier, K., and R. Anderson, "System Performance of a Photovoltaic-Powered Water Electrolysis System," *Proceedings of 10th World Hydrogen Energy Conference*, June 1994.

3. Block, D., and I. Melody, "Efficiency and Cost Goals for Photoenhanced Hydrogen Production Processes," *Int. J. Hydrogen Energy*, Vol. 17, No. 11, pp. 853-861, 1992.

4. Personal communication with Dr. Alexander Stuart of The Electrolyzer Corporation, October 16, 1995.

5. Personal communication with Mr. James Heffel of the Center for Environmental Research and Technology at the University of California at Riverside, November 15, 1995.

6. Garcia-Conde, A. G., and F. Rosa, "Solar Hydrogen Production: A Spanish Experience," *Int. J. Hydrogen Energy*, Vol. 18, No. 12 pp. 995-1000, 1993.

7. Kauranen, P. S., P. D. Lund and P. VanHanen, "Control of Battery-Backed Photovoltaic Hydrogen Production," *Int. J. Hydrogen Energy*, Vol. 18, No. 5, pp. 383-390, 1993.

8. Lehman, P. A., and C. E. Chamberlin, "Design of a Photovoltaic-Hydrogen-Fuel Cell Energy System," Int. J. Hydrogen Energy, Vol. 16, No. 5, pp. 349-352, 1991.

9. Hamilton, H. C., et al., "Design and Operation of the Solarex Two-Axis Tracking Linear Concentrating Collector System," Fourteenth IEEE Photovoltaic Conference, pp. 777-782, 1980.

10. Giuffrida, M., et al., "Parabolic Troughs Concentrators Photovoltaic Module," Fourteenth IEEE Photovoltaics Conference, pp. 749-753, 1980.

11. Kaplan, S. I., and C. M. Benson, "Experience With a Grid-Interactive Solar Photovoltaic Electric System," Fifteenth IEEE Photovoltaics Conference, pp. 90-91, 1981.

12. "Five-Year Research Plan, 1987-1991," Photovoltaic Energy Technologies Division, U.S. Department of Energy, DOE/CH 10093-7.

13. Photovoltaics Program Overview - Fiscal Year 1992, National Photovoltaics Program Plan, U.S. Department of Energy, DOE/CH100 93-190.

14. Maycock, Paul, "Carlson Describes Possible $.50/Watt Amorphous Silicon Production," *PV News*, March 1989.

15. Corsi, J., "Delivering Clean Energy Goods: Industry Ability to Respond to Market Acceleration Policies," Presented at Forum on Renewable Energy and Climate Change, Washington, DC, June 14, 1989.

16. "Typical Meteorological Year, Hourly Solar Radiation - Surface Meteorological Observations," National Climatic Center, Asheville, NC.

17. Beckman, W. A., S. A. Klein and J. A. Duffie, "Solar Heating Design by the F-Chart Method," John Wiley & Sons, Inc., 1977.

18. Personal communication with Mr. William Kincaide, of Teledyne Energy Systems, May 4, 1989.

TABLE I: PHOTOVOLTAIC EFFICIENCIES AND COSTS USED IN THE SYSTEMS ANALYSIS

PV Systems	Present Day	Ten Years
A. Flat Plate		
Module efficiency	12%	15%
Balance-of-system efficiency	90%	91%
Power conditioner efficiency	95%	96%
Module cost	$\$400/m^2$	$\$250/m^2$
Balance-of-system cost	$\$100/m^2$	$\$ 75/m^2$
Power-related cost	\$400/kW	\$250/kW
Operation and maintenance cost/yr.	$\$3/m^2$	$\$2/m^2$
Lifetime (years)	20	25
B. Flat-Plate Tracking		
Module efficiency Balance-of-system efficiency Power conditioner efficiency Module cost Balance-of-system cost	All values are the same as flat plate values.	
Power-related cost		
Tracking cost	$\$100/m^2$	$\$75/m^2$
Operation and maintenance cost/yr.	$\$3.75/m^2$	$\$2.50/m^2$
Lifetime (years)	20	25
C. Concentrators		
Module efficiency	18%	21%
Balance-of-system efficiency	90%	91%
Power conditioner efficiency	95%	96%
Optical efficiency of concentrator	90%	90%
Concentrator module cost	$\$600/m^2$	$\$400/m^2$
Balance-of-system cost	$\$100/m^2$	$\$ 90/m^2$
Power-related cost	\$400/kW	\$250/kW
Tracking cost	$\$100/m^2$	$\$ 75/m^2$
Operation and maintenance cost/yr.	$\$3.75/m^2$	$\$2.50/m^2$
Lifetime (years)	15	20
D. Electrolyzer		
Efficiency	60%	70%
O&M cost as percent of initial cost	10%	7.5%
Lifetime (years)	20	25

TABLE II: SITE INSOLATION DATA AND AVERAGE VALUES

Cities	Daily Horizontal Insolation kWh/m^2(Btu/ft^2)	Latitude (Degrees)	Global Cloudiness Index KT	Insolation Enhancement* for Fixed at Latitude Tilt and South Facing	Insolation Enhancement* for Two-Axis Tracking	Insolation Enhancement* for Two-Axis Direct Normal Tracking
Albuquerque, NM	5.80 (1840)	35.10	0.70	1.12	1.51	1.33
Daggett, CA	5.82 (1846)	34.87	0.70	1.09	1.47	1.30
Las Vegas, NV	5.93 (1882)	36.10	0.73	1.12	1.53	1.36
Phoenix, AZ	5.90 (1873)	33.40	0.70	1.09	1.46	1.28
Prescott, AZ	5.72 (1816)	34.65	0.69	1.10	1.52	1.33
DESERT SOUTHWEST AVERAGE:	5.83 (1851)	34.83	0.70	1.10	1.50	1.32
Dallas, TX	4.64 (1472)	32.83	0.55	1.08	1.39	1.14
Honolulu, HI	5.18 (1643)	21.30	0.56	1.02	1.25	0.96
Miami, FL	4.72 (1498)	25.80	0.52	1.05	1.29	0.98
Orlando, FL	4.66 (1477)	28.50	0.53	1.05	1.30	0.98
San Diego, CA	5.02 (1593)	32.40	0.59	1.09	1.36	1.12
SOUTHERN U.S. AVERAGE:	4.85 (1537)	28.17	0.55	1.06	1.32	1.04
Atlanta, GA	4.30 (1363)	33.70	0.51	1.07	1.35	1.06
Baltimore, MD	3.89 (1235)	39.20	0.49	1.09	1.38	1.08
Charleston, WV	3.55 (1126)	38.37	0.45	1.06	1.30	0.96
St. Louis, MO	4.21 (1335)	38.70	0.53	1.09	1.41	1.14
Washington, DC	3.83 (1215)	38.90	0.48	1.09	1.38	1.08
MIDDLE U.S. AVERAGE:	3.95 (1254)	37.77	0.49	1.08	1.36	1.06
Boston, MA	3.47 (1101)	42.40	0.46	1.09	1.42	1.13
Chicago, IL	3.83 (1215)	41.78	0.49	1.10	1.42	1.14
Minneapolis, MN	3.69 (1170)	44.90	0.51	1.13	1.48	1.21
Portland, OR	3.40 (1078)	45.60	0.47	1.05	1.36	1.05
Seattle, WA	3.25 (1032)	47.50	0.46	1.06	1.39	1.09
NORTHERN U.S. AVERAGE:	3.53 (1119)	44.44	0.48	1.09	1.41	1.12

*All insolation enhancement values are with respect to the horizontal insolation.

TABLE III: PHOTOVOLTAIC DC SYSTEM AND ELECTRICITY COSTS

PV Systems	Present	Ten Years
A. Flat Plate		
System Cost		
$/m^2 ($/ft^2)	500 (46)	325 (30)
$/kW$_p$	4870	2480
Electricity Cost		
Desert Southwest	$ 0.15/kWh	$ 0.07/kWh
Southern U.S.	0.19	0.09
Middle U.S.	0.23	0.11
Northern U.S.	0.26	0.12
B. Flat-Plate Tracking		
System Cost		
$/m^2 ($/ft^2)	600 (56)	400 (37)
$/kW$_p$	5850	3050
Electricity Cost		
Desert Southwest	$ 0.14/kWh	$ 0.06/kWh
Southern U.S.	0.19	0.09
Middle U.S.	0.22	0.10
Northern U.S.	0.24	0.11
C. Concentrating		
System Cost		
$/m^2 ($/ft^2)	800 (74)	565 (53)
$/kW$_p$	5776	3422
Electricity Cost		
Desert Southwest	$ 0.18/kWh	$ 0.09/kWh
Southern U.S.	0.28	0.14
Middle U.S.	0.34	0.17
Northern U.S.	0.36	0.18

TABLE IV: FLAT-PLATE NONTRACKING PV ARRAY SIZE TO PRODUCE 1000 Nm^3/YEAR

Location	Present	Ten Years
Desert Southwest	2.23 kW_p	1.93 kW_p
Southern U.S.	2.80	2.43
Middle U.S.	3.36	2.91
Northern U.S.	3.74	3.24

TABLE V: COST OF GASEOUS HYDROGEN USING PV-ELECTROLYSIS

PV Systems	Present	Ten Years
A. Flat Plate		
System Cost - $/$m^2$ ($/$ft^2$)	500(46)	325 (30)
H_2 Cost ($/MMBtu)		
Desert Southwest	85	37
Southern U.S.	104	45
Middle U.S.	123	52
Northern U.S.	136	57
B. Flat-Plate Tracking		
System Cost - $/$m^2$ ($/$ft^2$)	600 (56)	400(37)
H_2 Cost ($/MMBtu)		
Desert Southwest	76	34
Southern U.S.	101	44
Middle U.S.	118	51
Northern U.S.	127	55
C. Concentrating		
System Cost - $/$m^2$ ($/$ft^2$)	800 (74)	565 (53)
H_2 Cost ($/MMBtu)		
Desert Southwest	99	46
Southern U.S.	147	66
Middle U.S.	174	78
Northern U.S.	185	82
D. Electricity at $0.05/kWh		
H_2 Cost ($/MMBtu)	34	29

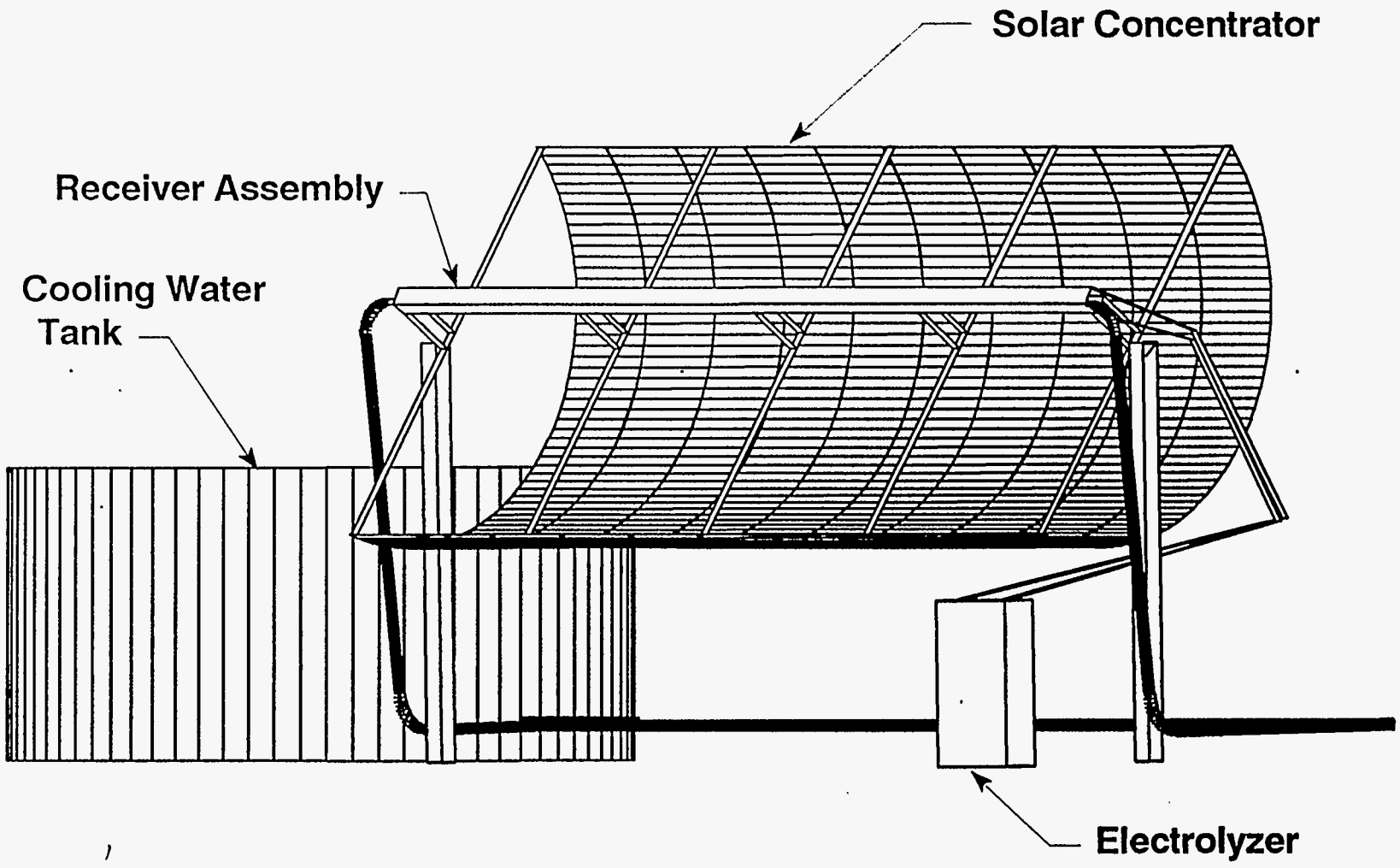

Fig. 1. PV-electrolyzer system.

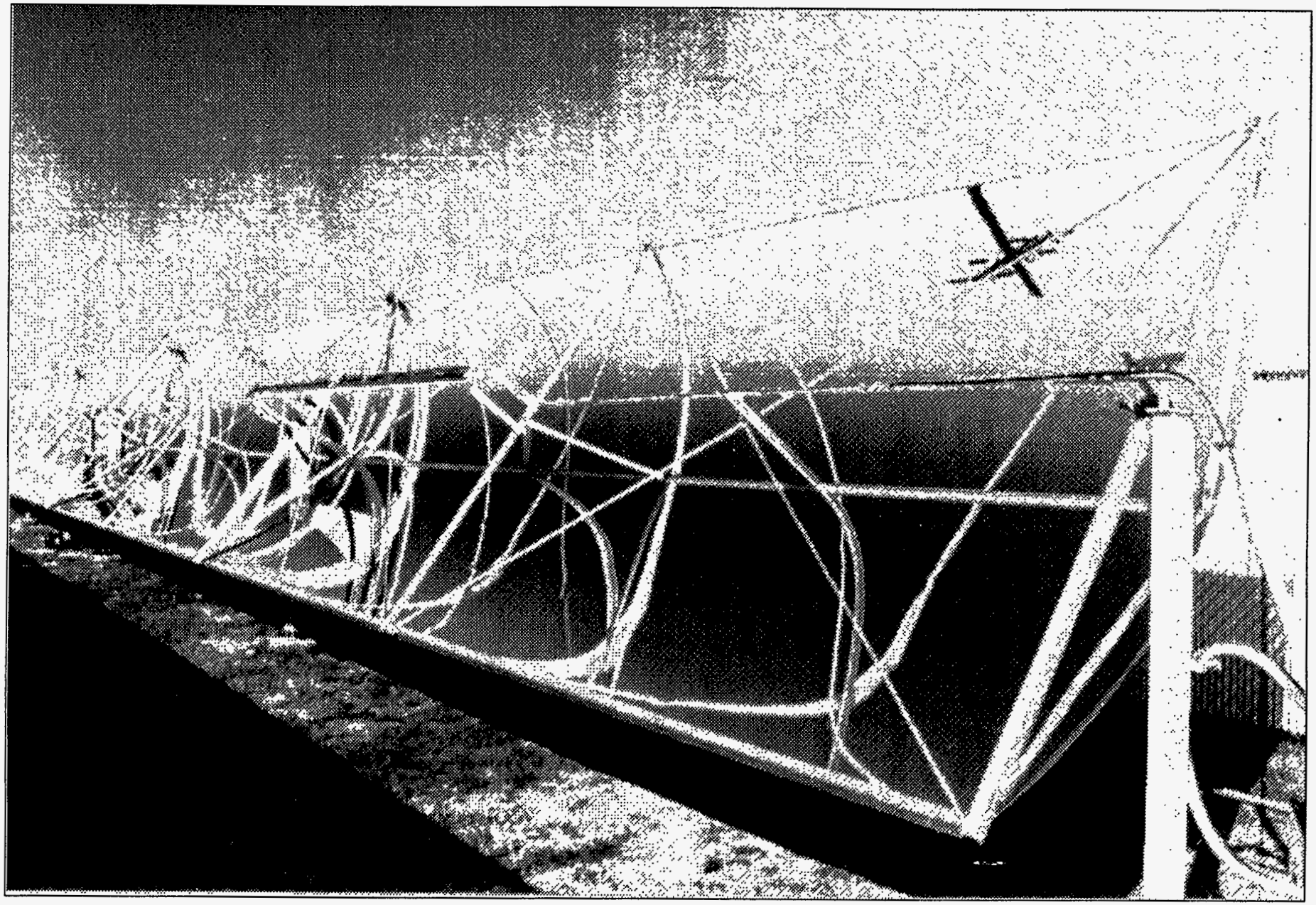

Fig. 2. IST collector system.

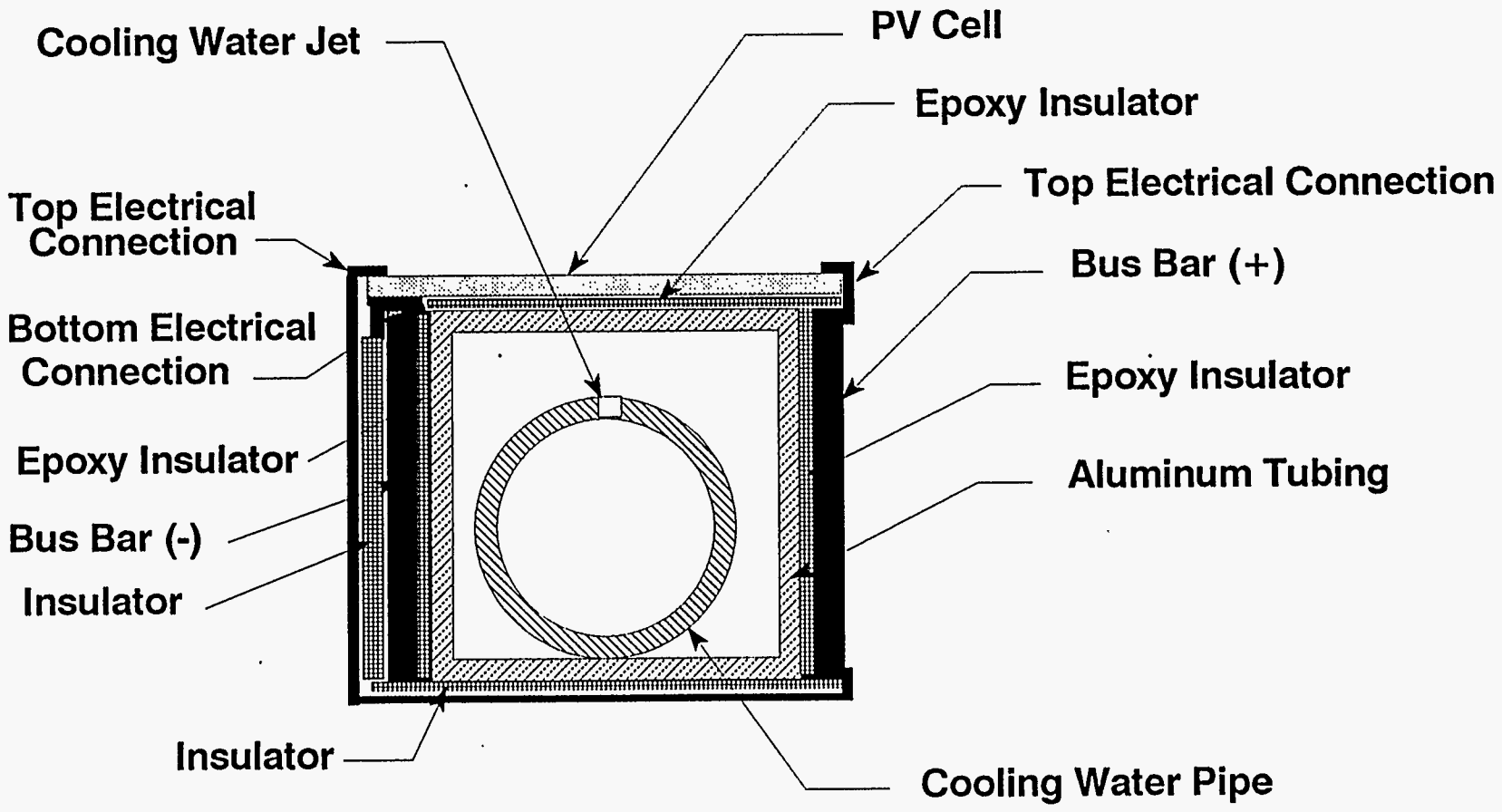

Fig. 3. Collector receiver assembly cross-section.

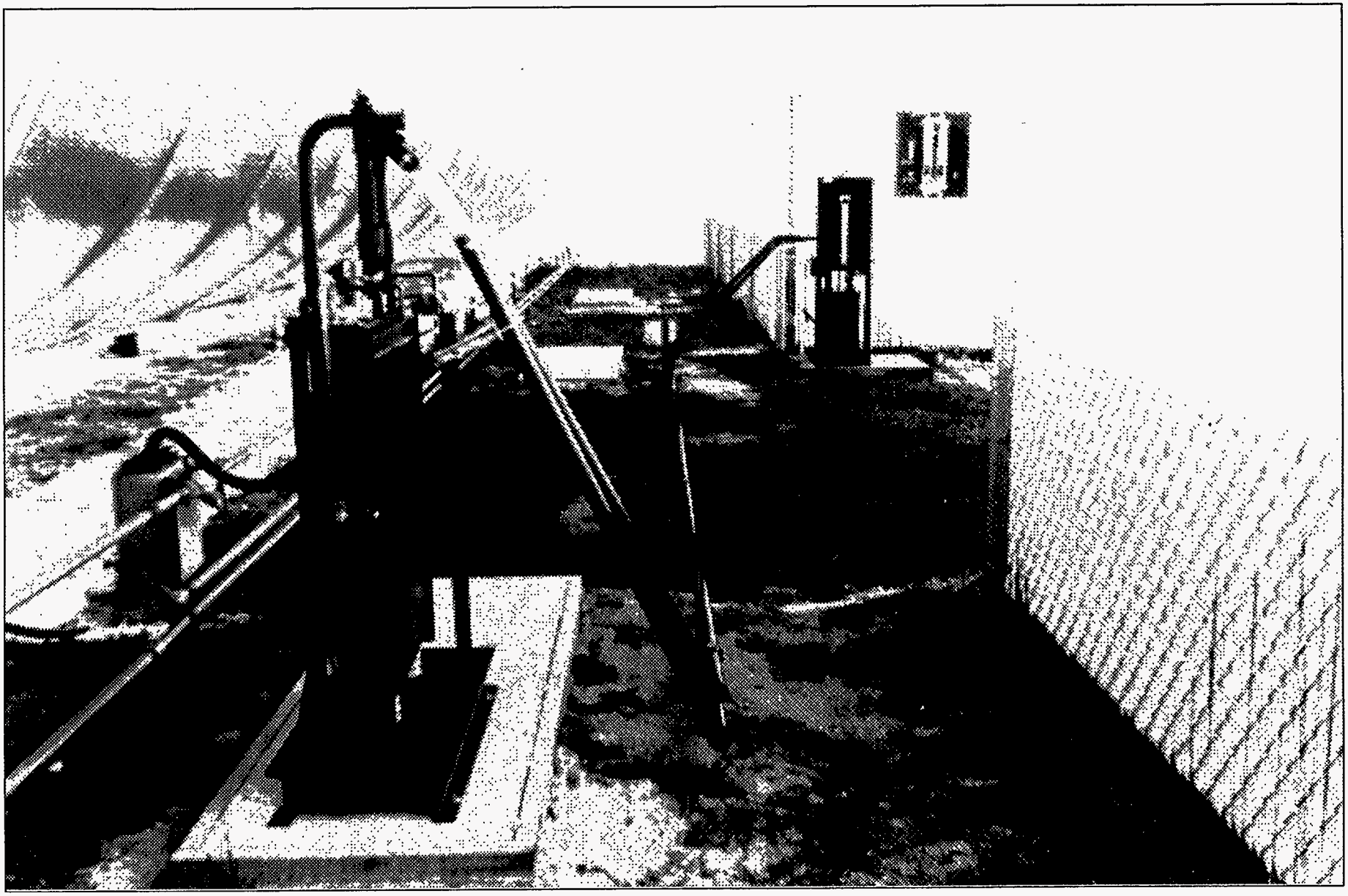

Fig. 4. Single-cell electrolyzer manufactured by The Electrolyzer Corp., Ltd.

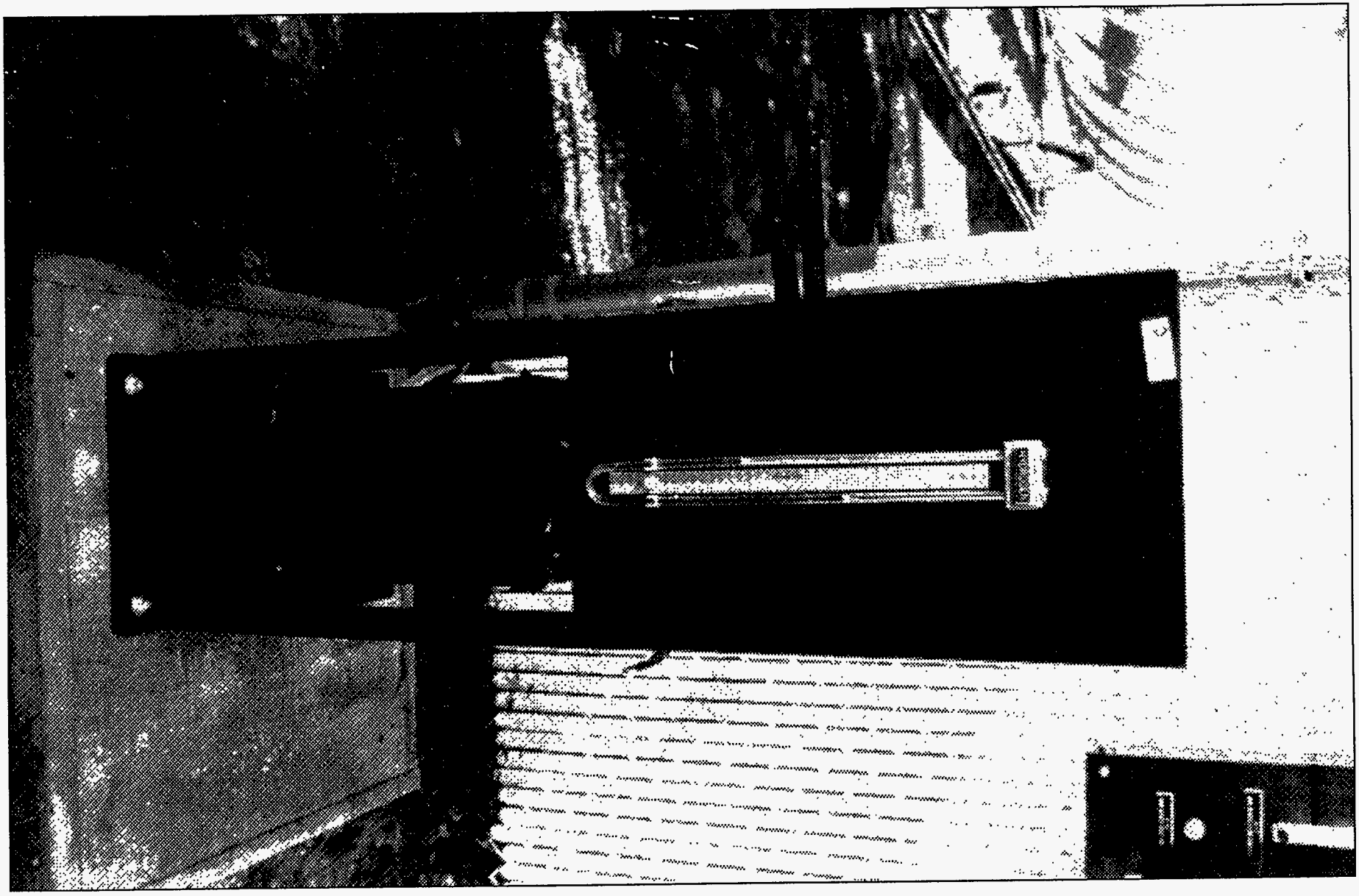

Fig. 5. Make-up water treatment hardware.

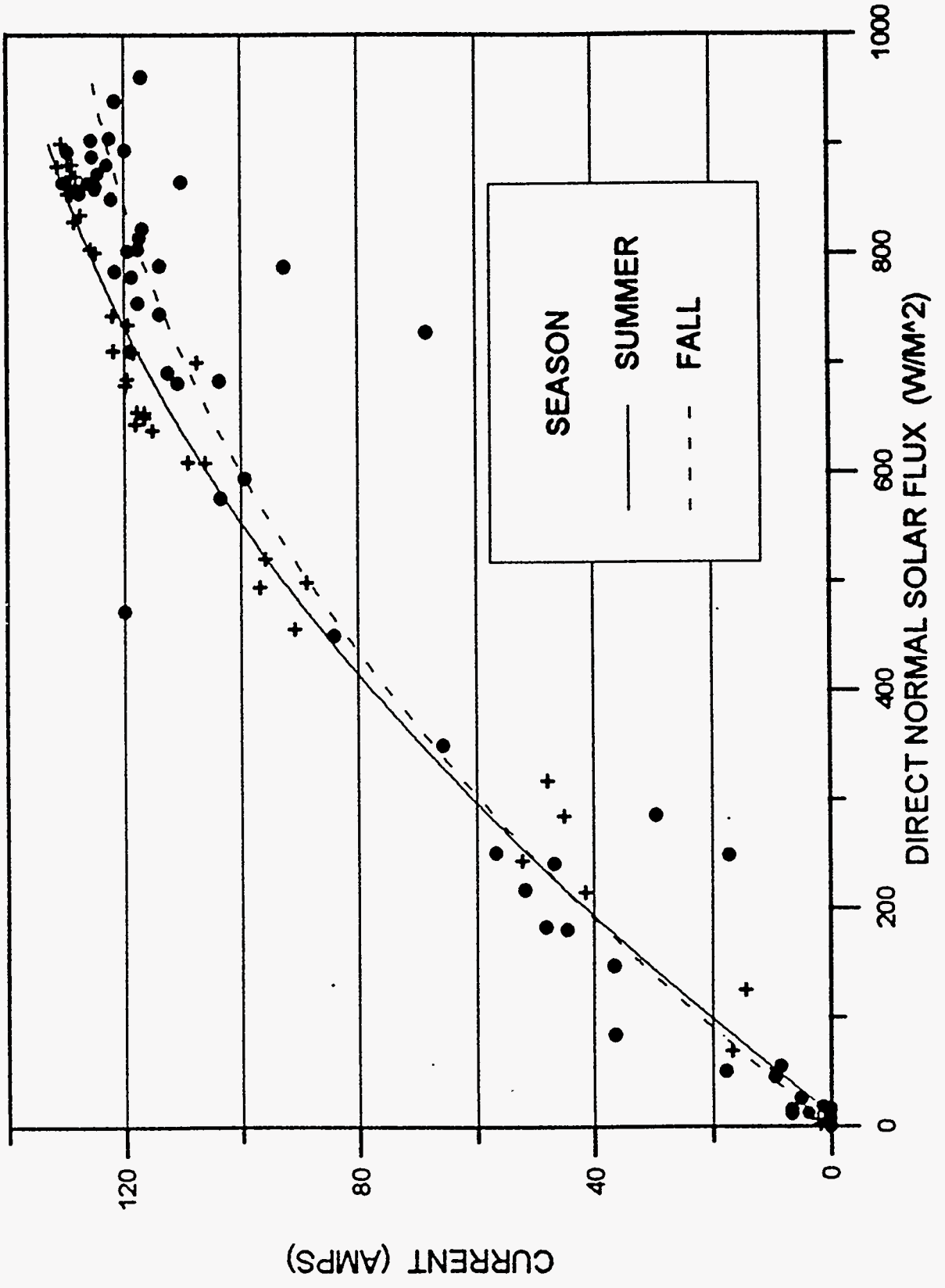

Fig. 6. Seasonal system performance.

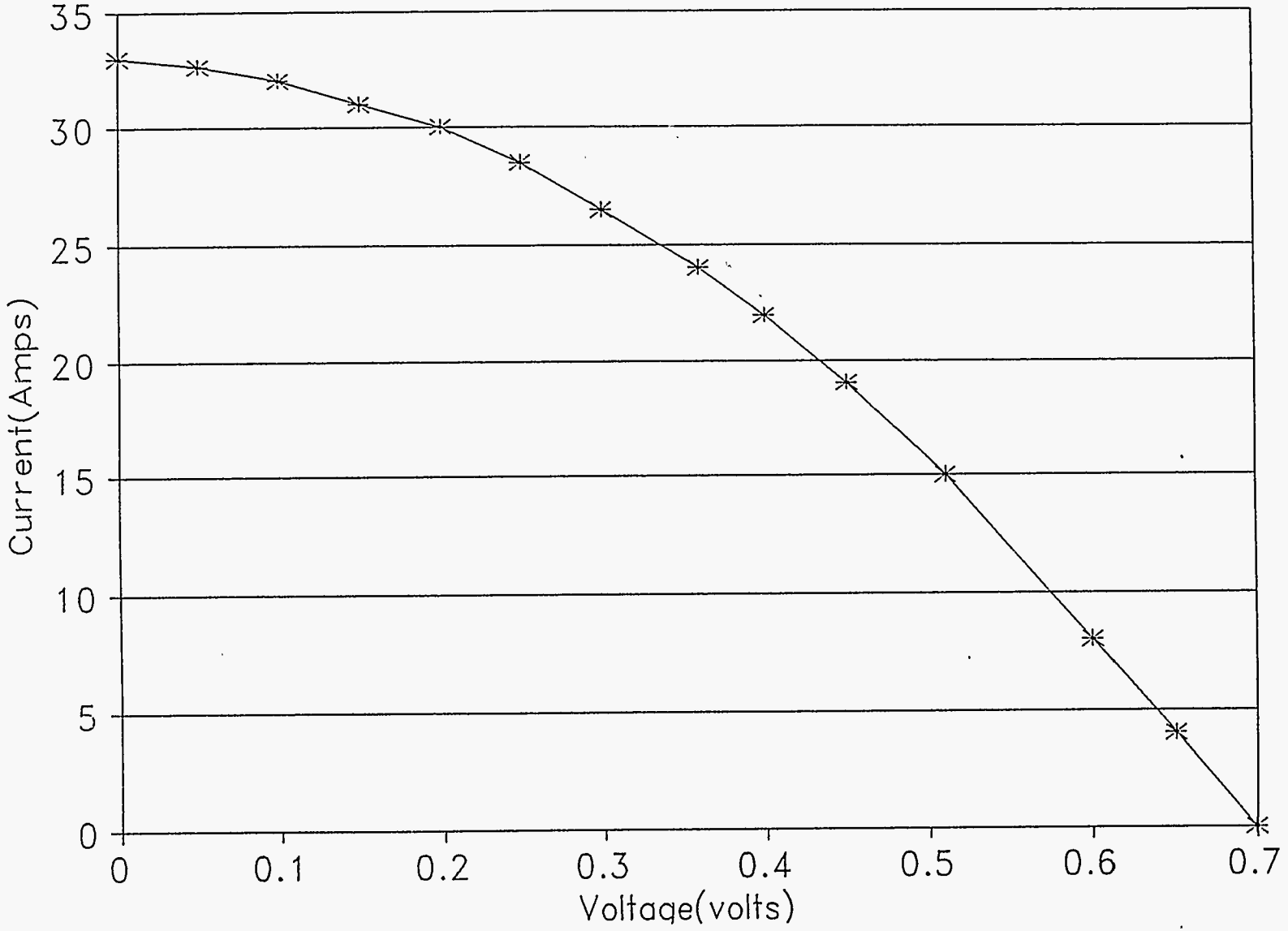

Fig. 7. Electrical characteristics of AstroPower cell.

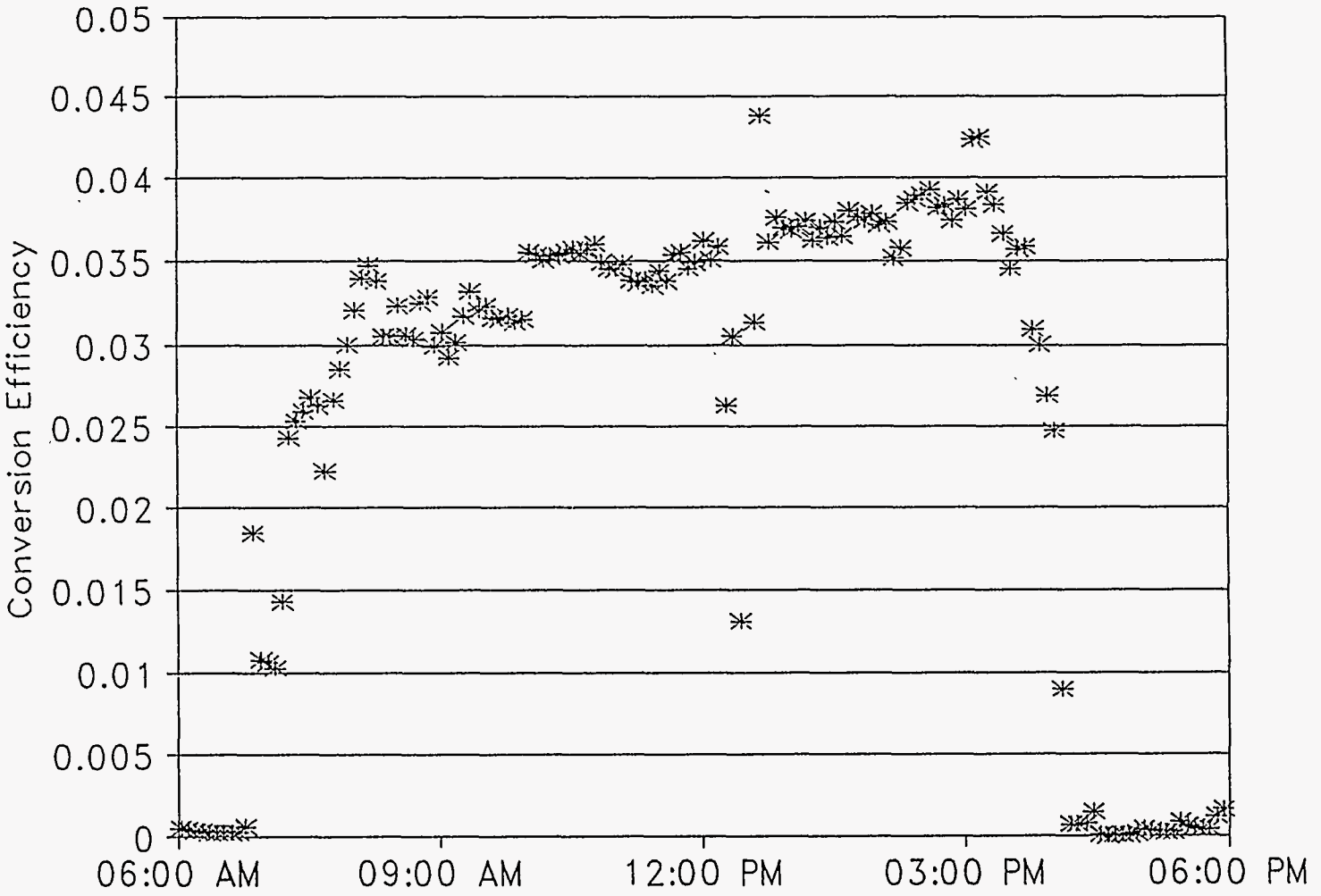

Fig. 8. Conversion efficiency for typical summer day.

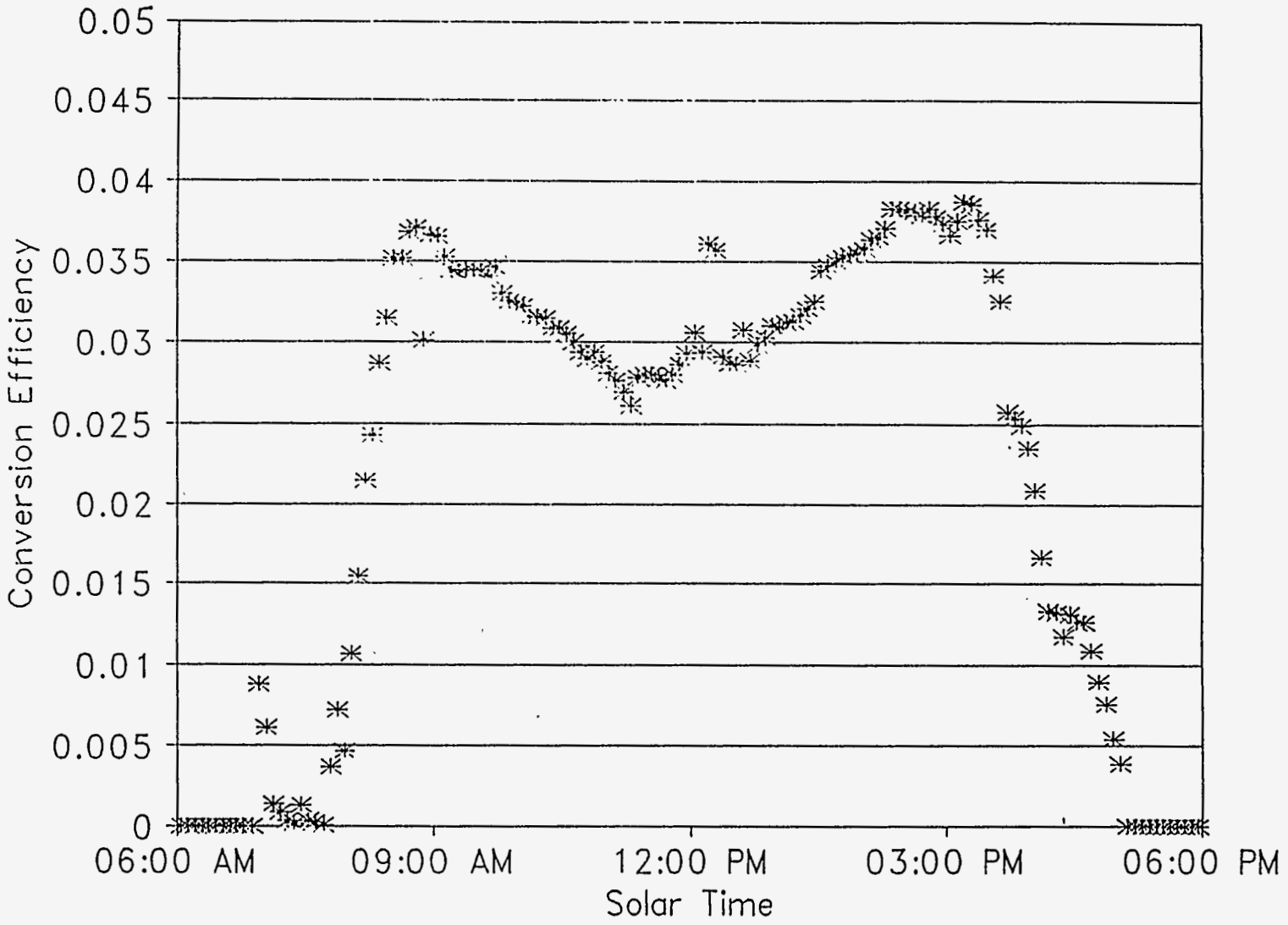

Fig. 9. Conversion efficiency for typical fall day.

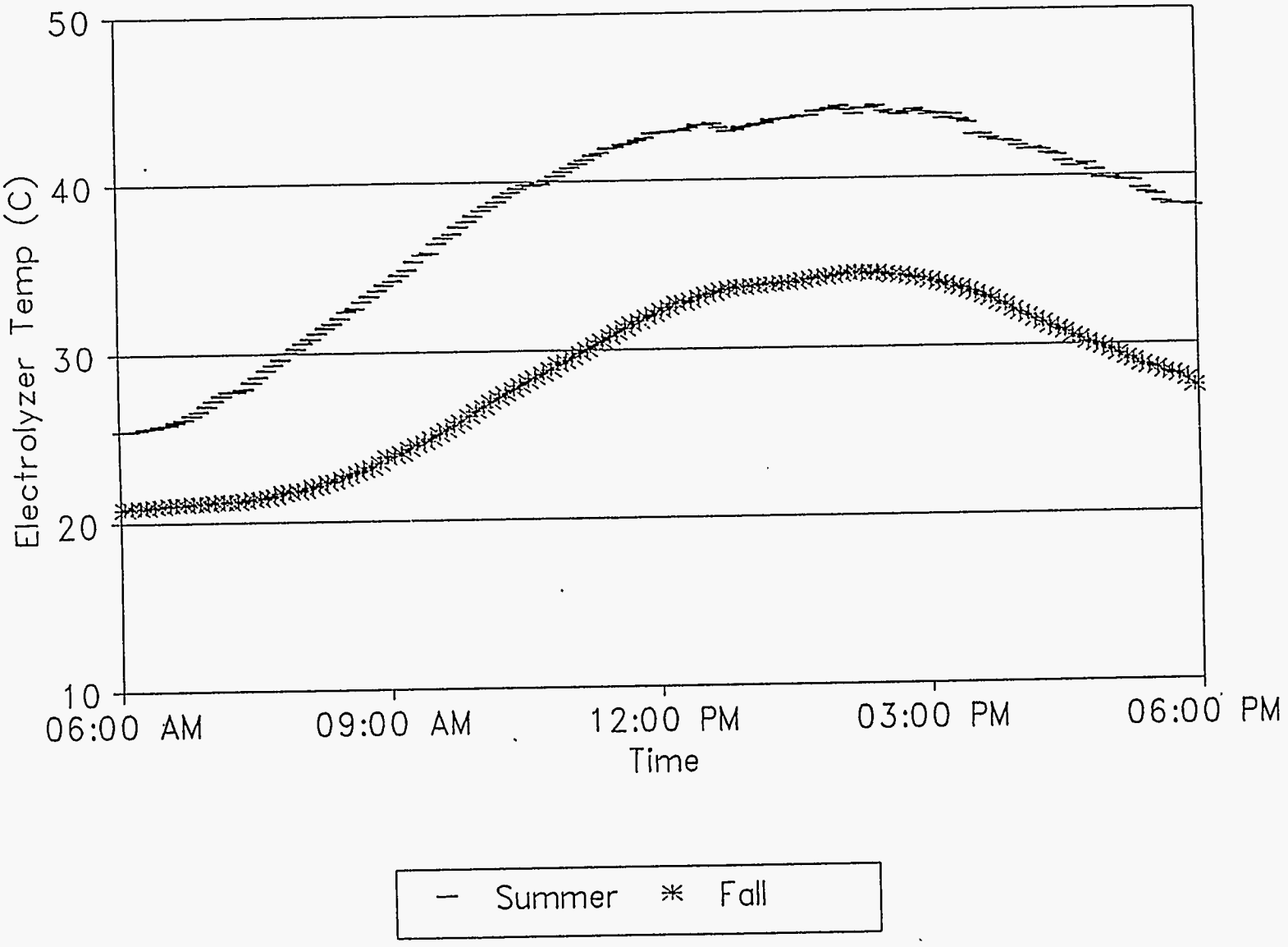

Fig. 10. Electrolyzer temperature vs. time of day.

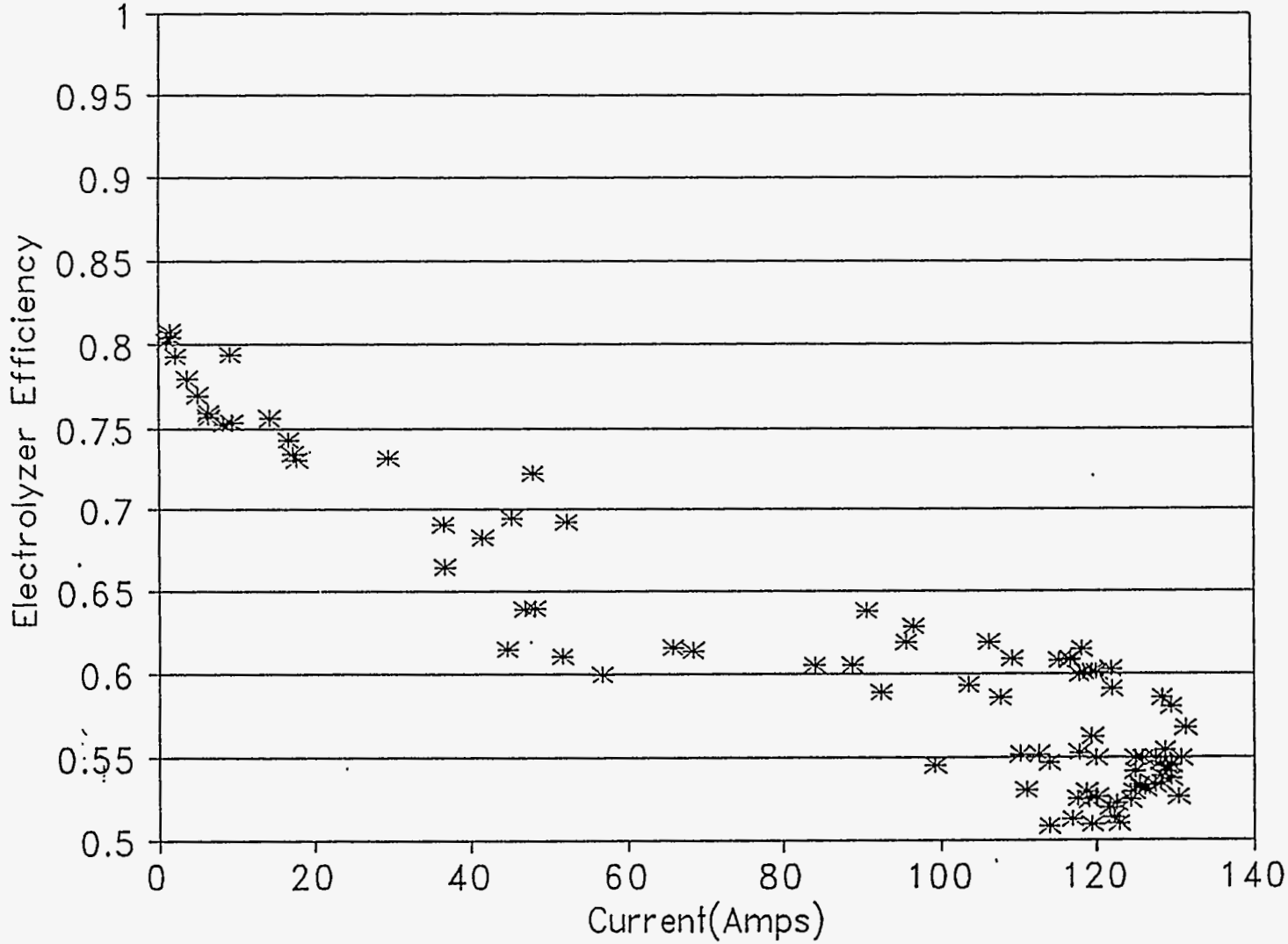

Fig. 11. Electrolyzer efficiency.

Task 2 Report

Solar Photocatalytic Hydrogen Production from Water Using a Dual Bed Photosystem

Annual Report

FSEC-CR-857-95
DOE Contract #DE-FG04-94AL85802
December 1995

Submitted to:
Neil Rossmeissl
Advanced Utility Concepts Division
Department of Energy
Washington, DC 20585

Submitted by:
Dr. Clovis A. Linkous
G. Thomas Mckaige
Darlene K. Slaterry
Anthony J.A. Ouellette
Beverly C.N. Austin

Florida Solar Energy Center
University of Central Florida
1679 Clearlake Road
Cocoa, Florida 32922-5703

SOLAR PHOTOCATALYTIC H_2 PRODUCTION FROM WATER USING A DUAL BED PHOTOSYSTEM

Dr. Clovis A. Linkous
G. Thomas McKaige
Darlene K. Slattery
Anthony J.A. Ouellette
Beverly C.N. Austin

Florida Solar Energy Center
University of Central Florida
1679 Clearlake Road
Cocoa, FL 32922-5703

1.0 SUMMARY

This work is an investigation into the use of photocatalytic particles in a dual bed configuration, so as to effect the solar-driven decomposition of water to its constituent elements, particularly hydrogen. The system envisioned would consist of two modules, each consisting of a shallow, flat, sealed container, in which micron-sized photocatalytic particles are immobilized. An aqueous solution containing a redox mediator is pumped between the two chambers. Different photoparticles and catalysts are chosen for their respective modules so as to effect oxidative water-splitting in one vessel to evolve oxygen gas, and reductive water-splitting in the other to evolve hydrogen. This is a direct photoconversion scheme that breaks down the energetic requirement for water decomposition into a 2-photon process, and enables separate production of hydrogen and oxygen.

Titanium dioxide, TiO_2, and indium phosphide, InP, were employed as photoparticles in the O_2- and H_2-evolving beds, respectively. Platinum catalysts were evaluated to promote H_2- evolution. Calculations on the energy band structure of free and immobilized particles provided guidance as to how the microstructure of the particles should be configured. A series of redox mediators, spanning a range of redox potentials, were tested. While many electron donors facilitated H_2-evolution, only the most oxidizing ones enabled O_2- evolution. A single redox couple, capable of charge exchange in both modules, is desirable to avoid system design complexity.

2.0 INTRODUCTION

In 1972 Fujishima and Honda pointed out that irradiation of wide band gap semiconductors such as TiO_2 could supply much of the energy required to electrolytically decompose water, evolving O_2 and generating protons that could be reduced at a dark electrode to produce hydrogen. This introduced photoelectrochemistry as a new approach to solar energy conversion.

Various problems arose as work progressed. One, the original wide band gap semiconductors, such as TiO_2 and SnO_2, required light energy well into the ultraviolet, making poor utilization of the solar spectrum; two, only highly crystalline, highly pure semiconductor specimens gave large photocurrents and quantum efficiencies, because of the limited lifetimes of the photogenerated charge carriers in the solid state; and three, semiconductors whose band gaps were better matched to the solar spectrum were subject to photoanodic corrosion, where the photogenerated hole could decay by dissolving a surface metal atom into the electrolyte.

It was also realized that the classic electrochemical configuration of two planar electrodes standing parallel to one another did not lend itself well to efficient use of the incoming solar photons. One either had to use an optically transparent counter electrode so that light could pass through it and the electrolyte to reach the semiconductor electrode, or deposit a thin film of semiconductor on glass and irradiate from the backside.

Since the essential feature of photoelectrochemical energy conversion was development of a barrier voltage at the semiconductor/electrolyte interface, it was realized that this could just as well be accomplished with the semiconductor in powder form. Conceptually this was a much simpler way to perform solar photoelectrolysis: just pour the semiconductor powder into water, expose the system to light, and H_2 and O_2 would bubble out.

New problems arose, however. The main one was separation of products. In an electrochemical cell, chemistry is performed by the occurrence of two half-cell reactions, each reaction proceeding at its own respective electrode. In the case of electrolyte-soluble products, an ion-conductive separator can also be included to ensure that the two chemical product streams do not mix with one another and back react. For the semiconductor particle system, the

microscopic nature of the half-cell reaction surfaces causes H_2 and O_2 to be evolved essentially together. The gas stream released from the photoparticle slurry would be 66% H_2 by volume, the balance mostly O_2, well within the combustible range.

Our work to date has been geared toward understanding how photoparticle systems operate, and how a large scale reactor system might be configured. We have found that fixed bed arrays of particulates would make the most economic use of the solar energy-converting material. Furthermore, the loss in conversion efficiency compared to loose colloidal systems is compensated by the technical advantages of having a flow system that moves the dissolved products of reaction out the photoreactor, lessening the extent of back reaction.

3.0 DESCRIPTION OF CONCEPT

We are attempting to take the fixed particle bed approach and apply it to the photocatalytic water splitting problem. The intrinsic problem of gaseous product separation could be solved by employing 2 particle beds, one for oxidation of water to evolve O_2, the other for reduction of water to evolve H_2. Figure 1 depicts how the system would work.

The general chemical mechanism for a dual bed concept photosystem would be as follows:

Photoreactor 1, PC-R: $4H_2O + 4M^\circ \rightarrow 2H_2 + 4OH^- + 4M^+$

Photoreactor 2, PC-O: $\underline{4OH^- + 4M^+ \rightarrow O_2 + 2H_20 + 4M^\circ}$

net: $2H_2O \rightarrow 2H_2 + O_2$

where, PC-R: photocatalyst for the reductive stage of the process
PC-O: photocatalyst for the oxidative stage of the process
M: redox mediator

The immediate task was to identify photoactive materials that could be used for either H_2 or O_2 evolution, and devise ways to immobilize them on a surface. Much of the work done over the

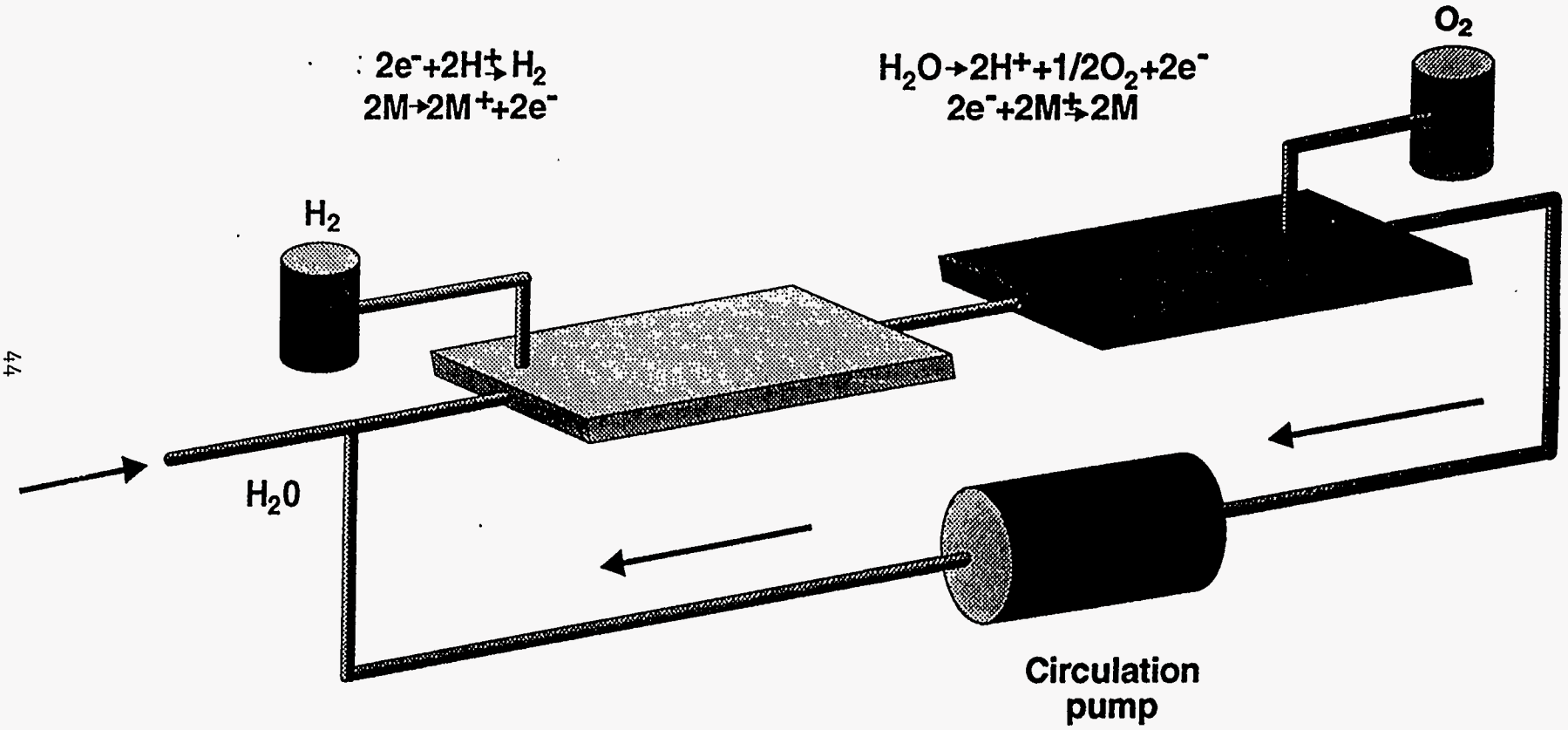

Figure 1. Schematic of the Dual Photoparticle Bed Concept for Water Splitting.

years in photoelectrochemical work could be built on for this task. As for O_2 evolution, one can identify 6 metal oxides that have achieved some measure of success as photoanodes: TiO_2, ZnO, SnO_2, WO_3, MoO_3, and Fe_2O_3. We have used TiO_2, as the greatest photoelectrochemical successes have been achieved with this material.

As for hydrogen evolution, comparably fewer materials have been identified. This is partly due to difficulties in p-type doping of materials that are stable in water, and also due to the use of Pt and other noble metals as rapid H_2-evolving electrodes that work in the dark while the anode is illuminated. Even so, a number of metal phosphides, such as InP and GaP, have been studied. We chose InP as the base material.

Also, a redox equivalent transfer agent or mediator should be identified to provide an anodic half-cell reaction in the H_2-evolving reactor and the cathodic half-cell back reaction in the O_2-evolving reactor. Charge transfer kinetics with the respective semiconductor powders should be reasonably rapid in order to make use of the photogenerated electrons and holes, but not so fast that the reverse reaction proceeds with equal facility. The respective back reactions between O_2 and M in one chamber and H_2 and M^+ in the other also represent an efficiency loss that should be accounted for.

The band characteristics of PC-R and PC-O will limit what redox agents could possibly serve as mediator in the dual particle bed system. As shown in Figure 2, the positive limit of redox potential is determined by the valence band edge of the p-type, H_2-evolving photocatalyst, while the negative limit is determined by the conduction band edge of the n-type, O_2-evolving photocatalyst. As band edges are difficult to determine, researchers frequently approximate them by measuring the flat band potential, V_{fb}.

To give an example, let PC-O be n-TiO_2. At pH 9, V_{fb} is calculated to be -0.375 V vs NHE, based on -0.7 V at pH 13. The previously mentioned approximation for n-type semiconductors is that $E_{cb} = V_{fb}$, and so -0.375 is the negative limit. Also let PC-R be p-InP. At the same pH, V_{fb} = +0.7 V, which approximates the InP valence band position. That enables a 0.7 - (-.375) = 1.07 volt range to work with.

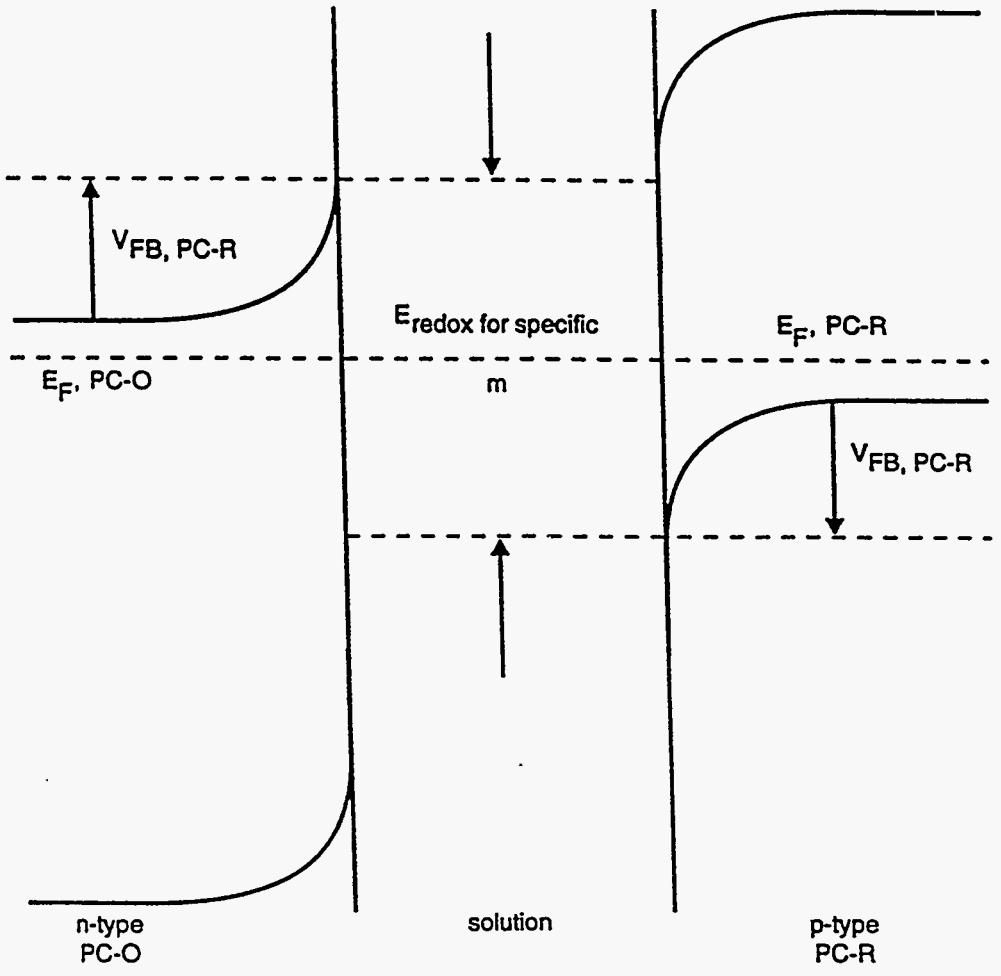

Figure 2. **Energy band diagram showing range of possible mediator redox potentials**

Various iron complexes, quinones, halogens, and other reasonably rapid charge transfer agents within the optimum redox potential range were examined. A listing of these reagents with their respective standard reduction potentials is given in Table I.

Table I. Listing of Redox Mediators

Ox	Red	E° (V vs NHE)
Sn^{4+}	Sn^{2+}	0.139
Anthraquinone-2,6-disulfonate	-	0.228
$K_3[Fe(CN)_6]$	$K_4[Fe(CN)_6]$	0.46 (NaOH)
1,4-Napthoquinone-2-sulfonate	-	0.47
Toluidine Blue	R.T.B.*	0.534
-	KI	0.535
thionine	leucothionine	0.563
-	$FeSO_4$	0.68
1,4-benzoquinone	hydroquinone	0.699
NO_3^-	-	0.84
V_2O_5 (VO_2^+)	$VOSO_4$	1.00
-	KBr	1.087
-	HCl	1.358
HIO_6	-	1.7

*R.T.B. = "reduced Toluidine Blue", produced via Zn reduction of the Ox form.

We tried wherever possible to test both the "Ox" and "Red" forms of the mediator, since positive results (i.e., H_2 and O_2 evolution, respectively) for both forms would constitute unambiguous proof that a good candidate had been found. In a few instances, where a particular redox state was not commercially available, it was generated in-house, as in Zn reduction of Toluidine Blue.

4.0 RESULTS

4.1 Theory: Band Structure of Catalyst/Photoparticle Configurations

On the microscopic level, there are many ways to configure the arrangement of catalyst and photoparticle. Certainly they must be in close proximity to each other, so that the photogenerated charge can flow from semiconductor to catalyst phase without recombination or other loss mechanisms. One normally thinks of a catalyst as precious material, dispersed as fine particles on an inert support. In our case, the catalyst would be deposited on a semiconductor powder, which is certainly not inert. The optimum size of a catalyst deposit, both in terms of its absolute size and size relative to the semiconductor particle that supports it, needs to be determined. Also, the proximity of one catalyst island to another is important, because too much catalyst could block the incoming light that is to be absorbed by the semiconductor.

If the catalyst is not too expensive, one could just as well consider depositing the semiconductor on the catalyst, or better still, deposit both semiconductor and catalyst on an inexpensive, but electronically conductive, substrate. That way, islands of semiconductor and catalyst could be placed side by side. This would cause some segregation of the respective oxidation and reduction reactions in each module, and would enable maximum light absorption by the photoparticle. It is intended to establish a theoretical basis for this approach.

Potential Distribution for a Flat, Infinite Semiconductor Surface

The model for the potential field in a semiconductor immersed in an electrolytic solution assumes a flat infinite semiconductor surface. A potential will develop according to Poisson's equation as follows:

$$\nabla^2 V(x) = \frac{-4\pi}{\epsilon_1}\rho \ , \qquad (1)$$

which states that the potential is a function of the charge density, ρ, and semiconductor dielectric constant, ϵ_1. The charge density can be written in terms of concentrations of electron, holes, donor levels, and acceptor levels as follows (n,p,N_D,N_A respectively):

$$\rho = e(-n+p+N_D-N_A) \quad . \tag{2}$$

Assuming complete ionization of donors and acceptors, free carrier concentration in the electric field can be determined by a Boltzmann distribution. Thus,

$$n(x) = n^{\circ}\exp^{\frac{e(V-V_b)}{kt}}; \qquad p(x) = p^0\exp^{-\frac{e(V-V_b)}{kT}}, \tag{3}$$

Where n_0, p_0, and V_b are concentrations of electrons, holes and the potential at the bulk of the semiconductor, k is the Boltzmann constant, and T is temperature. Substituting this result into equation (2) yields

$$\rho = e\left(-n^0 e^{\frac{e(V-V_b)}{kT}} + p^0 e^{-\frac{e(V-V_b)}{kT}} + N_D - N_A\right) \quad . \tag{4}$$

Substituting this into (1) results in

$$\nabla^2 V = -\frac{4\pi}{\varepsilon_1} e(-n^0 e^{\frac{e(V-V_b)}{kT}} + p^0 e^{-\frac{e(V-V_b)}{kT}} + N_D - N_A) \quad . \tag{5}$$

For an n-type semiconductor for which $N_D >> N_A$ and $n^0 >> p^0$ equation (5) can be simplified to

$$\nabla^2 V = -\frac{4\pi}{\varepsilon_1} e(-n^0 e^{\frac{e(V-V_b)}{kT}} + N_D) \quad . \tag{6}$$

Using only the first term of the series expansion of the exponential, equation (6) further simplifies to

$$\nabla^2 V = -\frac{4\pi}{\varepsilon_1} e\left(-n^0\left(1+\frac{e(V-V_b)}{KT}\right) + N_D\right) \quad . \tag{7}$$

Because there is no space charge in the bulk of the semiconductor, $-n^0 + N_D \approx 0$. Taking this into account,

$$\nabla^2 V = \frac{4\pi n^0 e^2}{\varepsilon_1 kT}(V - V_b) \quad . \tag{8}$$

Asserting that V_b is the reference potential, hence equal zero, the solution to the flat infinite surface is:

$$V(x) = (V_0 - V_b)e^{-\frac{x}{L}} - V_b \quad , \tag{9}$$

where L is the Debye length defined as

$$L = \sqrt{\frac{\varepsilon_1 kT}{4\pi e^2 n^0}} \quad . \tag{10}$$

Free Semiconductor Particle

Expanding on this general development, a spherical semiconductor particle immersed in an electrolytic solution will be considered. The form of Poisson's equation is shown below after simplifications of the same nature as those above have been applied. Additionally, $V_b=0$ is assumed.

$$\frac{1}{r^2}\frac{\partial}{\partial r}\left(r^2 \frac{\partial V}{\partial r}\right) = \frac{1}{L^2} V \tag{11}$$

Equation (11) is of the form of a modified spherical bessel function as generally shown below:

$$z^2 w'' + 2zw' - [z^2 + n(n+1)] = 0 \quad . \tag{12}$$

Because the potential at the center of the particle must be finite ($V|_{r=0}$=constant), rejection of all solutions except the i-type bessel functions is possible. Also because our initial equation restricts n to 0 or -1 we can consider the case of n=0. Because $i_0(r)=\sinh(r)/r$ the appropriate solution is:

$$V=\frac{r_0 V_o}{r}*\frac{\sinh\left(\frac{r}{L}\right)}{\sinh\left(\frac{r_0}{L}\right)} \tag{13}$$

for the boundary for the boundary conditions $V=1|_{r=r_0}$ and $V=\text{constant}|_{r=0}$.

Potential Distribution for Interstitial Catalyst System

The potential for a semi-spherical semiconductor particle interfaced to a conductive substrate on the flat side and immersed in an electrolytic solution is in the following.

It is assumed that symmetry exists in the θ direction. Thus equation (1) takes the form below in 2 dimensional spherical coordinates.

$$\frac{1}{r^2}\frac{\partial}{\partial r}\left(r^2\frac{\partial V}{\partial r}\right)+\frac{1}{r^2\sin\phi}\frac{\partial}{\partial\phi}\left(\sin\phi\frac{\partial V}{\partial\phi}\right)=\frac{-4\pi}{\varepsilon_1}\rho(r,\phi) \tag{14}$$

Applying the same assumptions as in the first section equation (8) is as follows:

$$\frac{1}{r^2}\frac{\partial}{\partial r}\left(r^2\frac{\partial V}{\partial r}\right)+\frac{1}{r^2\sin\phi}\frac{\partial}{\partial\phi}\left(\sin\phi\frac{\partial V}{\partial\phi}\right)=\frac{1}{L^2}(V-V_b) \tag{15}$$

Substituting $u=\cos\phi$, and again asserting that V_b is the reference potential (V_b=0) this becomes

$$\frac{1}{r^2}\frac{\partial}{\partial r}\left(r^2\frac{\partial V}{\partial r}\right)-\frac{1}{r^2}\frac{\partial}{\partial u}\left((1-u^2)\frac{\partial V}{\partial u}\right)=\frac{1}{L^2}V \tag{16}$$

Utilizing separation of variables, it is assumed that the solution takes the form:

$$V(r,\phi)=R(r)M(u) \ , \tag{17}$$

which leads to

$$\frac{1}{R}\frac{\partial}{\partial r}\left(r^2\frac{\partial R}{\partial r}\right)-\frac{1}{L^2}r^2=\frac{1}{M}\frac{\partial}{\partial u}\left((1-u^2)\frac{\partial M}{\partial u}\right) \tag{18}$$

Because functions of r are equal to functions of u the two sides of equation (18) must be equal to an arbitrary constant λ. Thus,

$$\frac{1}{R}\frac{\partial}{\partial r}\left(r^2\frac{\partial R}{\partial r}\right)-Kr^2=\lambda \tag{19a}$$

$$\frac{1}{M}\frac{\partial}{\partial U}\left((1-U^2)\frac{\partial M}{\partial u}\right)=\lambda \ , \tag{19b}$$

Where equation (19a) is recognizable as a Bessel equation, equation (19b) is of the form of Legendre's equation and λ is a positive integer and separation parameter.

The solution to equation (19b) is the well known Legendre polynomial expressed as

$$M(u)=A_nP_n(u) \ , \tag{20}$$

where

$$P_n(x)=\sum_{m=0}^{\frac{n}{2}}(-1)^m\frac{(2n-2m)!}{2^n m!(n-m)!(n-2m)!}x^{n-2m} \ . \tag{21}$$

The solutions of equation (19a) are the spherically modified bessel function $i_n(x)$ and $k_n(x)$. Because the potential must be finite at r=0 only the i function is possible. Thus, the solution is of the form:

$$R(r)=D_n\, i_n\left(\frac{1}{L}r\right) , \tag{22}$$

where

$$i_n\left(\frac{r}{L}\right)=2^{-(n+1)}\sqrt{\pi}\left(\frac{r}{L}\right)^n \sum_{k=0}^{\infty} \frac{\left(-\frac{re^{\frac{ni}{2}}}{4L}\right)^k}{k!\Gamma(n+.5+k+1)} . \tag{23}$$

Finally, substituting equations (20) and (22) into equation (17) results in the general form of the solution.

$$V(r,\phi)=\sum_{n=1}^{\infty} A_n D_n J_n\left(\frac{1}{L}r\right) P_n(\cos\phi) \tag{24}$$

Letting $a_n=A_nD_n$,

$$V(r,\theta)=\sum_{n=1}^{\infty} a_n i_n\left(\frac{1}{L}r\right) p_n(\cos\theta) . \tag{25}$$

The coefficient a_n is readily obtained by applying B.C. V=1 at$_0$r=r and the condition of orthogonality to the Legendre polynomial.

$$a_n=\frac{(2n+1)k}{2i_n\left(\frac{r_0}{L}\right)}\int_0^{\frac{\pi}{2}} P_n(\cos(\phi))\sin(\phi)\, d\phi \tag{26}$$

Thus, the complete solution is

$$V(r,\phi)=\sum_{n=1}^{\infty}\left(\left(\frac{(2n+1)k}{2i_n\left(\frac{r_0}{L}\right)}\int_0^{\frac{\pi}{2}}\sin(\phi)\cdot P_n(\cos(\phi))\,d\phi\right) i_n\left(\frac{r}{L}\right)\ P_n(\cos(\phi))\right) \quad . (27)$$

At this point, the particular solution awaits imposition of additional boundary conditions. Discontinuities are found at the edges the semiconductor particle where it contacts both the electrolyte and the conductive substrate. Finite element analysis may be necessary to define the potential distribution.

4.2 Redox Mediator Photochemistry

The first objective was to show that the two types semiconductor particles together can generate a sufficient photovoltage to break down water; at ambient temperature, the theoretical value is about 1.23 V. Based on realistic values of overpotentials and other losses, about 1.0 V per module needs to be generated. We chose n-TiO_2 and p-InP as the initial pairing of powders to be tested.

A series of redox reagents were irradiated with a Xe lamp in aqueous slurries of photocatalytic powders to probe the limits of energy storage that each semiconductor is capable of. It also provided some insight into what compounds may prove to be useful redox mediators. For example, if the voltage generation requirement is shared equally between the two photoreactors, the redox mediator will have a standard redox potential of 0.6 V (acidic standard state). The further the mediator's redox potential departs from that value, the more uneven the energy storage load becomes.

In Table II below, gas evolution results are given for one-hour irradiation of TiO_2 slurries in the presence of various redox reagents. It was expected that those with the highest redox potentials would perform best, while those with low redox potential would exhibit little or no gas evolution. As it turned out, gas evolution was observed in nearly every case. Therefore, gas chromatographic analysis of the product gases were performed to confirm the presence of O_2. In the majority of cases, the gas evolved was not O_2. Not surprisingly, the only clear cut case of O_2 evolution was found for H_5IO_6, periodic acid, the reagent with the highest redox potential.

Table II. Gas Evolution from TiO_2 Slurries

1 hr Xe lamp illumination

redox substrate	gas evolved (ml)	O_2 detection
1,4-napthoquinone disulfonic acid	12	no
2,6-anthraquinone disulfonic acid	15	no
toluidine blue	5	no
thionine	0	no
VO_2+	10	?
	20*	yes
H_5IO_6	5	yes
	13*	yes
NO_3^-	4	no

* ground admixture of TiO_2 and dried carbon paint.

O_2 evolution with H_5IO_6 does not clearly represent energy storage at all, since its redox potential is positive of water oxidation--the TiO_2 is acting as a photocatalyst, but not as an energy transducer.

Many representatives from the previous series of redox agents were tested as electron donors in the photocatalytic evolution of H_2 using InP. The experiment was essentially the same: irradiation of an InP semiconductor particle suspension, measurement of net gas evolution, and gas chromatographic analysis for H_2. Nine different redox agents were tested representing a span of approximately 1 volt of redox potential energy. Results are summarized in the Table III below:

Table III. Gas Evolution from InP slurries

Mediator	Solvent	Gas Evolution?	H_2 Evolution?
hydroquinone	NaOH	yes	no
$K_4[Fe(CN)_6]$	NaOH	yes	yes
$SnCl_2$	HCl	yes	yes
$FeSO_4$	H_2SO_4	yes	yes
Toluidine Blue	H_2SO_4	yes	?
KI	HCl	yes	yes
KBr	HCl	yes	yes
none	HCl	yes	yes
KI	H_3PO_4	yes	yes
KBr	H_3PO_4	yes	yes
$VOSO_4$	H_3PO_4	yes	no

The solvent is listed in each case, because it was determined midway through the experiments sequence that HCl was an active substrate for H_2 evolution. This was an unexpected result, as

the redox potential for Cl_2 evolution was thought to be too positive. Enough testing with alternative electrolytes was done to insure against false results.

In contrast to what had been seen earlier for TiO_2, all the redox agents tested evolved gas, and all but 2 or 3 of them had at least some H_2 as part of that gaseous evolution. Even the halides were found to work as redox substrates. In terms of redox potential, the hydroquinone should have worked, but also underwent uncharacterized decomposition reactions.

4.3 Future Work

Even though many possible redox mediator candidate were identified in the H_2 - evolution module, the lack of positive results in the O_2 - evolution module precluded identification of a reagent capable of shuttling electrons between the two modules. Either the TiO_2 needs to be made more active through doping or catalyst modification, or alternatives need to be found; ultimately, chromophore/photoconductor systems for O_2 and H_2 evolution must be developed.

It will also be necessary to: a) Determine level of sophistication needed for redox mediator. b) Balance light absorptive and catalytic activity of the chromophore. c) Consider whether the H_2 cell would benefit from a dye sensitization approach.

Finally, we will need to: 1. on the theoretical work, incorporate reverse chemical reaction kinetics into steady state equation. 2. use supersensitizers in conjunction with base chromophore. 3. catalysts for redox mediator oxidation and reduction.

5.0 ACKNOWLEDGEMENT

The author would like to thank Beverly Austin, Tom McKaige, Anthony Ouellette, and Darlene Slattery for their technical assistance on this work. The financial support of the Department of Energy, Office of Advanced Utility Systems, is gratefully acknowledged.

Task 3 Report

Development of Solid Electrolytes for Water Electrolysis at Intermediate Temperatures

Annual Report

FSEC-CR-857-95
DOE Contract #DE-FG04-94AL85802
December 1995

Submitted to:
Neil Rossmeissl
Advanced Utility Concepts Division
Department of Energy
Washington, DC 20585

Submitted by:
Dr. Clovis A. Linkous
Randy Anderson
Robert W. Kopitzke

Florida Solar Energy Center
University of Central Florida
1679 Clearlake Road
Cocoa, Florida 32922-5703

DEVELOPMENT OF SOLID ELECTROLYTES

FOR WATER ELECTROLYSIS AT

INTERMEDIATE TEMPERATURES

Clovis A. Linkous
Randy Anderson
Robert W. Kopitzke
Florida Solar Energy Center
Cocoa, FL 32922-5703

1.0 SUMMARY

This project is an attempt to synthesize and fabricate proton exchange membranes for hydrogen production via water electrolysis that can take advantage of the better kinetic and thermodynamic conditions that exist at higher temperatures. Current PEM technology is limited to the 125-150^0 C range. Based on previous work evaluating thermohydrolytic stability, some 5 families of polymers were chosen as viable candidates: polyether ketones, polyether sulfones, fluorinated polyimides, polybenzimidazoles, and polyphenyl quinoxalines. Several of these have been converted into ionomers via sulfonation and fashioned into membranes for evaluation. In particular, the sulfonated polyetheretherketone, or SPEEK, was tested for water uptake, thermo-conductimetric analysis, and performance as the solid electrolyte material in an electrolysis cell. Results comparable to commercial perfluorocarbon sulfonates were obtained.

2.0 BACKGROUND

2.1 Advantages in Performing Water Electrolysis at Elevated Temperature

If an electrolyzer could operate at higher temperatures, several benefits would accrue. The first is that the thermodynamic electrical energy requirement to drive the reaction would be reduced. As shown in Figure 1, supplying the total enthalpy of reaction at any temperature involves a combination of electrical and thermal energy inputs. Because of the positive entropy associated with water decomposition, the thermal contribution increases as temperature rises, allowing the free energy requirement to decrease.

Thus the open circuit voltage, V_{oc}, for water splitting drops as temperature rises. At room temperature, V_{oc} for water decomposition is 1.229 V. At 400^0 C, voltage requirement has

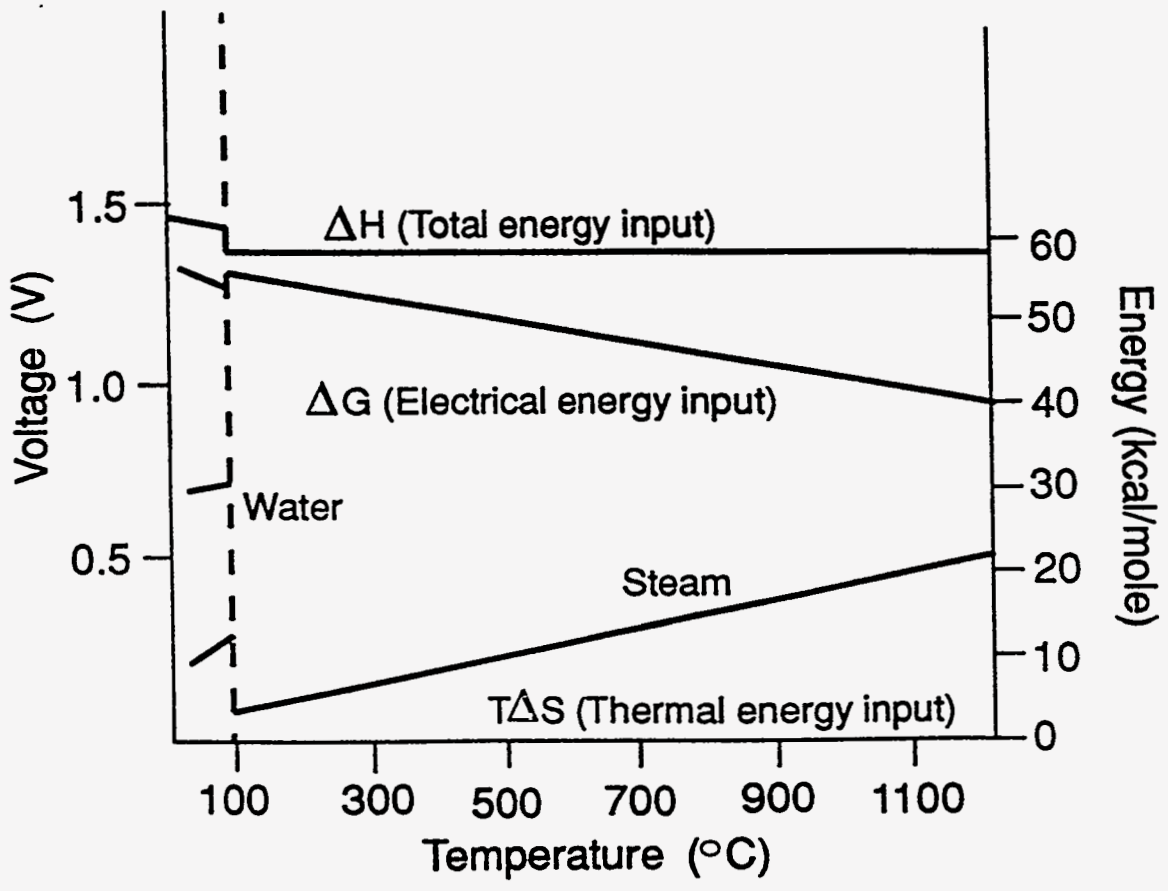

Figure 1. Energy relationships in water electrolysis

dropped to 1.1 V; at 1000^0 C, it is only 0.92 V. Since electricity is a more expensive form of energy on a btu basis, the more energy taken from the thermal surroundings the better. Moreover, this thermal energy content could be solar-derived. While the cost of solar thermal energy varies in the range of $360-900/peak kilowatt, the installed cost of photovoltaic electricity is in the range of $4,000-5,000/peak kilowatt. Thus if one is compelled to erect an array of photovoltaic panels to generate the e.m.f. necessary to split water, substituting as much area with thermal collectors as possible represents a substantial cost savings.

A second benefit is that activation barriers for the various electrode surface chemical reactions are more easily surmounted as temperature increases. As it stands now, expensive noble metals are frequently required in electrolyzers to keep cell voltages acceptably close to the thermodynamic value. For a unit operating at higher temperature one may be able to substitute cheaper, less catalytic metals with higher intrinsic activation energies toward O_2 and H_2 evolution.

This same consideration may likely be applicable to the electrolyte itself. Ionic motion in solids is frequently modeled as a hopping process, where the mobile ionic species, in our case H^+ or H_3O^+, makes activation-limited jumps from one binding site to an adjacent one. Thus one could anticipate reduced ohmic overpotential loss from the electrolyte as well.

2.2 Current Proton Exchange Membrane Technology

In principle, this type of electrolyzer would include any electrolyte consisting of a polymeric material that could be fabricated into a gas impermeable membrane that could transport ions necessary to support water electrolysis. A number of other polymeric proton exchange membranes have been reported in recent years. Doping polyethyleneoxides with various salts results in proton conducting membranes with conductivities on the order of 10^{-5}-10^{-4} S/cm at room temperature and greater than 10^{-3} S/cm at 100^0 C (1). Polymers doped with inorganic acids have been prepared and resulted in conductivities as high as 1.4×10^{-2} S/cm at 100^0 C for a polyacrylamide doped with sulfuric acid (2). A final example, poly(benzyl sulfonic acid) siloxane showed conductivities ranging from 2×10^{-3} to 10^{-2} S/cm at room temperature (3).

In practice, proton exchange membrane technology, or PEM, has come to mean those cells employing a perfluorinated hydrocarbon sulfonate ionomer, such as Du Pont's Nafion™. Originally developed as a substitute for other types of cell separators utilized in the chlor-alkali industry, it has come to occupy a place of prominence in the search for more efficient, less expensive ways to electrolytically produce H_2.

To exhibit protonic conductivity, Nafion must be pre-swelled with water, usually by boiling it. In this state it has a conductivity on order of 0.01 $(ohm\text{-}cm)^{-1}$. In comparison to a 1 M HCl solution (0.1 $(ohm\text{-}cm)^{-1}$), it is a factor of 10 too resistive, but can be fabricated and mounted in a cell with much closer tolerances, so that the absolute resistance is comparable. The uptake of water can amount to 28% by weight (4).

The water uptaken into Nafion is for the most part free and unbound, since it is quickly lost once temperature exceeds 100^0 C. By pressurizing the system, one can increase operating temperature; however, by the time temperature has been raised to 150^0 C, the thermal stability of the perfluorinated ionomer itself is brought into question. The normally light brown or clear membrane irreversibly becomes dark and brittle. Thus currently one cannot operate PEM electrolysis cells at temperatures above 150^0 C.

The sulfonated ionomer is acidic in nature, and so other components, especially the anode and its external electrical contacts, must have some corrosion resistance. To date this has required that the anode be either a noble metal such as Pt or a transition metal alloy based on Ir or Ru (5).

2.3 Development of Intermediate Temperature Solid Electrolytes

At the current level of water electrolysis technology, there exists an 800-900 degree gap, between zirconia-based ceramic membranes at the high end and PEM cells at the low end, in which there are no electrolytic systems suitable for water electrolysis. Even if one includes all of the fuel cell technologies that could possibly be run in reverse, such as phosphoric acid at up to 200^0 C and molten carbonate as low as 600^0 C, there still exists a 400 degree gap. In terms of striking a balance between faster kinetics and lower open circuit voltage by raising

temperature, and reducing corrosion and materials compatibility problems by lowering it, operation in the 200-400^0 C range appears to be desirable.

Most efforts to develop high temperature proton conductors have involved hydrated inorganic oxides (6,7). A less explored avenue would be to consider engineering polymers, those specialized polymers whose structures allow them to be used in applications requiring extremes of temperature and corrosivity. However, since they were developed for other applications such as flame retardant materials, seals for electronic components in hostile environments, and autoclavable medical supplies (8), their behavior in an electrolytic situation at elevated temperature has not been well characterized.

2.4 Previous Work on Engineering Polymers

A less tried route that could allow for higher operating temperatures is to use engineering polymers. These polymers are designed for use at temperatures in excess of 300^0 C and can be modified to yield ion conducting materials. For example, a polyimide containing quaternary copolymer was found to have a conductivity of 10^{-6} at 250^0 C (4). Aromatic polyethersulfones have been sulfonated and used as experimental water electrolysis membranes although no conductivity data for this system was reported (10). The derivatization of the aromatic polyetheretherketone (PEEK) to its sulfonic acid ionomer and the characterization of this ion containing polymer have been extensively studied (11-15), although its ion conducting properties have not been reported.

In previous work, over 40 different polymeric materials, each known for their thermal and chemical resistance, were examined under steam/O_2 and steam/H_2 conditions. This was done to simulate conditions that would be observed in the anode and cathode compartments of a steam electrolysis cell (16). Of these, several polymer families showed good stability: liquid crystal aromatic polyesters, polybenzimidazoles, and some of the polyimides were stable at 200^0 C. The polyphenylene sulfides, polysulfones, polyethersulfones, the various polyketones, and some of the polyimides were stable at 300^0 C. None of the polymers tested could withstand the combination of steam and O_2 at 400^0 C; however, some of the polyketones did survive at 400^0 C under the reducing environment.

The above list of polymers makes a fair representation of those families that are most likely to succeed as high temperature solid electrolytes. Some of the polymers of interest consisted of 1,4-disubstituted phenyl groups separated by any of a number of linkages:

$$-[X\text{-(phenyl)-}Y\text{-(phenyl)-}Z\text{-(phenyl)}]_n ,$$

where X,Y,Z = -O-, -C(O)-, $-C(CH_3)_2-$, $-SO_2-$, -S-, etc.

for PEEK, X = Y = -O-, Z = -C(O)-;

for PES, $X = -SO_2-$, Y = -O-, etc.

In the present work, our task has been to sulfonate these materials, converting them to ionomers, and then characterize their thermohydrolytic and proton-conducting behavior.

3.0 EXPERIMENTAL

3.1 Sulfonation Reaction

Electrophilic aromatic sulfonation of the PEEK was done following established literature methods (14). A typical reaction is as follows: 10 g of oven dried PEEK was dissolved in 100 ml of 96% H_2SO_4. The tan PEEK dissolved within 2 hours to give a deep red, viscous solution. The time and the temperature of the reaction were varied in order to achieve the desired level of sulfonation. The reaction was quenched by slowly pouring the acidic solution into one liter of distilled water. The polymer precipitated instantly, forming a continuous white string. The polymer was extensively washed to remove the excess acid, dried in a vac-oven at 100^0 C, and titrated to determine the level of sulfonation.

The above sulfonation technique was attempted on each of the polymer candidates. As it turned out, more often than not the results were unsatisfactory: sometimes the polymers was so

heavily sulfonated it was completely water soluble and thus unsuitable for membrane fabrication and testing, and in others the polymer would simply dissolve and reprecipitate unreacted. Therefore, a number of other sulfonation procedures were adopted that will be described in the Results section.

3.2 Membrane Formation

Initially, four levels of sulfonation were selected for testing: 20%, 30%, 45% and 65%. Thin films were made by solvent casting 10% wt:wt solutions of the polymers in dimethylformamide (DMF) onto either a glass plate or into a beaker. The solvent was removed by gentle heating until the film could be peeled off the substrate. The films used for the water electrolysis studies were cast onto glass onto which had been spread 4 mg/cm^2 of iridium black powder. These membranes, once dried, were coated on one side only with the iridium catalyst. All of the membranes were hydrated before use by heating them in distilled water. The temperature and duration of heating varied with the membranes' resistance to dissolution in the water.

3.3 Water Uptake

H_2O uptake by the ionomer membranes was determined by soaking the films in distilled water for one hour. It is uncertain whether the degree of water uptake so obtained truly constituted saturation - certainly the recommended procedure for swelling Nafion is more severe, involving boiling for several hours. Many of the test membranes, however, were not stable under boiling conditions, and so milder water uptake conditions had to be used.

The water uptake of the S-PEEK samples was determined as follows: the membranes were dried in a vacuum oven, weighed, soaked in distilled water overnight at room temperature, blotted dry to remove any surface moisture and reweighed. The water uptake is reported as the weight percentage of the membrane.

3.4 Degree of Sulfonation

Degree of sulfonation was determined via a combination of acid/base titrimetry and gravimetry. A dry sample of the test material would be weighed and then thoroughly soaked in 1 M HCl(aq) to completely protonate all of the sulfonic acid moieties contained within. It would then be rinsed with distilled water to remove excess acid and placed in a 3 M NaCl solution. This action would displace all of the labile protons and release them to the surrounding salt solution. The acidified salt solution would then be titrated with standardized NaOH solution. The results were used to calculate either degree of sulfonation (%), with 100% meaning 1 sulfonic acid group per repeating unit, or acid density (milliequivalents/g).

3.5 Thermo-Conductimetric Analysis

Resistance measurements were made using an a.c. bridge at 1000 Hz. The membrane conductivity cell was patterned after the work done at Los Alamos (17). Sample membranes were suspended in a holder and clamped with platinum contacts at opposite edges. The conductivity cell was immersed in deionized water within a Parr reactor equipped with electrical feedthroughs and ramped at 0.5^0 C/min. Resistance values so obtained would be corrected by the dimensions of the sample membrane to yield conductivity.

It was decided that since conductivity was a valid parameter in assessing the viability of a candidate membrane, we could use the conductivity bridge in a type of thermal analysis. To perform the "thermoconductimetric" analysis, the conductivity cell was suspended inside a Parr reactor that was equipped with electrical feedthroughs to enable connection with the a.c. bridge. Temperature was slowly ramped while measuring conductivity. In each case, temperature was raised until failure of the membrane occurred. This would be noted by a precipitous drop in conductivity.

3.6 Electrolysis Performance

The test cell, as shown in Figure 2, consisted of two graphite blocks bored out to allow the evolved gases to escape from the cell. The iridium coated polymer was sandwiched between two

pieces of carbon cloth, one of which was electrolytically imbedded with platinum. This current distributor was placed at the cathode, positioned on the side of the polymer not coated with iridium. The carbon cloth provided acceptable electrical conductivity as well as gas and water permeability. The membrane assembly was centered between the graphite blocks and the entire cell was bolted together. Poppet check valves were placed in the exiting gas lines to pressurize the cell during higher temperature testing. Feed water was contained in a vertical column connected to the inlet port of the cathode.

Once completely assembled, the current versus voltage curves were generated. The power to the cell was controlled with a variable direct current power supply. A temperature controller connected to heat tape adhered to the test cell walls maintained the operating temperature during testing.

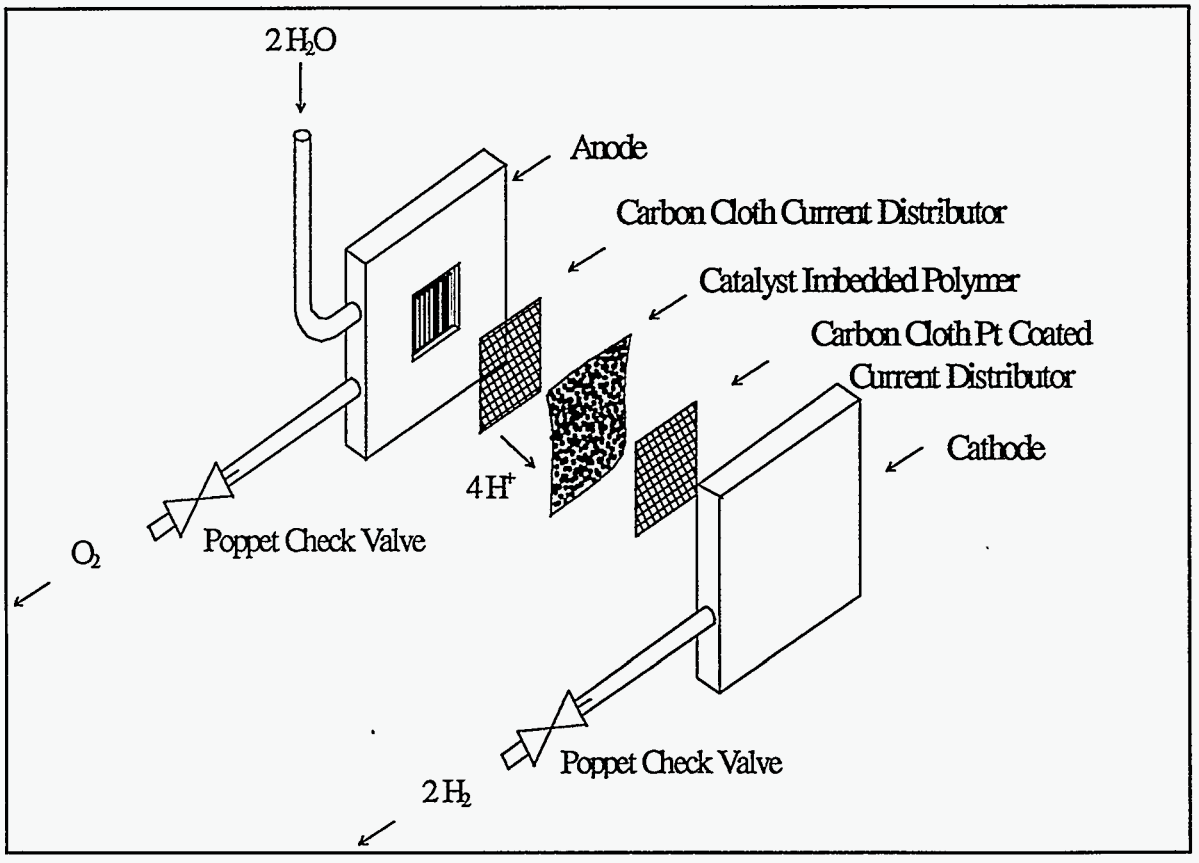

Figure 2. Proton exchange membreane electrolysis test cell.

4.0 RESULTS AND DISCUSSION

4.1 Ionomer Synthesis and Membrane Fabrication

PEEK

PEEK was sulfonated at various levels between 20%-75% by varying either reaction time or temperature. The sulfonation was performed by dissolving a sample (10g) of PEEK in concentrated sulfuric acid. Once the reaction time was completed, the reaction was quenched by adding the viscous acid solution dropwise to cold, rapidly stirring water.

Once the polymer had been sulfonated and obtained as solid white strands and droplets, it was usually necessary to convert it into thin sheets for characterization. Films were cast by dissolving the polymer in DMF, casting the solutions in a crystallizing dish, and evaporating the solvent to dryness. Films were hot-pressed to uniform thickness at 100^0 C and several thousand psi.

PES

Sulfonated PES was prepared using the concentrated sulfuric acid method. The levels of sulfonation obtained were 7%, 17.5% and 29.5%. All attempts to cast films from solvent resulted in cracked films. The suspicion was that the concentrated sulfuric acid used in the reaction was causing some decomposition of the polymer and resulting in shorter chain length. Attempts to sulfonate at greater than 29.5% resulted in H_2O soluble polymers (actually the 29.5% sample was soluble in hot water).

Blends of SPES with commercial PES were made to try and form a non-brittle film. A 1:1 blend of 29.5% SPES and PES gave a film that did not crack. This obviously limits the degree of sulfonation.

Higher degrees of sulfonation were finally achieved using a literature procedure with dissolved sulfur trioxide, SO_3, as the sulfonating agent (18,10). By varying the molar ratio of SO_3 to base polymer, 10% and 70% sulfonation levels were obtained.

PBI

Sulfonation of PBI was attempted using the concentrated sulfuric acid method, but was not successful. The polymer simply dissolved and re-precipitated after water dilution without reaction. Sulfonation was subsequently accomplished by soaking membranes, which were cast from a DMF solution doped with LiCl, in a 10% H_2SO_4 solution and then heating the swollen membrane at 300^0 C. This was based on a procedure obtained from Hoechst-Celanese (19). Initially, the swollen membranes were heated for one hour; this gave very brittle films that were not useful. Shortening the heating period to 1-2 minutes seems to improve the characteristics of these membranes. Attempts to make a membrane pliable enough for trials in the Parr reactor are still underway.

PPQ

Sulfonation of PPQ was also unsuccessful using the sulfuric acid method, but the soak and bake method using 35% H_2SO_4 has produced flexible membranes. The PPQ membranes used in this procedure are obtained from Cemota (Centre d'Études des Matériaux Organiques pour Technologies Avancées). The percent sulfonation (as determined by weight) can be controlled by varying the soaking period.

FPI

EYMYD films were cast from the supplied resin from the Ethyl Corporation and cured according to the prescribed procedure to give the polyimide film. Curing of a free film (not coated on any substrate) caused a crumpling of the membrane.

Attempts to sulfonate the polyimide were made using concentrated H_2SO_4, concentrated H_2SO_4 at elevated temperature, and 30% oleum. In all cases some discoloring of the solution occurred,

but no significant dissolution or reaction was observed. The problem seemed to be the resistance of these films to any moisture uptake.

Attempts to sulfonate the diamine portion of the monomer were made using simple dissolution in concentrated H_2SO_4. The diamine dissolved readily and was apparently sulfonated based on ^1H NMR at almost 200% after overnight reaction (one SO_3H group on each of the amine bearing aromatic rings). This sulfonated material would not dissolve in NMP (N-methyl pyrrolidone), however, when an attempt was made to do the polymerization reaction. Reducing the sulfonation reaction time from overnight to 6 hours gave a solid that was soluble in NMP. However, the polymerization reaction run under the hood with dry solvent and dry materials resulted in a brittle film when the reaction mixture was solvent cast. The assumption is that the polymerization reaction is producing low molecular weight polymer which forms a brittle film.

The polymerization reaction was performed using non-sulfonated diamine as a test of the polymerization reaction procedure. Attempts made in both the glove box and in the fume hood did not result in a usable film. Further consultation with the literature will be made before continuing this particular synthetic effort.

4.2 H_2O Uptake

It was anticipated that sulfonation of the base polymers would render them hygroscopic and capable of substantial water uptake. This effect can have a direct bearing on how well the ionomer conducts protons. Since most of our synthetic effort had been directed toward SPEEK, we were able to look at its water uptake ability in some detail.

In Table I, water uptake by SPEEK membranes as a function of degree of sulfonation is shown.

Table I. SPEEK Water Uptake Data

% sulfonation	% water uptake	# H_2O's / SO_3H
20	19	23
30	25	22
45	41	33
65	60	49

As can be seen, substantial amounts of water were indeed sorbed into the membranes, and was directly related to the degree of sulfonation. Of particular interest is the number of water molecules per sulfonic acid group. Waters of hydration alone could only account for possibly 6 H_2O's per acid group. The size of the numbers shown above indicate swelling and separation of the polymer strands. Indeed, samples with higher degrees of sulfonation would expand in their lateral dimensions and were quite weak mechanically. Thus either cross-linking groups must be introduced or the degree of sulfonation must be kept low. This latter solution would unfortunately work against high protonic conductivity.

4.3 Thermoconductimetric Results

As was mentioned in the previous section, SPEEK showed substantial water uptake, which at first glance this would be considered a positive attribute, but the moisture uptake also brought on the loss of mechanical properties. At 80^0 C in the Parr reactor, a 32% degree of sulfonation SPEEK sample showed a resistance of 75 kΩ at 81^0 C. At saturation its H_2O uptake was 47% by weight of the original dried film. This corresponds to 25.6 H_2O molecules/sulfonic acid. Upon examination, the membrane had swollen into a gel-like state, and was unusable for further testing. H_2O absorbence was also tested on 20% SPEEK at 80^0 C to see if it possessed the rigidity to act as a good membrane; this too swelled to a gel-like state and was unusable.

After much trial and error, we were able to produce membranes with as high as 65% degree of sulfonation that were mechanically strong enough to perform a thermoconductimetric

examination. An exponential rise in conductivity versus temperature was obtained, consistent with Arrhenius-type behavior, as shown for in Figure 3. This was also generally the case with the other polymer candidates.

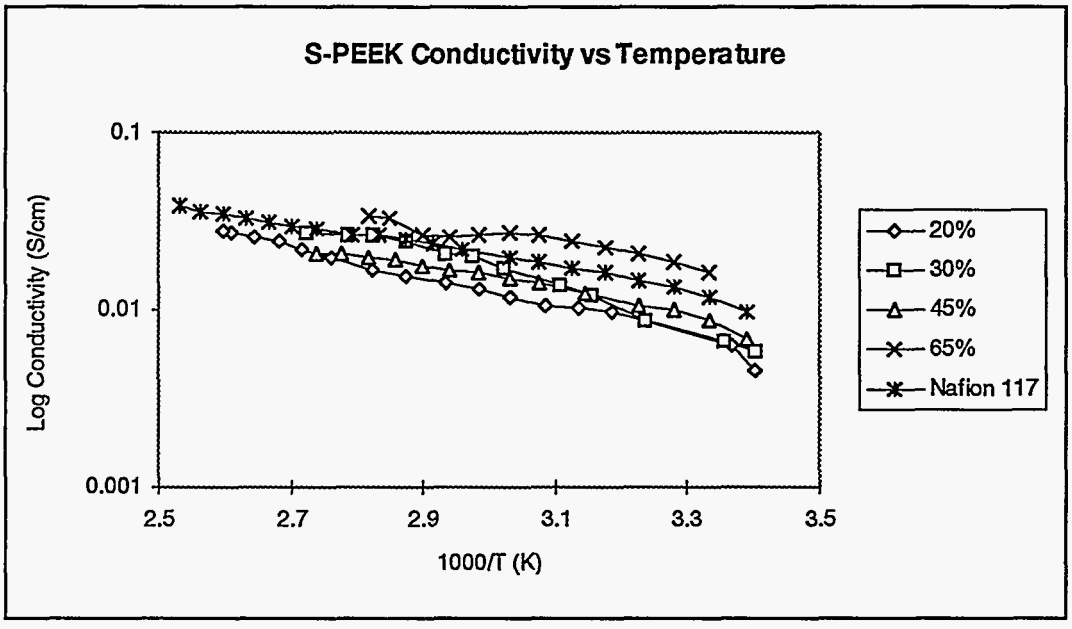

Figure 3. SPEEK conductivity vs reciprocal temperature.

A thick film cast with 10% SPES showed only 3% H_2O uptake and was highly non-conductive (> 1100 kΩ). Films using 70% SPES gave measurable results.

A resistance experiment was done with an SPPQ sample (% sulfonation unknown) which had an H_2O uptake of 23.2%. At 80° C the resistance was in the range of 30-35 kΩ. A second piece of SPPQ (no H_2O uptake information-but it had a longer soaking period) gave a resistance of 1.3 kΩ at 80° C. At elevated temperatures the membrane gave a minimum resistance of 525 Ω at 119° C. The membrane subjected to the higher temperatures (up to 165 C) had completely dissolved (or decomposed) when the reactor was opened up.

A resistance experiment was performed using SPPQ sulfonated at 100% degree of sulfonation (one SO_3H unit/monomer). The H_2O absorbence at this level of sulfonation is 13.8%. This is a rather resistive system, since at 80° C the resistance is 200 kΩ.

A resistance experiment on Nafion 117 was run using the Parr reactor setup; it gave a value of 850 Ω at 81° C and a minimum of 400 Ω at 167 C. The stability of the Nafion in high temperature steam was better than the other sulfonic acid polymers. The temperature reached a maximum of 270° C, and after cooling the reactor down, the membrane remained intact, although discoloration of the membrane had occurred.

A summary of the performance data for the ionomer membranes is shown in Table 2. As was discussed in the synthetic section above, degrees of sulfonation well in excess of the commercial product were achieved. In terms of thermal stability, only the SPPQ compared favorably with Nafion. Activation energies, as determined from the slope of their respective $\ln(\sigma_{H+})$ vs T^{-1} plots, were decidedly higher than that for Nafion, indicating some difficulty in the proton transfer process.

Table 2. Thermoconductimetric Data for Candidate Polymers

Sample	% SO_3H	n (meq/g)	T_{max}	E_{act} (kcal/mol)	σ_{H+} (Ω-cm)$^{-1}$ 100° C
Nafion	13	0.83	150	0.9	0.18
SPEEK	32,xl	1.02	98	8.1	0.025
SPES	70	2.42	121	6.2	0.022
SPPQ	107	1.87	153	3.9	0.005

Proton conductivities were compared at 100° C. Since the SPEEK membranes were typically unstable at that temperature, a cross-linking reaction using 1,1'-carbonyl diimidazole followed by reaction with bis-(4-aminophenyl) sulfone (18) was performed on a 32% sulfonated sample. Nevertheless, conductivities were below that of Nafion.

The combination of high degree of sulfonation and low conductivity with respect to Nafion points to a difference in conductivity mechanism. Water uptake measurements, while not given for all the samples, were generally quite substantial, commensurate with the high degree of sulfonation. Nafion is a perfluorinated hydrocarbon sulfonic acid ether; the acid is attached to the end of a 6-atom (on average) side chain. The aryl sulfonic acid polymers prepared in this work have sulfonic acid groups attached directly to the phenylene backbone, thus removing that degree of freedom. The base polymers typically have large glass transition temperatures, a good attribute as far as mechanical stability is concerned, but possibly detrimental with respect to proton conduction. Tertiary structure, i.e., how the polymer strands bind to one another, is another attribute that may be important to ionic conduction.

4.4 SPEEK Electrolysis Testing

The main variation in all the SPEEK samples prepared was the degree of sulfonation. While directly measuring water uptake and conductivity was informative, it was nevertheless interesting to see the aggregate effect of how well they performed in an electrolysis cell. Figure 3 represents the results of the conductivity testing, while the results of the electrolysis testing are presented in figures 4 through 8. The testing consisted of electrolyzing water at increasing cell temperatures in 10° C increments. Each membrane's testing continued until its performance declined.

The effect of temperature is quite evident: a general 3-4 fold increase in current density was obtained by increasing temperature from 60 to 100° C. Higher degrees of sulfonation enabled

modest improvements in current density: by doubling the density of ionic groups from 20 to 46.5% sulfonation the current density at 2.00 V increased from 50 to 70 mA/cm^2.

In Figure 7, a comparison between SPEEK at 65% sulfonation and the commercially available Nafion 117 is shown. The operating temperature for this comparison was only 60o C, because at this level of sulfonation the water uptake was substantial, so that at higher temperature the SPEEK was prone to creep. At low voltages, where activation overvoltages are at play, the two membranes perform essentially the same; however, at higher voltages and current densities, the SPEEK membrane performance actually exceeded the commercial material. While mechanically very fragile, the membrane was quite conductive, and so was less limiting at the higher applied voltages.

One other aspect of cell performance is the coulombic or current efficiency. While high current density at low voltage is a worthwhile objective, it constitutes wasted effort if the amount of charge going to generate H_2 remains the same. Coulombic efficiency was determined by dividing the integrated steady state current into the volume of H_2 produced. Figure 8 reveals the electrolysis current density of 20% SPEEK with the corresponding coulombic efficiency versus the cell voltage. While some losses are seen at the highest voltages, coulombic efficiency remains above 90%.

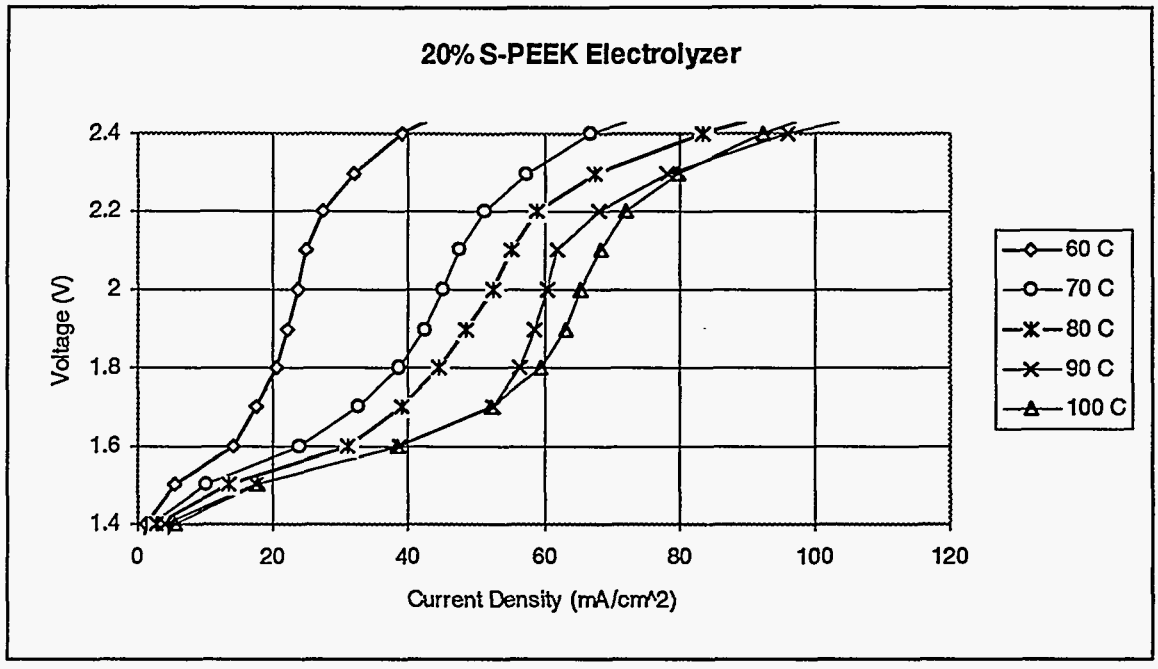

Figure 4. Water electrolysis curve for SPEEK membrane as a function of temperature; 20% degree of sulfonation.

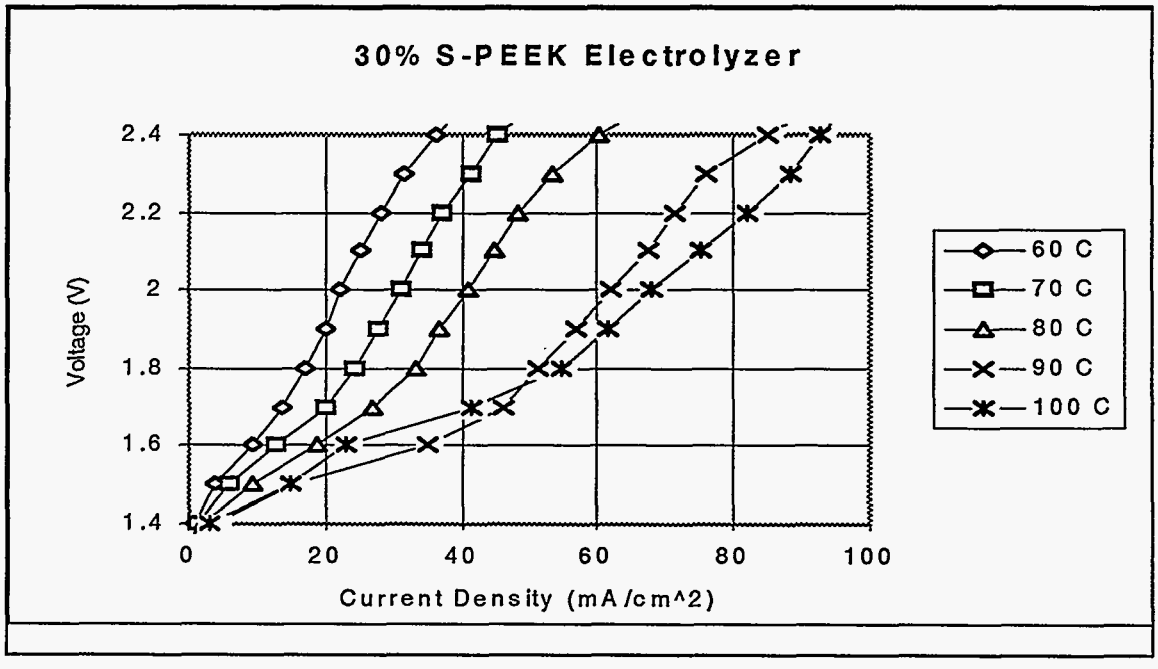

Figure 5. Water electrolysis curve for SPEEK membrane as a function of temperature; 30% degree of sulfonation.

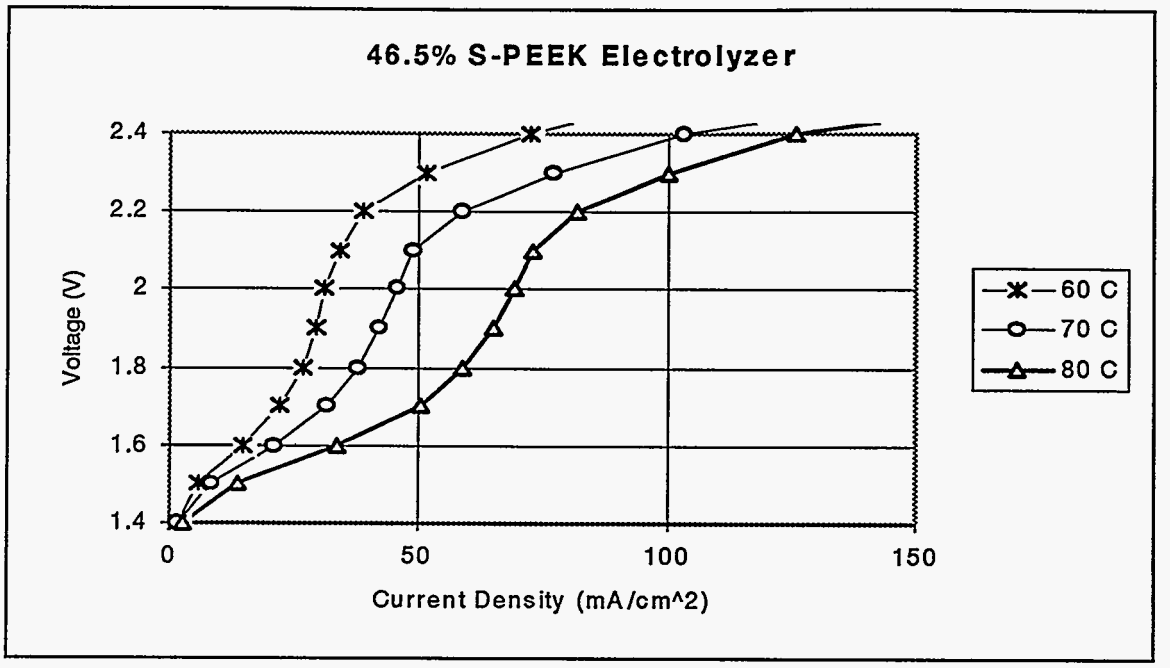

Figure 6. Water electrolysis curve for SPEEK membrane as a function of temperature; 46.5% degree of sulfonation.

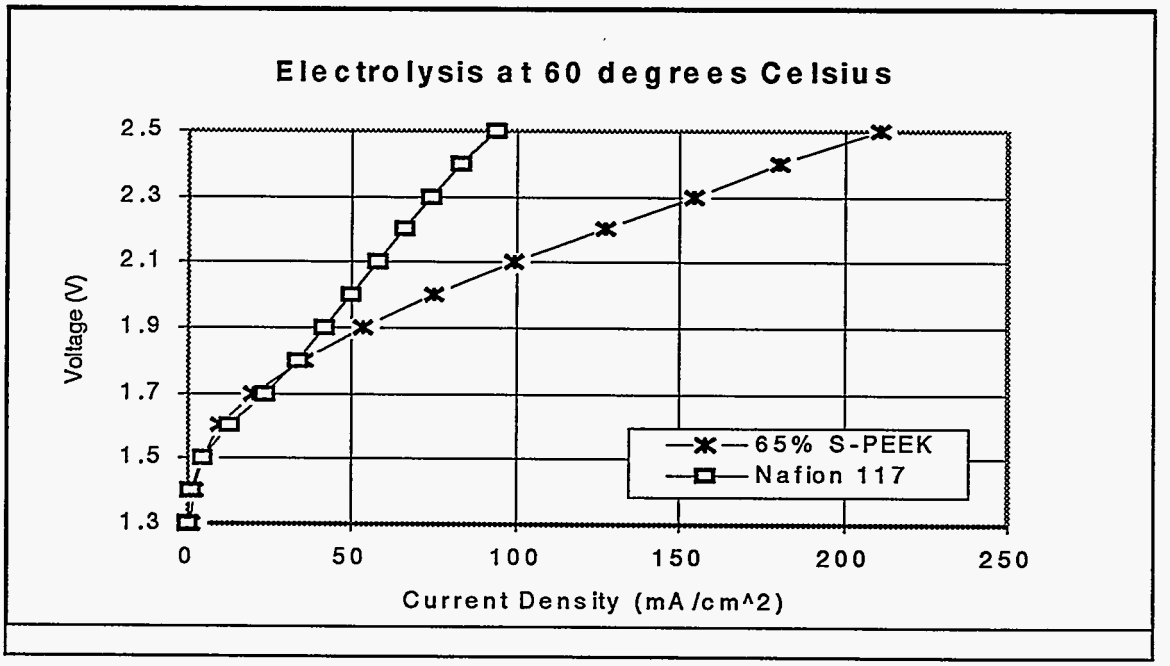

Figure 7. Performance comparison between Nafion 117 and 65% SPEEK.

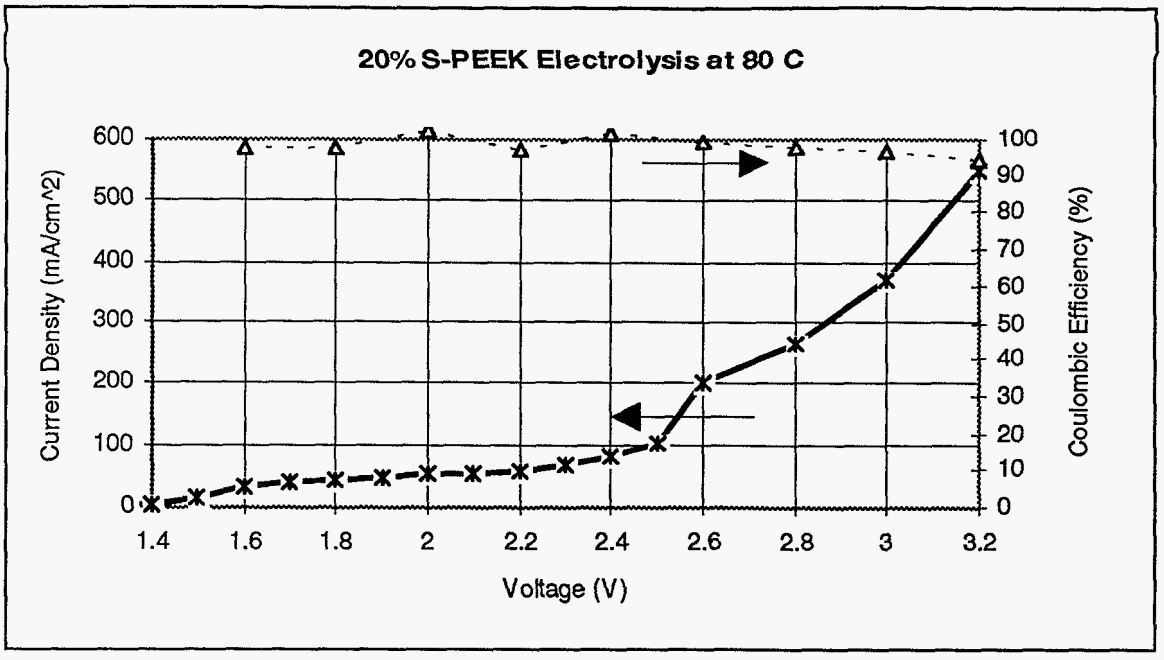

Figure 8. Correlation between current density and coulombic efficiency for 20% SPEEK.

5.0 CONCLUSION

Representative compounds from five engineering polymer families have been evaluated for utilization as a proton exchange membrane in a high temperature electrolyzer. Each was sulfonated with varying degrees of success. The SPEEK polymer was the most thoroughly studied, because it could easily be sulfonated and could be produced at a wide range of sulfonic acid content. Preliminary testing in an electrolysis cell showed performance comparable to existing commercial ionomer membranes.

6.0 ACKNOWLEDGMENTS

The authors would like to thank Dr. Gordon Nelson of the Florida Institute of Technology Chemistry Department for his guidance on this work. Financial support from the U.S. Department of Energy, Office of Advanced Utility Concepts is gratefully acknowledged.

7.0 REFERENCES

1. Z. Florjanczyk, W. Krawiec, W. Wieczorek and M. Siekierski, *J. Poly. Sci. Part B: Poly. Phys.*, **33**, 629 (1995).

2. J.C. Lassegues, B. Desbat, O. Trinquet, F. Cruege and C. Poinsignon, *Solid State Ionics*, **35**, 17 (1989).

3. J.Y. Sanchez, A. Denoyelle and C. Poinsignon, *Poly. Adv. Technol.*, **4**, 99 (1993).

4. P.W.T. Lu, and S. Srinivasan, *J. Appl. Electrochem.*, **9**, 269 (1979).

5. International Energy Agency Program of Cooperative Research and Development. 1987. *Task IV. Electrolytic Hydrogen Production*, 1986 Annual Progress Report, U.S. Department of Energy.

6. L. Glasser, *Chem. Rev.*, **75**, 21 (1975).

7. K. Kreuer, *J. Molecular Structure*, **177**, 265 (1988).

8. M.S. Reisch, *Chem. and Eng. News*, **67**, 21 (1989).

9. J. Bradshaw, S.B. Tian and G. Xu, *Solid State Ionics*, **73**, 147 (1994).

10. R. Nolte, K Ledjeff, M. Bauer and R. Mulhaupt, *J. Memb. Sci.*, **33**, 211 (1993).

11. X. Jin, M.T. Bishop, T.S. Ellis and F.E. Karasz, *Brit. Poly J.*, **17**, 4 (1985).

12. M.T. Bishop, F.E. Karasz, P.S. Russo and K.H. Langley, *Macromolecules*, **18**, 86 (1985).

13. J. Devaux, D. Delimoy, D. Daoust, R. Legras, J.P. Mercier, C. Strazielle and E. Nield, *Polymer*, **26**, 1994 (1985).

14. C. Bailly, D. J. Williams, F.E. Karasz and W.J. MacKnight, *Polymer*, **28**, 1009 (1987).

15. L. Leung, C. Bailly, J.F. O'Gara, D.J. Williams, F.E. Karasz and W.J. MacKnight, *Polym. Comm.*, **28**, 20 (1987).

16. C.A. Linkous, "Development of solid electrolytes for water electrolysis a intermediate temperatures," in vol I of *Hydrogen Energy Progress IX. Proceedings of the 9th World Hydrogen Energy Conference*, 419-427. T.N. Veziroglu, et al, eds., Paris, France, June 22-25, 1992, M.C.I., Paris.

17. T.A. Zawodzinski, Jr., M. Neeman, L.O. Sillerud and S. Gottesfeld, *J. Phys. Chem.*, **95**, 6040 (1991).

18. B.C. Johnson, I. Yidgor, C. Trans, M. Iqbal, J.P. Wightman, D.R. Lloyd, and J.E. McGrath, *J. Polym. Sci., Poly.. Chem. Ed.*, **22**, 721 (1984).

19. E.J. Powers and G.A. Serad."Histroy and Development of Polybenzimidazoles." In *High Performance Polymers: Their Origin and Development*, 355-373. R.B. Seymour and G.S. Kirshenbaum, eds., 1986, New York.

Task 4 Report

Production of Hydrogen by Thermocatalytic Cracking of Natural Gas

Annual Report

FSEC-CR-857-95
DOE Contract #DE-FG04-94AL85802
October 1995

Submitted to:
Neil Rossmeissl
Advanced Utility Concepts Division
Department of Energy
Washington, DC 20585

Submitted by:
Nazim Z. Muradov
Florida Solar Energy Center
1679 Clearlake Road
Cocoa, Florida 32922-5703

1.0 SUMMARY

In the next few decades hydrogen production will continue to rely on fossil fuels (primarily, natural gas). The conventional methods of hydrogen production from natural gas, for example, steam reforming (SR), are complex multi-step processes. These processes also result in the emission of large quantities of CO_2 into the atmosphere. One alternative is the single-step thermocatalytic cracking (TCC) (or decomposition) of natural gas into hydrogen and carbon. The comparative assessment of SR and TCC processes was conducted.

The series of experiments on the thermocatalytic cracking of methane over various catalysts and supports in a wide range of temperatures (500-900°C) and flow rates was conducted at the Florida Solar Energy Center. Two types of fix bed catalytic reactors were designed, built and tested: continuous flow and pulse reactors. The temperature dependence of the hydrogen production yield using metal and metal oxide type catalysts was studied. Ni-Mo/Alumina and Fe-catalysts demonstrated relatively high efficiency in the methane cracking reaction at the range of temperatures 600-800°C. Fe-catalyst demonstrated fairly good stability, whereas alumina-supported Pt-catalyst rapidly lost its catalytic activity. Methane decomposition reaction over Ni-Mo/alumina was studied over wide range of space velocities (3.8-67.8 min^{-1}) in a continuous flow fixed bed catalytic reactor. The experimental results indicate that the hydrogen yield decreases noticeably with an increase in the space velocity of methane. The pulse type catalytic reactor was used to test the activity of the catalysts. It was found that induction period on the kinetic curve of hydrogen production corresponded to the reduction of metal oxide to metallic form of the catalyst. SEM method was used to study the structure of the carbon deposited on the catalyst surface.

2.0 INTRODUCTION

2.1 Background

Energy systems based on hydrogen as an energy carrier coupled with renewable energy resources are considered as ultimate long term option. Natural gas appears to be a viable near term option. According to Marchetti (1979) and Nakicenovic (1990), natural gas will become, globally, the major source of energy during the next century. It is widely accepted that in the short- to medium-term hydrogen production will continue to rely on natural gas. On the other hand, the use of natural gas as a chemical feedstock and a fuel for the conventional processes of hydrogen production, for example, steam reforming (SR) or partial oxidation (PO), results in the emission of large quantities of CO_2 that produce adverse ecological effects. SR of natural gas is a complex process consisting of four processing steps:

1) feedstock purification

2) steam reforming of methane to hydrogen and carbon monoxide:

$$CH_4 + H_2O \leftrightarrow CO + 3H_2 + 206\ kJ \qquad (1)$$

3) water-gas shift reaction:

$$CO + H_2O \leftrightarrow CO_2 + H_2 - 41\ kJ \qquad (2)$$

4) gas purification (CO_2 removal)

The reforming reaction is a strongly endothermic, high temperature (800-900°C) process. To ensure a maximum conversion of CH_4 into the products , the process generally employs an excess of steam (steam/carbon ratio 3-5). The process thermal efficiency of the steam reformer is seldom greater than 50% (Cromarty 1992). Because of the energy intensive stages of SR process the usage of natural gas as a fuel is almost equal to its usage as a chemical feedstock. As a result the production of every cubic meter of hydrogen is accompanied by the emission of 0.5 cubic meter of CO_2. CO_2 can be removed from flue gases by several methods (*e.g.* adsorption by molecular sieves, cryogenic separation, membrane separation, etc.) which are energy and

investment intensive processes. However the real problem is what to do with accumulating volumes of CO_2 that are not released into the atmosphere. Simple calculations indicate that the amounts of CO_2 generated by reforming/scrubbing process would be truly enormous: the disposal of 10 millions tons of CO_2 would be the price to pay for each million ton of hydrogen produced. Although several proposals have been reported in literature (for example, Cheng and Steinberg 1986) on CO_2 disposal in natural underground reservoirs, depleted natural gas fields, the deep ocean, etc., concern was expressed by some experts on the possible ecological effects of high concentrations of CO_2 in the ocean or other disposal sites on the local biosphere (Nakicenovic 1993).

2.2 Thermal Cracking of Methane

One alternative to SR is a single-step thermal cracking (TC) of natural gas into hydrogen and carbon:

$$CH_4 \rightarrow C + 2H_2 + 75.6\ kJ \qquad (3)$$

The energy requirement per mole of hydrogen produced for TC is somewhat less than that for SR reaction: 37.8 and 41.2 kJ/mole H_2, respectively. The process is slightly endothermic, so only an insignificant amount of hydrogen produced could be used as a source of the thermal energy for the process. The H_2/CH_4 ratio for both TC and SR processes is approximately 2 (considering fuel usage of methane). In addition to hydrogen as a major product, the process produces a very important by-product: clean carbon.

A comparative assessment of hydrogen production processes by TC and SR of natural gas yields the following conclusions:

1) The energy and feedstock consumption per unit of hydrogen produced for the processes are comparable.

2) TC of natural gas is a technologically simple one-step process without energy and material intensive gas separation stages, while SR is a multi-step process.

3) The maximum temperature of the SR process is still high (815 °C) despite many decades of intensive operation and improvement. This leaves a very low probability for further reductions in the reaction temperature. In contrast, the TC process has a great potential for decreasing the maximum temperature of the process (by several hundred degrees centigrade) by using effective catalysts.

4) There is a very valuable by-product of TC process: pure carbon, while SR produces no useful by-products.

5) TC produces practically no CO_2 emissions.

It was shown (Steinberg and Cheng 1988) that the cost of hydrogen produced by TC of natural gas is somewhat lower than that for the conventional processes and is equal to \$1.64 per 10^3 SCF after by-product carbon credit is taken.

2.3 Thermocatalytic Decomposition of Methane

The thermodynamic data show that the methane decomposition can be realized at relatively moderate temperatures. Thus, the use of catalysts is needed for the realization of thermal decomposition of methane at comparatively low temperatures. Attempts have been made to use catalysts for the cracking of methane and light hydrocarbons. For example, authors used alumina, silica-alumina, silica-magnesia, etc. at 800-1000°C (Pohleny and Scott 1966) and Co, Cr, Ni, Pt-based catalysts at 895-1100°C (Callahan 1974). The carbon produced was then burned off the surface of the catalyst.

In this regard, these processes exhibit no significant advantages over conventional processes (for example, SR) because of high operational temperatures and large CO_2 emissions.

Our approach is based on the selection of the active catalysts for the methane decomposition operating at moderate temperatures (650-850°C) and carbon recovery. It is more attractive from technical and ecological points of view to store carbon rather than CO_2. Since TCC of natural gas does not produce CO_2 emissions it can be considered as a transition process linking the fossil fuel and the renewable energy resource-based economies. In the short-term, this process can be used for on-site production of hydrogen-methane mixtures in gas-filling stations and for CO_2-free production of hydrogen for fuel cell driven prime movers.

3.0 EXPERIMENTAL

3.1 Reagents and Catalysts

The gases: methane (99.0%, BITEC) and nitrogen (99.999%, BITEC) were used without further purification. Pt(1%)/alumina catalyst was prepared by soaking-drying technique using γ-alumina and 1% w solution of H_2PtCl_6, with subsequent reduction in a stream of hydrogen. Fe-catalyst was prepared from Fe_2O_3 (Fisher). $NiO-MoO_3$/alumina catalyst (surface area 180 m^2/g, pore volume 0.5 cm^3/g) was provided by Haldor Topsoe, Inc.

3.2 Reactors

Some consideration was given to the reactor material. We studied the catalytic activity of various materials which could potentially be used for the reactor construction for methane decomposition process. A quartz was found to be the most inert material in methane cracking reaction followed by alumina. Metals (e.g.stainless steel demonstrated noticeable catalytic activity in methane decomposition process and can not be used a reactor material in the catalyst activity measurements.

Two types of catalytic reactors were used in this work: continuous flow (material-quartz, reaction zone volume 58.4 mL, catalyst amount 3-6 g) and pulse (material-quartz, reaction zone volume 3.2 mL, catalyst amount 0.5 g). Both continuous flow and pulse catalytic reactors were made out of quartz tubes with O.D. 15 mm and 7 mm, respectively.

3.3 Experimental Set-up

The schematic diagram of the catalytic system with continuous flow reactor is depicted in Figure 1. The experimental set-up consists of 3 subsystems: fixed bed catalytic reactor, gas introduction and sampling subsystem and analytical subsystem. The reactor is placed in a temperature-controlled (Love Controls Corp.) oven. Ovens were manufactured by Thermcraft Inc. CH_4 and N_2 flow rates were measured by flowmeters MKS Instruments, Inc. and Teledyne, Hastings-Raydist, respectively. Before introducing methane into the continuous flow reactor at the operational temperatures and flow rates, slow flow of nitrogen (25 mL/min) was passed through the reactor to remove air. At the end of the experiment, the flow of nitrogen was again introduced into the reactor to remove metane and hydrogen from hot reactor.

Figure 2 depicts the schematic diagram of the catalytic system with pulse reactor which consists of a microreactor (volume 3.2 mL) with a catalyst, 6-port sampling valve with 1 mL sampling loop and gas chromatograph. In a "stand-by" position of 6-port valve the carrier gas (nitrogen) entered in tandem the 6-port valve, the microreactor and GC-column. Methane entered 1 mL sampling loop and vented off. In the "injection" position of the 6-port valve, the pulses (1 mL each) of methane were injected into the microreactor and the methane cracking products entered GC.

3.4 Analytical System

The products of methane decomposition and partial oxidation were measured gas-chromatographically. Gas chromatograph SRI 8610 (nitrogen-carrier gas, thermal conductivity detector, silicagele column) was used for the analysis of hydrogen. Varian 3000 (helium-carrier gas, flame-ionization detector, Hysep D_B column) was used for $CO, _2CO$ and traces of hydrocarbons analysis. SEM (Amray 1810) was used to study the carbon deposited on the catalyst surface

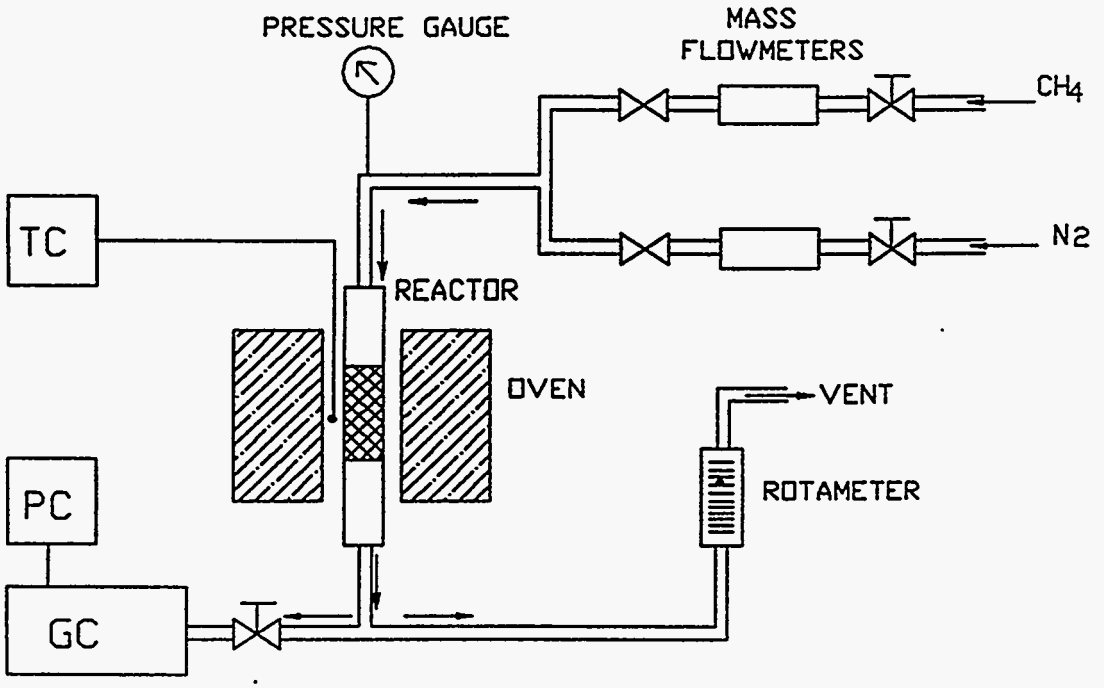

Figure 1. Schematic Diagram of Continuous Flow Thermocatalytic System for CH_4 Cracking. Reactor Volume: 58.4 mL. Catalyst: 6 g.

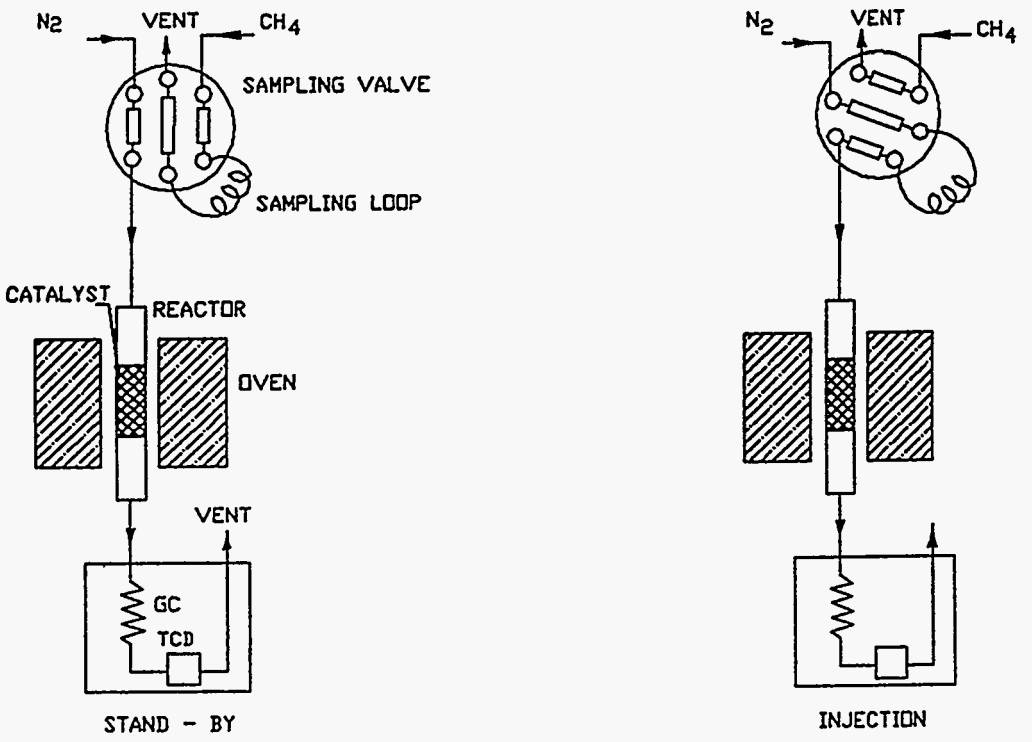

Figure 2. Pulse Reactor System for the Methane Thermocatalytic Cracking. Reactor Volume: 3.2 mL. Catalyst: 0.5 g.

4.0 RESULTS AND DISCUSSION

4.1 Temperature Dependence of Hydrogen Yield

We studied thermocatalytic decomposition of methane over various catalysts and contacts in a wide range of temperatures 500-900°C. It was observed that the hydrogen production rate is a function of the temperature. Figure 3 depicts the temperature dependence of the hydrogen concentration (% vol) in the effluent gas using different catalysts and refractory materials including the reactor material: quartz. It was found that quartz as well as graphite and alumina showed no or insignificant activity in the methane decomposition reaction at temperatures below 700°C. Alumina-supported Ni-Mo and Fe-catalysts demonstrated high catalytic activity in the range of 650-800°C and 800-900°C, respectively. It should be noted that in some cases we observed a decline in the hydrogen yield as the run proceeded due to the carbon build-up on the catalyst surface. Therefore, only maximum values of hydrogen yields were considered in plotting the temperature dependence of the methane decomposition reaction.

It was observed that the shape of the kinetic curve for hydrogen production is mostly determined by the chemical composition of the contact. For example, alumina-supported Pt-catalyst demonstrated high catalytic activity only during first several minutes and then the rate of the methane decomposition drastically dropped and reached the stationary level which corresponds to the hydrogen concentration in the effluent gas equal to approximately 20% vol. (Figure 4). In case of oxide type catalysts the maximum yield of hydrogen is reached after the induction period corresponding to the catalyst reduction to its metallic state. Figure 5 depicts the time dependence of H_2 concentration in the product of the methane decomposition in presence of alumina-supported Fe-catalyst. After a relatively long induction period, the stationary process of methane decomposition over the catalyst surface with the formation of gas (95% vol. H_2) was observed. It should be noted that in this experiment the hydrogen production rate did not decline for at least two hours. Another behavior was demonstrated by the alumina-supported Ni-Mo catalyst. The maximum hydrogen yield was reached after a short induction period (5 min) followed by slow decrease in the catalytic activity. The kinetic curves of the hydrogen and carbon oxides production in presence of Ni-Mo catalyst are shown in Figure 6.

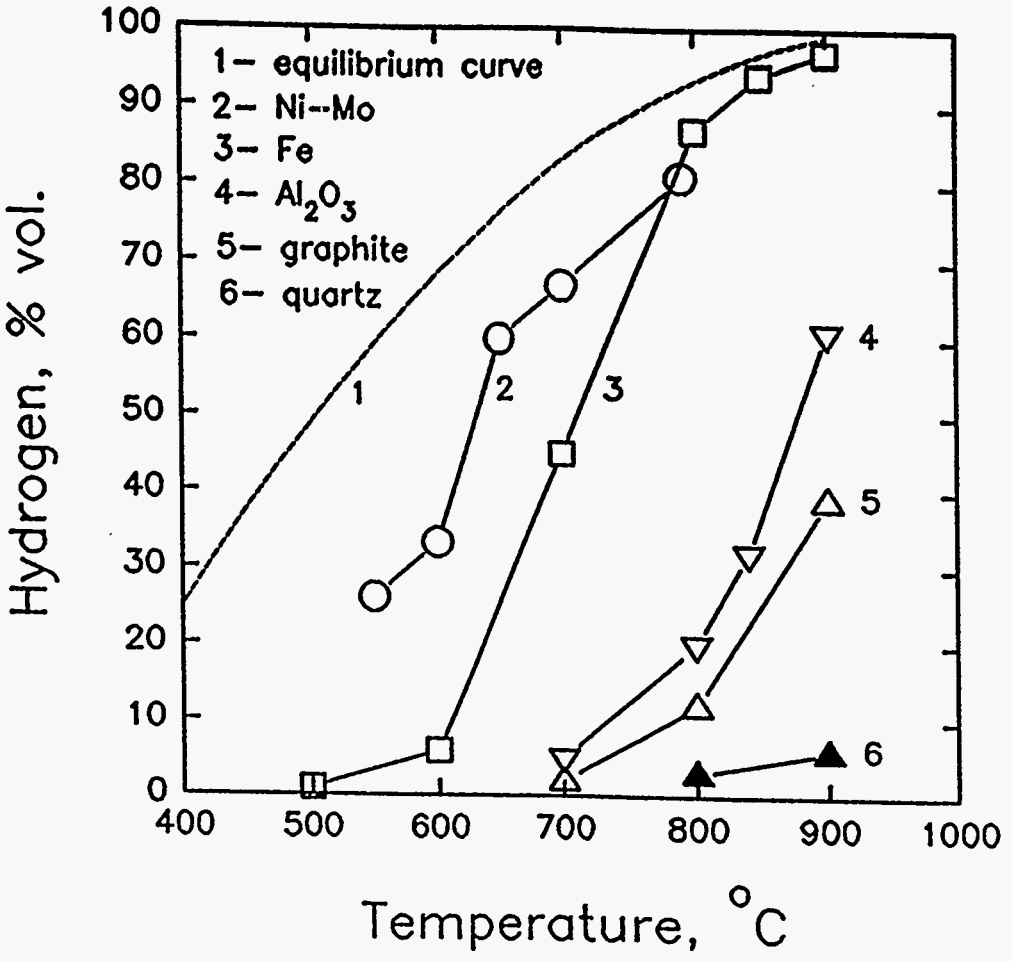

Figure 3. Temperature Dependence of Hydrogen Concentration in the Effluent Gas Using Various Catalysts and Contacts. Continuous Flow Reactor.

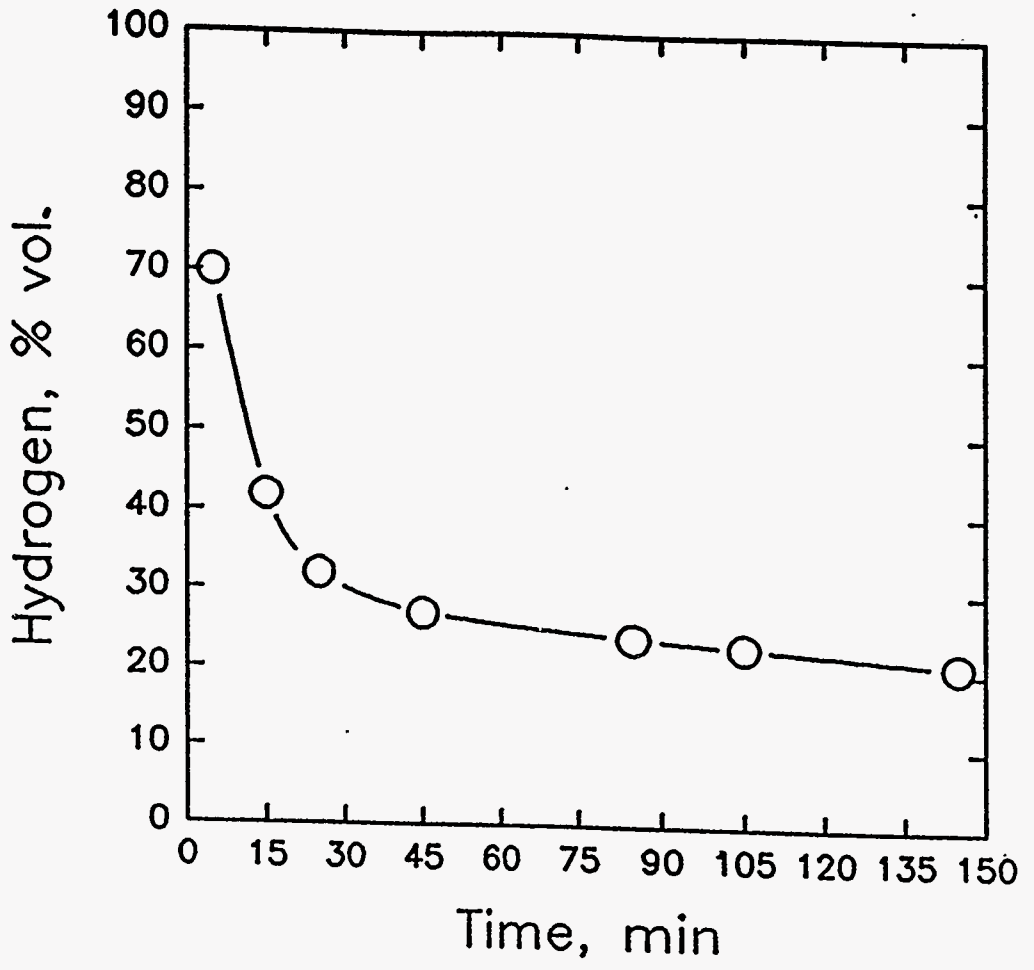

Figure 4. Time Dependence of Hydrogen Concentration in the Effluent Gas in the Presence of Alumina-Supported Pt-Catalyst. Continuous Flow Reactor. Temperature: 900°C.

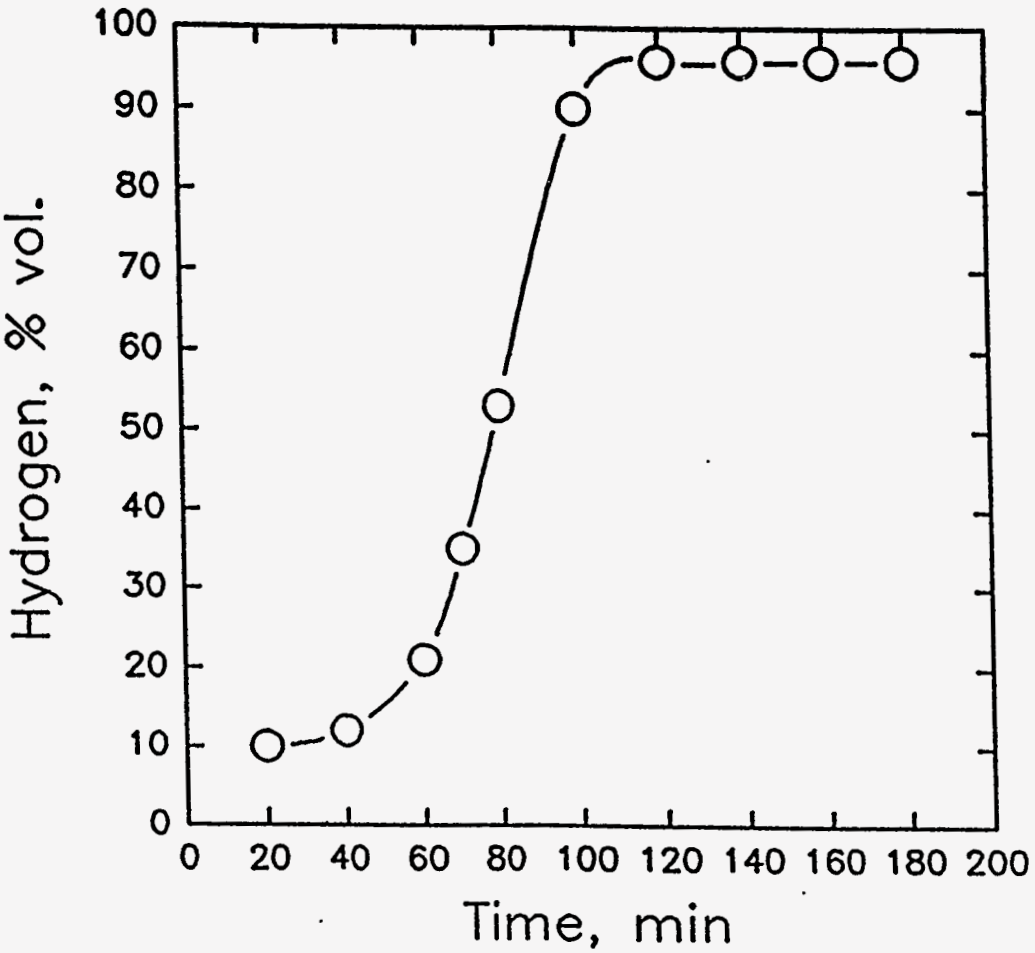

Figure 5. Time Dependence of Hydrogen Concentration in the Effluent Gas in the Presence of Fe-Catalyst. Continuous Flow Reactor. Temperature: 900°C.

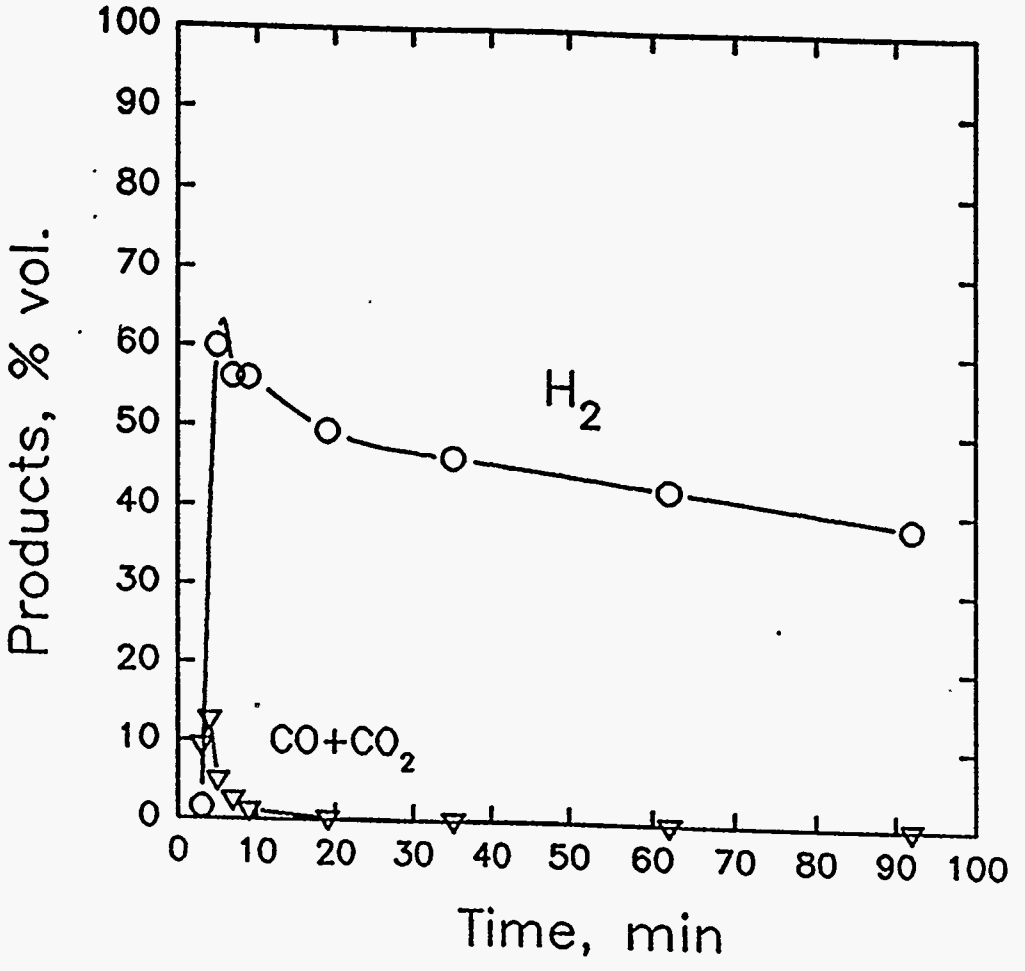

Figure 6. Time Dependence of Methane Decomposition Products Concentrations in the Effluent Gas Using Alumina-Supported Ni-Mo Catalyst. Continuous Flow Reactor. Temperature: 650°C.

4.2 Space Velocity Dependence of Hydrogen Yield

The rationale for this series of experiments was to study the effect of the residence time of methane within the continuous flow reactor on the hydrogen yield at given temperature. We conducted series of experiments on the methane catalytic cracking in wide range of flow rates from 25 to 450 mL/min at 700°C. NiO-MoO_3/alimina was used as a catalyst. Figure 7 depicts the kinetic curves of hydrogen production at various flow rates. After short induction period 1-10 minutes hydrogen concentration in the effluent gas reaches the maximum value and then gradually declined. GC analysis showed that during induction period the effluent gas is rich with carbon oxides. Figure 8 shows the dependence of the maximum hydrogen yield on the space velocity of methane. Increase in methane space velocity from 3.8 to 67.8 min^{-1} resulted in significant drop in the hydrogen yield from 75.9 to 24.8%.

4.3 Pulse Reactor Experiments

The continuous flow reactor experiments demonstrated that it was very difficult to accurately measure the maximum yields of hydrogen production. Relatively short induction period and the longevity of GC analysis (up to 7 minutes) were main sources of these difficulties. To solve this problem we problem we used pulse reactor, depicted in Figure 2. 1 mL pulses of CH_4 at regular intervals (corresponding to the time of GC analysis) were injected into the catalytic microreactor and the reaction products entered the GC analyzer. In a typical experiment we conducted up to 90 of such injections. Figure 9 depicts the dependance: the methane decomposition products yields *vs* the number of 1 mL methane injections. First injections result in a deep oxidation of the methane into the carbon oxides and the reduction of the catalyst to its reduced (probably, metallic) form. We observed the onset of the hydrogen formation after 13 injections with the maximum hydrogen yield corresponding to 25-40 injections. Beginning from the 30th injection hydrogen was the only product of the methane decomposition. The most important result of this series of experiments is that the maximum concentration of hydrogen in the effluent gas is fairly close to its equilibrium (*i.e.* theoretical) value which is an indication of an active catalyst.

It can be concluded from these experimental results that the induction period corresponds to the reduction of metal-oxide form of the catalyst into metallic form.

$$3NiO + CH_4 \rightarrow 3Ni + CO + 2H_2O \qquad (4)$$

$$12Fe_2O_3 + CH_4 \rightarrow 8Fe_3O_4 + CO_2 + 2H_2O \qquad (5)$$

$$12Fe_3O_4 + CH_4 \rightarrow 12FeO + CO_2 + 2H_2O \qquad (6)$$

$$3FeO + CH_4 \rightarrow 3Fe + CO + 2H_2O \qquad (7)$$

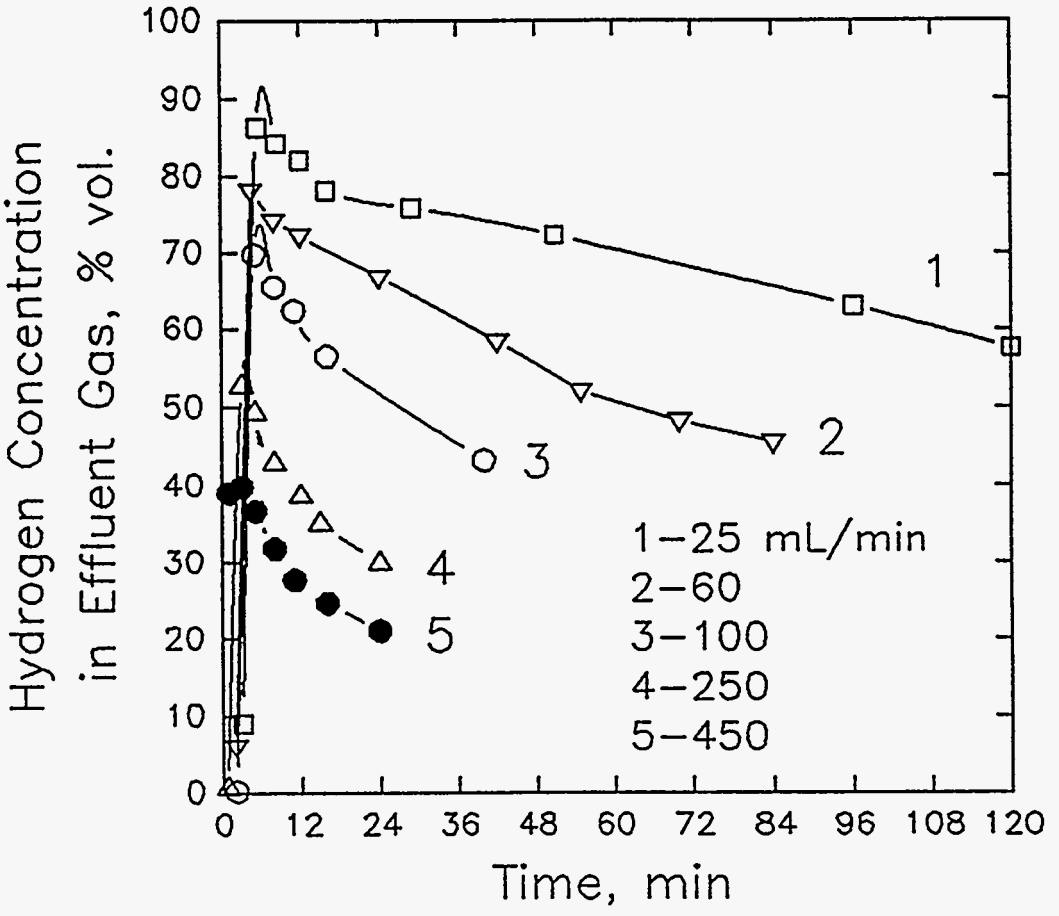

Figure 7. Kinetic Curves of Hydrogen Production at Different Flow Rates. Continuous Flow Reactor. Catalyst Ni-Mo/Alumina. Temperature 700°C.

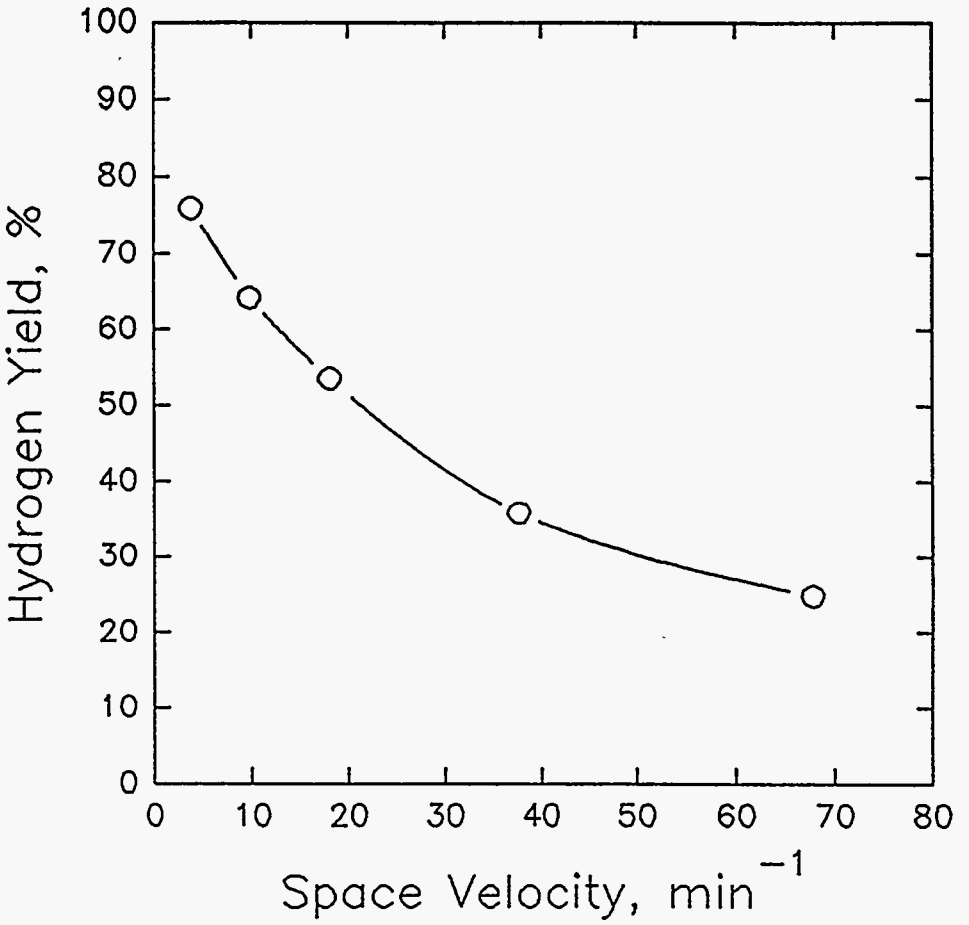

Figure 8. Hydrogen Yield *vs* Space Velocity of Methane. Continuous Flow Reactor. Catalyst Ni-Mo/Alumina. Temperature 700°C.

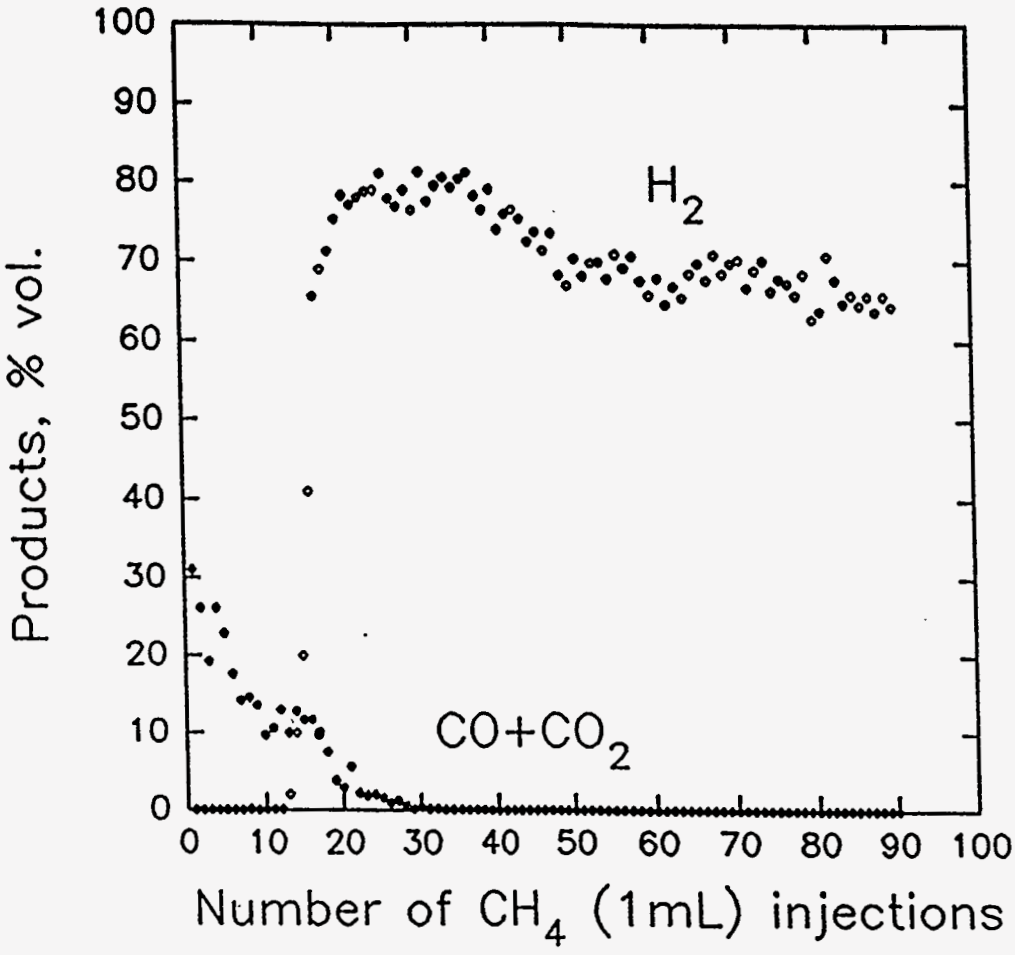

Figure 9. Methane Decomposition Products Concentrations in the Effluent Gas as a Function of the Number of Methane (1 mL) Injections into Reactor. Pulse Reactor. Alumina-Supported Ni-Mo Catalyst. Temperature: 650°C.

Once the active metallic form of the catalyst was produced, the effective cracking of methane molecules on the catalyst surface with formation of hydrogen and carbon begins. The carbon blocks the active sites on the catalyst surface which results in the reduction of the catalyst activity.

We have conducted SEM studies of the carbon deposited on the catalyst surface at different temperatures. After the catalytic cracking of methane, the reactor was allowed to cool to the room temperature in the stream of nitrogen. The carbon was carefully removed (mechanically) from the catalyst surface and analyzed by SEM method. Figure 10 depicts typical SEM micrograph of the carbon removed from Ni-Mo catalyst. It was found that the carbon formed on the catalyst surface at the range of temperatures 500-800°C had an amorphous structure.

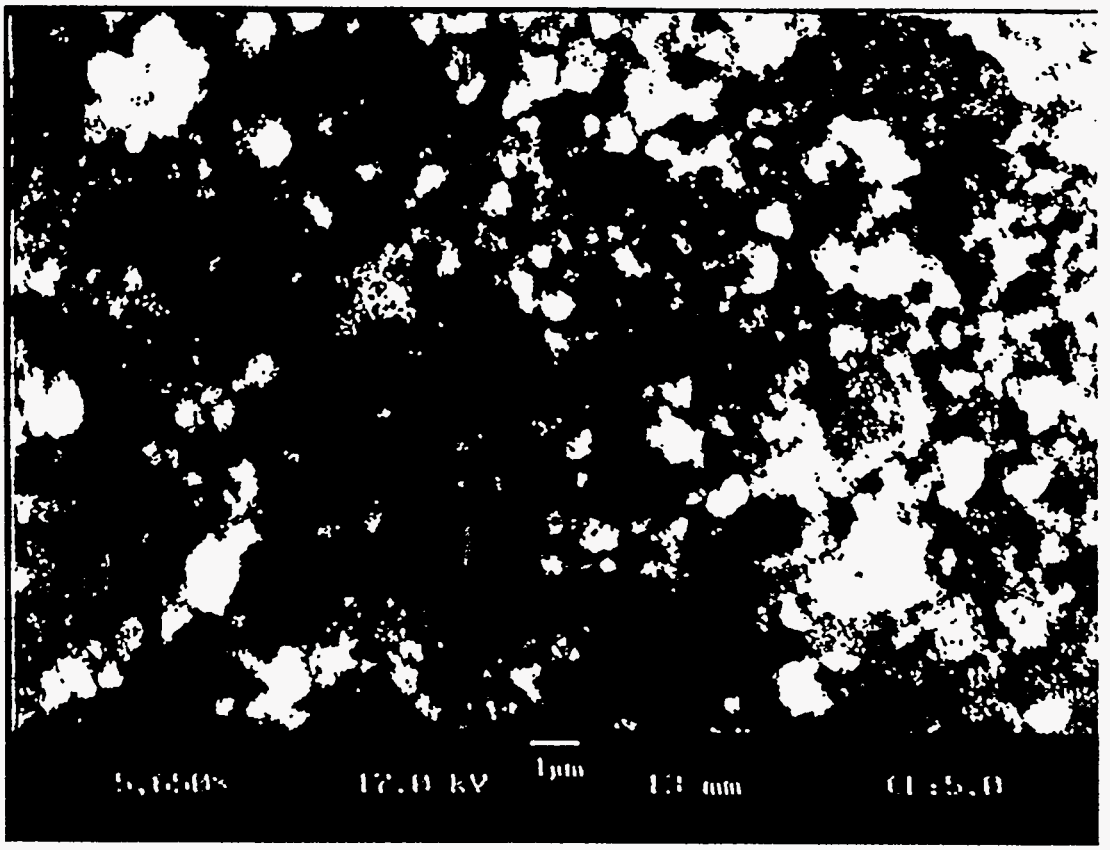

Figure 10. SEM Micrograph of Carbon Removed from Ni-Mo/Alumina Catalyst Surface.

5.0 CONCLUSIONS

Thermocatalytic cracking of the natural gas has several advantages over conventional processes of hydrogen production: i) it is technologically simple one-step process, ii) it produces a valuable by-product: pure carbon and iii) it produces practically no CO_2 emissions.

Thermocatalytic cracking of the methane over various catalysts and contacts was studied in this work. Catalyst activity and stability tests were conducted using two types of thermocatalytic systems: fixed bed continuous flow and pulse reactors, in a wide range of temperatures (500-900°C) and space velocities (3.8-67.8 min^{-1}). Alumina-supported Ni-Mo and bulk Fe catalysts demonstrated high catalytic activity at 650 and 800°C, respectively. Pt/alumina catalyst rapidly lost its catalytic activity. Among materials tested quartz demonstrated lowest catalytic activity in methane decomposition reaction and, hence, can be used as a material for the reactor construction. It was found that the concentration of hydrogen in the effluent gas is a function of temperature and gas flow rate. For example, the H_2-CH_4 mixtures with the hydrogen concentration 30 and 80% vol. can be produced at 600 and 790°C, respectively, using alumina-supported Ni-Mo catalyst. Fe-catalyst is thermally more stable than Ni-Mo/alumina catalyst and at elevated temperatures produces gas with the concentration of hydrogen up to 95% vol. The activity of the catalysts was tested using pulse catalytic reactor. The induction period preceded the effective hydrogen production using both Ni and Fe catalysts. It was found that the induction period corresponded to the reduction of metal oxide to metallic form of the catalyst. The carbon deposited on the catalyst surface was studied using SEM method.

6.0 REFERENCES

1. Callahan, M. **1974.** "Catalytic Pyrolysis of Methane and Other Hydrocarbons". In *Proceedings of 26th Power Sources Symposium,* 181-184. Red Bank, N.J.

2. Marchetti, C. and N. Nakicenovic. **1979.** *The Dynamics of Energy Systems and the Logistics Substitution Model,* IIASA, RR-79-13, Laxenburg, Austria.

3. Nakicenovic, N. **1993.** *Energy Gases: The Methane Age and Beyond,* IIASA Working Paper WP-93-033, Laxenburg, Austria.

4. Pohleny, J. and N. Scott. **1966.** U.S.Patent No 3,284,161 (UOP).

5. Steinberg, M. and H. Cheng. **1988.** "Modern and Perspective Technologies for Hydrogen Production from Fossil Fuels". In *Proceedings of 7th World Hydrogen Energy Conference,* 699-730. Moscow, USSR.